JYU DISSERTATIONS 689

Virva Kinnunen

Improving the Accuracy of Single Particle ICP-MS Analyses of Au and Ag Nanoparticles

UNIVERSITY OF JYVÄSKYLÄ
FACULTY OF MATHEMATICS
AND SCIENCE

JYU DISSERTATIONS 689

Virva Kinnunen

Improving the Accuracy of Single Particle ICP-MS Analyses of Au and Ag Nanoparticles

Esitetään Jyväskylän yliopiston matemaattis-luonnontieteellisen tiedekunnan suostumuksella
julkisesti tarkastettavaksi Ylistönrinteen auditoriossa Kem4
syyskuun 15 päivänä 2023 kello 12.

Academic dissertation to be publicly discussed, by permission of
the Faculty of Mathematics and Science of the University of Jyväskylä,
in Ylistönrinne, auditorium Kem4, on September 15, 2023, at 12 o'clock.

JYVÄSKYLÄN YLIOPISTO
UNIVERSITY OF JYVÄSKYLÄ

JYVÄSKYLÄ 2023

Editors
Rose Matilainen
Department of Chemistry, University of Jyväskylä
Päivi Vuorio
Open Science Centre, University of Jyväskylä

ISBN 978-951-39-9720-5 (PDF)
URN:ISBN:978-951-39-9720-5
ISSN 2489-9003

Permanent link to this publication: http://urn.fi/URN:ISBN:978-951-39-9720-5

ABSTRACT

Kinnunen, Virva
Improving the accuracy of single particle ICP-MS analyses of Au and Ag nanoparticles
Jyväskylä: University of Jyväskylä, 2023, 67 p.
(JYU Dissertations
ISSN 2489-9003; 689)
ISBN 978-951-39-9720-5 (PDF)

The remarkable advancements of nanotechnology have incorporated nanomaterials (NMs) in almost all fields of activity and product categories, which has raised concerns about the potential environmental and human health risks. The realistic risk assessment of NMs requires advanced analytical techniques suitable even for complex sample matrices, for which single particle inductively coupled plasma mass spectrometry (SP-ICP-MS) is an efficient alternative. However, some remaining challenges still need to be addressed to improve the accuracy of the results.

This thesis offers different approaches for improving the accuracy of the SP-ICP-MS analyses of Au and Ag nanoparticles (NPs). The literature review describes the fundamentals and a few of the existing applications of the SP-ICP-MS technique. Some of the remaining challenges of this technique and the existing procedures used to overcome these issues are discussed. The experimental section presents the different approaches used in the original papers to improve the accuracy of NP characterization and quantification.

First, the optimization of instrumental conditions for SP-ICP-MS measurements of gold was carried out using a design of experiments (DoE) approach, significantly enhancing the instrument sensitivity. The 15% reduction in the NP size limit of detection allowed more accurate detection and determination of the Au NPs. This was followed by the development of a simple sample pretreatment procedure using solid phase extraction (SPE) materials for dissolved silver (AgD) removal, thus allowing a more accurate determination of Ag NPs. Finally, a novel sample pretreatment method was presented using functional 3D printed scavengers for AgD removal. 3D printing enabled the incorporation of an efficient SPE material into highly porous 3D scavengers, allowing efficient removal of AgD while preserving the original Ag NP properties of the sample. Thus, more highly accurate sizing and counting of Ag NPs was achieved.

Keywords: Single particle inductively coupled plasma mass spectrometry, Nanomaterials, Ag NPs, Au NPs, Optimization, Dissolved analyte interference, Solid phase extraction materials, 3D printing, Functional 3D scavengers

TIIVISTELMÄ (ABSTRACT IN FINNISH)

Kinnunen, Virva
Au ja Ag nanopartikkeleiden määrityksen tarkkuuden parantaminen yksittäispartikkeli ICP-MS:lla
Jyväskylä: Jyväskylän yliopisto, 2023, 67 s.
(JYU Dissertations
ISSN 2489-9003; 689)
ISBN 978-951-39-9720-5 (PDF)

Nanoteknologian nopean kehittymisen seurauksena nanomateriaaleja (NM) hyödynnetään lähes kaikilla toiminta-aloilla ja tuotekategorioissa, joka on herättänyt huolta mahdollisista ympäristö- ja terveysriskeistä. NM:en realistinen riskinarviointi vaatii monimutkaisille matriiseille soveltuvia kehittyneitä analyysitekniikoita, johon yksittäispartikkeli induktiivisesti kytketty plasma massaspektroskopia (SP-ICP-MS) on varteenotettava vaihtoehto. Joitakin jäljellä olevia haasteita on kuitenkin vielä ratkaistava tulosten tarkkuuden parantamiseksi.

Tämä väitöskirja tarjoaa erilaisia ratkaisuja Au ja Ag nanopartikkeleiden (NP) määrityksen tarkkuuden parantamiseksi SP-ICP-MS:lla. Kirjallisuuskatsauksessa kuvataan SP-ICP-MS tekniikan perusteita ja olemassa olevia sovelluksia. Eräitä tekniikan jäljellä olevia haasteita ja käytettyjä ratkaisukeinoja käydään läpi. Kokeellisessa osuudessa kuvataan alkuperäisissä julkaisuissa esitetyt keinot NP:en määrityksen tarkkuuden parantamiseksi.

Ensiksi tilastollista koesuunnittelua hyödynnettiin olosuhteiden optimoinnissa kullan SP-ICP-MS mittauksia varten, joka johti herkkyyden huomattavaan parantumiseen. Saavutettu 15 %:n lasku nanopartikkeleiden koon määritysrajassa mahdollisti tarkemman Au NP:en havainnoinnin ja määrittämisen. Seuraavaksi kehitettiin yksinkertainen näytteen esikäsittelymenetelmä liuenneen hopean poistamiseen käyttäen kiinteäfaasiuutto (SPE) materiaaleja, joka mahdollisti tarkemman Ag NP:n määrittämisen. Lopuksi esiteltiin näytteen esikäsittelymenetelmä liuenneen hopean poistamiseen hyödyntäen funktionaalisia 3D tulostettuja sieppareita. 3D tulostus mahdollisti tehokkaan SPE materiaalin yhdistämisen huokoiseen 3D siepparii, joka mahdollisti tehokkaan liuennen hopean poistamisen säilyttäen samalla näytteen alkuperäiset Ag NP:en ominaisuudet. Tämän seurauksena Ag NP:n koon ja konsentraatiomäärityksen tarkkuutta saatiin huomattavasti parannettua.

Avainsanat: Yksittäispartikkeli induktiivisesti kytketty plasma massaspektroskopia, Nanomateriaalit, Ag NP:t, Au NP:t, Optimointi, Liuenneen analyytin häiriö, Kiinteäfaasiuuttomateriaalit, 3D tulostus, Funktionaaliset 3D siepparit

Author Virva Kinnunen
Department of Chemistry
University of Jyväskylä
Finland
Virva.v-t.kinnunen@jyu.fi
ORCID 0000-0002-7533-6495

Supervisors Doctor Rose Matilainen
Department of Chemistry
University of Jyväskylä
Finland

Doctor Siiri Perämäki
Department of Chemistry
University of Jyväskylä
Finland

Reviewers Professor Kevin J. Wilkinson
Department of Chemistry
University of Montreal
Canada

Professor Gábor Galbács
Department of Inorganic and Analytical Chemistry
University of Szeged
Hungary

Opponent Associate Professor Katrin Löschner
DTU National Food Institute
Technical University of Denmark

PREFACE

This doctoral thesis work was conducted in the Department of Chemistry at the University of Jyväskylä during 2019-2023. The research has been funded by the Department of Chemistry, University of Jyväskylä.

First and foremost, I wish to express my deepest gratitude to my supervisors, Rose Matilainen and Siiri Perämäki, for sharing their precious time and knowledge to guide me on my path to a Ph.D. It goes without saying that without their warm guidance and encouragement during these years, the accomplishment of this work would not have been possible. I wish to thank both for all our discussions during these past years, which often helped me see things in a new light. I especially wish to thank you, Rose, for all your hard work during these past challenging months, for which I'll be forever gratefull. My reviewers, Professor Kevin J. Wilkinson and Professor Gábor Galbács, are greatly acknowledged for their careful review and valuable comments on this thesis.

I wish to thank Professor Ari Väisänen for giving me the opportunity to pursue a doctoral degree as a member of his team and for his comments on this thesis. I would also like to thank all my present and former colleagues in Team Väisänen for their support and all the fun memories over the years. It has been a privilege to be surrounded by such hard-working and innovative people, and I wish nothing but the best for all of them. I wish to thank all my other colleagues in the Department of Chemistry for creating such an inspiring working atmosphere. I especially wish to thank Kaisa Lampinen and Elina Hautakangas for offering me an extra pair of hands in the laboratory when needed, and Hannu Salo for SEM analysis.

I want to express my gratitude to my family and friends for their encouragement throughout this challenging process. They have always been there for me and never doubted my chances of completing this task. They helped me to keep my head in the clouds and my feet on the ground, for which I am grateful. Finally, I would like to thank my husband Esko for his loving support during these past years. I am grateful for his remarkable patience when listening to me jabbering about my work in the sauna and for all the encouraging words and hugs which have kept me going even through the darkest of times. He is one in a million and, for me, the only one.

Jyväskylä 1.6.2023
Virva Kinnunen

LIST OF ORIGINAL PUBLICATIONS

This thesis is based on the following original publications, which are referred to in the text by Roman numerals:

I Kinnunen, V., Perämäki, S, and Matilainen, R., Optimization of instrumental parameters for improving sensitivity of single particle inductively-coupled plasma mass spectrometry analysis of gold, *Spectrochim. Acta B*, 2021, **177**, 106104.

II Kinnunen, V., Perämäki, S, and Matilainen, R., Solid phase extraction materials as a key for improving the accuracy of silver nanoparticle characterization with single-particle inductively coupled plasma mass spectrometry in natural waters through dissolved silver removal, *Spectrochim. Acta B*, 2022, **193**, 106431.

III Kinnunen, V., Frimodig, J., Perämäki, S, and Matilainen, R., Application of 3D printed scavengers for improving the accuracy of single-particle inductively coupled plasma mass spectrometry analyses of silver nanoparticles by dissolved silver removal, *Spectrochim. Acta B*, 2023, **203**, 106662.

Author's contribution

In papers I-III, the author had the main role in planning and executing the experimental work, performing all SP-ICP-MS, ICP-MS, ICP-OES, and TEM measurements, interpreting the experimental results, and writing the manuscripts. In publication III, the author conducted all experimental work except for 3D printing and SEM analysis.

Other related publications by the author:

IV Lahtinen E., Kukkonen E., Kinnunen V., Lahtinen M., Kinnunen K., Suvanto S., Väisänen A. and Haukka M., Gold Nanoparticles on 3D-Printed Filters: From Waste to Catalysts, *ACS Omega*, 2019, **4**, 16, 16891-16898.

V Minelli C., Wywijas M., Bartczak D., Cuello-Nuñez S., Infante H. G., Deumer J., Gollwitzer C., Krumrey M., Murphy K. E., Johnson M. E., Montoro Bustos A. R., Strenge I. H., Faure B., Høghøj P., Tong V., Burr L., Norling K., Höök F., Roesslein M., Kocic J., Hendriks L., Kestens V., Ramaye Y., Contreras Lopez M. C., Auclair G., Mehn D., Gilliland D., Potthoff, A., Oelschlägel K., Tentschert J., Jungnickel H., Krause B. C., Hachenberger Y. U., Reichardt P., Luch A., Whittaker T. E., Stevens M. M., Gupta S., Singh A., Lin F., Liu Y-H., Costa A. L., Baldisserri C., Jawad R., Andaloussi S. E. L., Holme M. N., Lee T. G., Kwak M., Kim J., Ziebel J., Guignard C., Cambier S., Contal S., Gutleb A. C., Tatarkiewicz J., Jankiewicz B. J., Bartosewicz B., Wu X., Fagan J. A., Elje E., Rundén-Pran E., Dusinska M., Kaur I. P., Price D., Nesbitt I., O'Reilly S., Peters R. J. B., Bucher G., Coleman D., Harrison A. J., Ghanem A., Gering A., McCarron E., Fitzgerald N., Cornelis G., Tuoriniemi J., Sakai M., Tsuchida H., Maguire C., Prina-Mello A., Lawlor A. J., Adams J., Schultz C. L., Constantin D., Thanh N. T. K., Tung L. D., Panariello L., Damilos S., Gavriilidis A., Lynch I., Fryer B., Carrazco Quevedo A., Guggenheim E., Briffa S., Valsami-Jones E., Huang Y., Keller A. A., Kinnunen V., Perämäki S., Krpetic Z., Greenwood M., and Shard A. G., Versailles project on advanced materials and standards (VAMAS) interlaboratory study on measuring the number concentration of colloidal gold nanoparticles, *Nanoscale*, 2022, **14**, 4690-4704.

CONTENTS

ABBREVIATIONS

AgD	Dissolved silver
ANOVA	Analysis of variance
BSD	Backscatter electron detection
C115HMR	Purolite C115HRM
CE	Capillary electrophoresis
COD_{Mn}	Chemical oxygen demand (Mn)
CPE	Cloud point extraction
DLS	Dynamic laser scattering
DOC	Dissolved organic carbon
DoE	Design of experiments
FFF	Field-flow fractioning
ICP-MS	Inductively coupled plasma mass spectrometry
ICP-OES	Inductively coupled plasma optical emission spectrometry
LC	Liquid chromatography
LLE	Liquid-liquid extraction
LOD_{size}	Size limit of detection
LOQ	Limit of quantification
MDL	Method detection limit
MSPE	Magnetic solid phase extraction
NIST	National Institute of Standards and Technology
NM	Nanomaterial
NP	Nanoparticle
NTA	Nanoparticle tracking analysis
PA-12	Polyamide-12
PP	Polypropylene
PS	Polystyrene
RSM	Response surface methodology
SB TA	SiliaBond Tosic Acid
SEM	Scanning electron microscopy
SLS	Selective laser sintering
SPE	Solid phase extraction material
SP-ICP-MS	Single particle inductively coupled plasma mass spectrometry
STS	Sodium thiosulphate
TEM	Transmission electron microscopy
TMAH	Tetramethyl ammoniumhydroxide
TPU	Thermoplastic polyurethane
TSPP	Tetrasodium pyrophosphate
UP	Ultrapure

1 INTRODUCTION

Nanotechnology and nanoscience are novel and rapidly developing fields expected to bring new opportunities to many areas of research and technology. The disciplines deal with the study, production, modification, and application of engineered nanomaterials (NMs) having a size in the nanoscale range (ca. 1 – 100 nm). The extremely small size of these materials gives rise to exceptional physical, chemical, and biological properties different from those found in materials at a larger scale. These unique characteristics can be beneficiated in various innovative applications used in e.g., consumer products, renewable energy production, water treatment, and even smart drugs allowing highly targeted drug delivery in specific parts of the body. It is thus widely recognized that nanotechnology has the potential to bring considerable health, environmental, and financial advantages in many areas. However, the increased use of NMs and their novel and enhanced properties have raised concerns about their effects on the environment and human health.[1,2]

The risk assessment of NMs requires an in-depth understanding of their environmental behavior and toxic effects. For this purpose, sophisticated analytical techniques able to accurately characterize these materials are needed.[3,4] One of the most promising techniques for NM determination is single particle inductively coupled plasma mass spectrometry (SP-ICP-MS). The strength of the technique lies in the versatility of the analytical information that can be obtained from relatively simple measurements, including nanoparticle (NP) size, size distribution, particle concentration, and dissolved content. SP-ICP-MS combines the benefits of element-specific and sensitive detection capabilities of an ICP-MS instrument with those of particle counting techniques, thus delivering information on a particle-by-particle basis.[5,6] However, although the technique's feasibility for the analyses of NPs was demonstrated nearly two decades ago,[7] remaining challenges still need to be addressed to develop the technique further. Compared to other techniques used for NM characterization, the relatively high size limit of detection (LOD_{size}) restricts the application of SP-ICP-MS to determine samples with small NPs. In addition, coexisting dissolved analyte can increase the LOD_{size} values even further, thus preventing the detection of the

smallest NPs. These factors directly affect the accuracy of the technique and may cause a biased determination of the sample properties.[8–10]

This thesis discusses some of the remaining challenges of the SP-ICP-MS technique affecting the accuracy of NMs characterization and quantification. Then, different means to improve the accuracy of NM sizing and particle concentration determination are presented by addressing some of the remaining challenges.

2 AIMS OF THE STUDY

This study aims to deepen the knowledge of the SP-ICP-MS technique and develop strategies allowing more accurate determination of NPs' size and concentration. Accurate characterization and quantification of these materials are crucial for their commercial production and for understanding the related potential environmental and human health risks. Although SP-ICP-MS was introduced for NP determination two decades ago, the technique still needs further development. This objective included the following aspects:

- Optimizing the SP-ICP-MS instrumental parameters for gold to improve the accuracy of NP detection by decreasing the LOD_{size} values.

- Studying the interfering effect of coexisting dissolved silver (AgD) on the accuracy of Ag NPs' sizing and concentration determination.

- Evaluating the applicability of using solid phase extraction materials (SPE) for AgD removal in Ag NP dispersions and selecting the most suitable materials for different water matrices.

- Developing an effective sample pretreatment method for AgD removal in Ag NP dispersions using functional 3D printed scavengers, thus allowing a more accurate characterization and quantification of Ag NPs.

3 NANOMATERIALS

3.1 Properties and applications

Nanomaterials are usually defined as materials having a size in the 1-100 nm range[11] and can be classified either as natural or anthropogenic (man-made), depending on their origin. Although natural NMs have been an inseparable part of human history since the beginning of time, the intentional manufacturing of these materials by tuning their properties at the nanoscale is less than a century old.[12,13] Since then, the field of nanotechnology has evolved rapidly. It is recognized as potentially providing innovative solutions to challenges related to food production,[14] water treatment,[15] clean energy production,[16] and diagnosis and treatment of diseases[17].

NMs are appealing for various applications for their unique physicochemical properties, which can differ significantly from those of chemically identical bulk materials. These properties arise from the extremely small size of the materials, increasing their reactivity and affecting their optical, mechanical, and magnetic behavior.[2] These characteristics can be exploited to improve or modify the properties of other materials for specific purposes. For example, carbon nanotubes can be used to improve the energy conversion efficiency of wind turbines by developing lighter and stronger materials used in wind turbine blades[16,18] or to increase concrete's mechanical strength and durability[19]. NMs are also frequently exploited in various fields and consumer products for their antimicrobial properties, such as Ag NPs in textiles, water purification systems, and health care products.[20,21] In addition, the properties of Ag and Cu NPs, for example, can be exploited to develop antimicrobial coatings and surfaces used in public spaces, thus preventing the spread of infectious pathogens through surfaces.[22]

3.2 Risks related to NMs

With various nano-enabled products and applications already on the market, and new ones being continuously developed, NMs are clearly here to stay. However, the increased production and use of these materials will inevitably increase the risk of environmental and human exposure. Thus, for the sustainable production and use of NMs, assessing these materials' potential environmental and health risks is required.[1]

For a realistic risk assessment and regulatory development point of view, careful evaluation of both exposure and effects of NMs is needed.[23,24] In recent years, a vast amount of research has been conducted to evaluate the release of NPs from nano-enhanced products and their effects on the environment and human health.[24–29] Several studies have shown the release of NPs from various consumer products during their use, such as Ag NPs in baby products[30] and toothbrushes[31] and TiO_2 from textiles.[32] The released NPs will enter the environment and, on the other hand, serve as a direct route for human exposure (e.g., through oral ingestion or dermal contact).[25]

Once in the environment, NPs are expected to be distributed to all environmental compartments, such as air, water, and soil,[33] where they have the potential to interact with various organisms. Upon exposure, NPs can be taken up by organisms through different entry routes (such as inhalation, skin contact, and oral ingestion) and further distributed as intact particles to various organs, tissues, and cells.[34–37] Recently, Xiao *et al.*[38] reported the biomagnification of Ag NPs in the fish food web for the first time, thus posing a greater risk for higher-level predators. In addition to the effects on the exposed species, the distribution of NPs or their ionic counterparts within the organism can serve as a potential route for direct human exposure after oral ingestion. Edible plants, such as tomatoes, garden cress, and white mustard, have been shown to uptake Au[34] and Pt NPs[37] through their roots, where they were further distributed to shoots as intact particles. On the other hand, plants can also uptake dissolved ions originating from NPs, as was demonstrated for ZnO NPs.[39]

The toxicity of NPs and the underlying toxicity mechanisms have been studied extensively during previous years.[1,25,26,28,40] NPs have shown various adverse effects, such as reduced plant growth and seed germination in plants,[28,41] development of preneoplastic lesions and inflammatory responses in mammals,[42,43] and increased mortalities and development of malformations in aquatic species.[28] Recently, Bettini *et al.*[43] reported findings about a possible link between food-grade TiO_2 NPs and autoimmune diseases and even colorectal cancer in humans. The exact mechanisms causing NP toxicity are complex[40] and may be due to NPs, their dissolved species, or possibly both.[28,29,44,45] The observed toxic effects are dependent on several parameters, such as the physicochemical parameters of the NPs themselves (e.g., size, shape, and chemical composition).[40] They are also affected by conditions where toxicity studies were performed, as these may affect the properties of the NPs (such as surface[46] or concentration[35,47]).

Despite the vast amount of research already conducted, there are still many uncertainties related to the risk assessment of NMs. Most toxicity studies are performed with pristine NPs in carefully controlled laboratory environments, and in some cases, with relatively high concentrations.[40] However, NPs may undergo various transformation processes affecting their behavior and toxicity in the environment, including dissolution, agglomeration, sedimentation, and sulfidation.[27,48–50] These processes are known to be complex and affected by the physicochemical properties of the NMs and the characteristics of the surrounding environment (such as pH, presence of other compounds, and sunlight).[51–60]

3.3 NM characterization techniques

Understanding the potential risks related to NMs requires accurate characterization of these materials, for which several techniques exist. All techniques pose their strengths and limitations and differ based on the information they can provide. The choice of the technique is thus based on the desired information and is also affected by the sample type itself.[3,4,61] Considering the assessment of the environmental behavior and toxicity of NPs, careful determination of the NPs' physicochemical properties in the real exposed media is required. Knowledge of the existing environmental concentrations and the various transformational processes possibly taking place is also needed for a realistic NM risk assessment.[24,33,40,62,63] As such, often multiple techniques are needed for a more thorough characterization of NPs.

Electronic microscopy techniques, such as scanning and transmission electron microscopy (SEM and TEM), are mature and widely applied for NP detection and characterization. These techniques can visualize individual NPs and thus provide information on their size and form.[3,4,61,64] They are also often used with other techniques either to verify or complement the obtained analytical information.[65–67] However, gaining representative and statistically significant results requires imaging a vast number of NPs. As such, these techniques are not well-suited for analysis of samples with low particle concentration, which is often the case, e.g., in environmental,[27,68] toxicological,[35] and migration studies.[30,31] Sample preparation may also cause changes in original sample properties, which can lead to biased characterization.[3,4,61,64]

Light scattering techniques, such as dynamic light scattering (DLS) and nanoparticle tracking analysis (NTA), can be used to obtain information on NP size and size distribution. These techniques utilize light scattering and the Brownian motion of NPs to obtain information on the hydrodynamic diameter of the NPs. In DLS, the fluctuations in the scattering intensity are recorded as a function of time, resulting in intensity-based NP size distribution. However, as the intensity of scattered light depends on particle size, the determination of polydisperse samples with DLS is a challenge. On the other hand, NTA tracks individual particles, removing the limitations of DLS concerning sample

polydispersity and thus allowing more accurate NP sizing and even particle concentration determination.[3,4,69] However, as shown in a recent interlaboratory study on measuring the particle concentration of Au NPs, further development of the technique is still needed to improve the accuracy and reproducibility of the results.[V]

Spectrometric techniques, such as inductively coupled plasma mass and optical emission spectrometry (ICP-MS, ICP-OES) and electrothermal atomic absorption spectroscopy, are often applied for NPs determination for their element-specific and highly sensitive detection capabilities. However, these techniques alone can provide only the total concentration of the elements. They thus cannot directly be used to determine whether the analyte is present in nanoparticulate or dissolved form, or both. No information can be obtained from the other physicochemical characteristics of the NPs, such as particle size. As such, these techniques are often used in combination with other separation or fractioning methods, such as liquid chromatography (LC), field-flow fractioning (FFF), or capillary electrophoresis (CE). These techniques allow the separation of NPs based on their size, surface, or charge characteristics, making them valuable tools in NMs' characterization from complex samples.[3,4,70] They can even be used to discriminate NPs from their ionic counterparts.[71–73] Alternatively, off-line extraction methods, such as magnetic solid phase extraction (MSPE)[74–77] or cloud-point extraction (CPE),[78–80] can be applied to separate NPs from their ionic species and sample matrix, followed by determination with spectrometric methods.

In addition to the various techniques discussed above, SP-ICP-MS is considered a powerful technique for the determination of NPs, which is discussed in more detail in the following Chapter 4.

4 SP-ICP-MS

4.1 Fundamentals

SP-ICP-MS has become a relevant technique for determining NPs over the years. The strength of the technique lies in the diversity of the analytical information obtained within a single run, including NP size, size distribution, particle concentration, and dissolved content at environmentally relevant concentrations.[5,6] Degueldre *et al.* first demonstrated the feasibility of SP-ICP-MS for the analysis of colloidal suspensions in a series of papers[7,81–84] almost two decades ago. Since then, the applicability of the technique for the detection, characterization, and quantification of NPs has been demonstrated in various matrices, such as environmental and biological samples and cosmetics.[9,10]

The detection of individual NPs in SP-ICP-MS is based on operating the ICP-MS instrument as a particle-counting technique, thus being able to deliver information on a particle-by-particle basis. In SP-ICP-MS, a sample solution is introduced in plasma as a fine aerosol, resulting in an analyte element's vaporization, atomization, and ionization. The intensity of the generated ions is then recorded at a given mass/charge ratio using very short dwell times (e.g., 1 ms or less) and plotted individually as a function of time, resulting in thousands of intensity readings. The detection of individual NPs is based on separating the intensities originating from NPs over a constant background signal caused by the coexisting dissolved element and instrumental noise. As the dissolved element is distributed evenly in the aerosol droplets, the mass of the element entering to plasma and finally being detected as ions will be rather stable, thus producing a relatively stable intensity signal. However, if the sample solution also contains NPs, the analyte atoms will no longer be homogenously dispersed but instead concentrated in discrete particles, arriving randomly in plasma. The ionization of a single NP in plasma will generate a burst of ions traveling to the detector as a

pack of ions, producing a spike in intensity, clearly separating from the background.[5,6]

An example of raw data obtained with SP-ICP-MS is shown in **Fig. 1**, which is further processed to differentiate the NP events from the background signal by applying a specific threshold limit. Different means exist to obtain this value, such as visually inspecting the intensity distribution histograms[85] or applying mathematical algorithms.[68,86] Typically, the threshold value is, however, calculated based on the mean and standard deviation (σ) of the background signal using an iterative "mean+nσ" calculation, where n is the applied coefficient (generally 3 or 5).[5,87] After extracting all NP events, the remaining data set represents the background signal, which can be used to obtain the dissolved analyte concentration using an external calibration.[6]

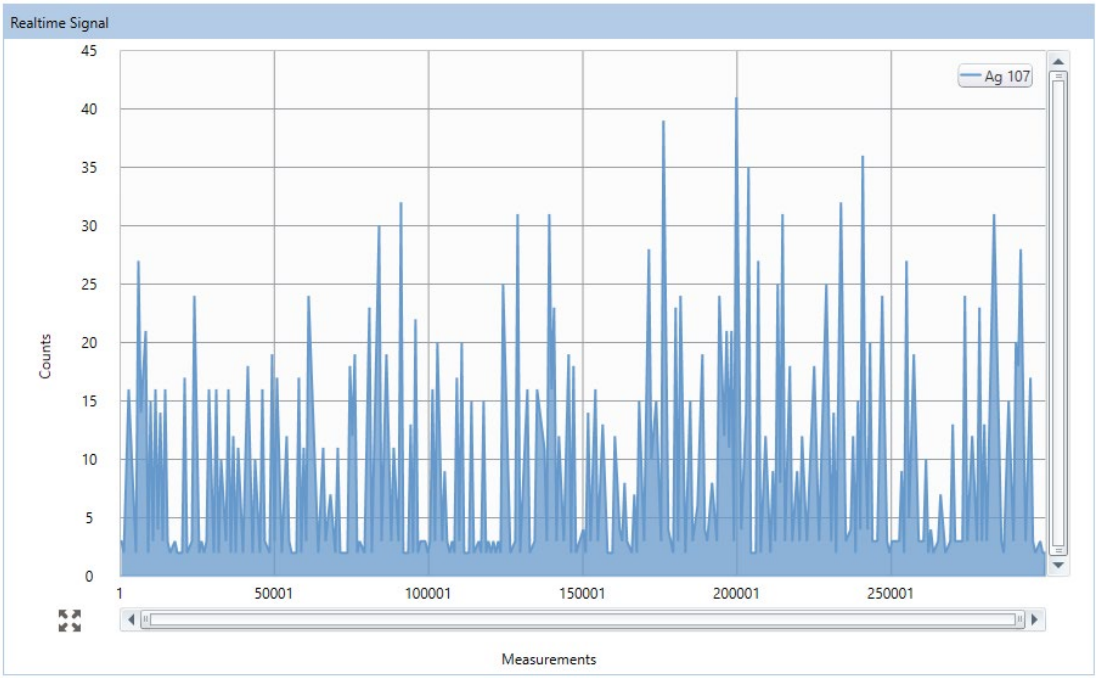

FIGURE 1 An example of SP-ICP-MS raw data obtained for a dispersion containing 50 nm Ag NPs (ca. 30000 part. g^{-1}) and AgD (1.0 µg kg^{-1}). The numerous signals above the continuous background signal originate from individual NPs. Measurement time 30 s, dwell time 100 µs.

The basic principle of SP-ICP-MS is that NP dispersions introduced in plasma should be sufficiently diluted to ensure the arrival of individual NPs in plasma one by one. If true, each observed NP event should represent a single particle. As such, the number of observed pulses (N_{NP}) in a given acquisition time (t, minutes) is related to particle concentration (C_p, particles g^{-1}) according to Eq. 1, where Q_{sam} is the sample flow rate (g min^{-1}) and η_n is the transport efficiency (%):[5]

$$C_p = \frac{N_{NP}}{Q_{sam} \cdot t \cdot \eta_n} \quad (1)$$

The η_n in Eq. 1 defines the ratio of analyte in plasma to that of the aspirated sample. Although several methods can be used to obtain this value,[8,88] the most often used is the particle frequency method described by Pace *et al.*,[5] which utilizes well-characterized NP reference standards with a known particle concentration according to Eq. 2:

$$\eta_n = \frac{N_{NP}}{Q_{sam} \cdot t \cdot C_p} \cdot 100\% \quad (2)$$

The intensity of the detected NP events is directly related to particle mass, which can be converted to particle size, assuming that additional information on the NP shape and density is available. The most straightforward way to obtain the particle mass of unknown samples is to calibrate the instrument with NP standards with known mass or size. The mass of the particles (m_p, ng) can then be obtained directly from the calibration curve and further converted to particle size (d, nm) assuming a spherical geometry using Eq. 3, where ρ is the particle density (g cm^{-1}):[5]

$$d = \sqrt[3]{\frac{m_p \cdot 6}{\rho \cdot \pi \cdot 10^{-12}}} \quad (3)$$

However, well-characterized NP standards are not available for all elements, limiting the use of this approach for NP sizing. In these cases, particle size can be obtained by using dissolved standards for calibration. The analyte mass per event (W, µg/event) needs to be calculated according to Eq. 4 to relate the obtained intensity to elemental mass, where t_{dt} is dwell time (min/event), and C is the standard concentration (µg g^{-1}):[5]

$$W = \eta_n \cdot Q_{sam} \cdot t_{dt} \cdot C \quad (4)$$

4.2 Applications

Since its first introduction at the beginning of 2000, SP-ICP-MS has evolved as a valuable tool in NMs analysis. During these two decades, the technique has been applied not only to determine pristine NPs' properties as such but also in various studies concerning their release, behavior, fate, and toxic effects. These studies, together with some excellent review articles,[3,8–10,89] have raised our understanding of the behavior and effects of NPs and the various possibilities and the existing limitations of the SP-ICP-MS technique.

Some studies regarding the analysis of NMs from various matrices are presented in **Table 1**. In ideal cases, samples can be analyzed with SP-ICP-MS directly or after a simple sample dilution. Although this might be sufficient for some sample types (such as NP standard suspensions or aqueous samples), additional sample preparation is often needed for more complicated sample matrices and solid samples. These may include, e.g., alkaline or enzymatic digestion of biological or environmental samples (such as tissues, organs, or soil samples), liquid- or solid-phase extraction, or separation of the matrix components. However, these might alter the original NP properties of the sample by, e.g., causing changes in NP size or concentration.[3,9,89] For example, a commonly employed sample preparation step—filtration—has been frequently shown to cause significant NP losses.[90–93] As such, independent of the applied sample treatment method, its effect on the original NP properties should be carefully estimated to avoid changes in sample properties, which could lead to biased determination.

TABLE 1 Examples of the existing applications of SP-ICP-MS for the analysis of NMs.

Sample type	NP analyzed	Sample preparation	Reference
Consumer products			
Toothbrushes	Ag	Extraction in tap water	31
Food containers and baby products	Ag	Food containers: Extraction in ultrapure water, 3% acetic acid, and 10% ethanol; Baby products: Extraction in artificial saliva	30
Textiles	TiO_2	Extraction in ultrapure water	32
Environmental samples			
River water	Ag	CPE using Triton X-114	94
Wastewater	Ag, TiO_2	Dilution	95
Tap, river, and wastewater	Ag	MSPE	96
Soil extracts, standard suspensions of Au and Ag	Ag, Au	Soil extracts: Alkaline extraction using TSPP[1]; Standard suspensions: Dilution	97
Biological samples			
Human breast cancer cells	Au	Alkaline digestion with TMAH[2]	98
Tomato (shoots)	Au	Enzymatic digestion with macerozyme R-10	34
Chicken (liver and yolk)	Ag	Enzymatic digestion with proteinase K	36
Zebrafish (liver, gill, intestine)	Ag, Au	Alkaline digestion with TMAH[2]	35

[1] Tetrasodium pyrophosphate
[2] Tetramethyl ammoniumhydroxide

4.3 Remaining challenges

The results obtained with SP-ICP-MS have been extensively compared to those obtained with other available techniques for NM characterization over the years, showing similar or better accuracy in particle sizing.[65,67,99–101] However, as shown in interlaboratory studies on Au NP sizing[102] and particle concentration determination,[V] further development is still required to improve the overall quality of the results. This is especially the case for the smaller NPs (e.g., ≤30 nm), which determination is more challenging compared to larger ones.[102] Some key factors affecting the accuracy of the results are discussed in the following paragraphs.

4.3.1 The effect of instrument sensitivity

Although SP-ICP-MS can detect NPs at extremely low concentrations (e.g., 100-1000 particles mL^{-1}),[87,103] the LOD_{size} values for most elements are currently ≥10 nm and even higher for oxides (e.g., 25-130 nm for TiO_2).[10,87,104] As such, the accurate determination of samples with small NPs (e.g., <30 nm for Ag NPs in environmental samples)[68,105,106] is currently a challenge for SP-ICP-MS. In these cases, the high LOD_{size} can prevent the detection of NPs entirely or lead to only a partial capture of the NP size distribution. This would result in an overestimation of the particle mean size and an underestimation of the particle concentration and, thus, biased determination.[9,1] As such, improving the LOD_{size} values is one of the most important aspects in developing the SP-ICP-MS technique.

The smallest detectable particle size in SP-ICP-MS is defined as the smallest NP signal intensity that can be separated from the background signal and depends on the detection efficiency of the instrument.[87,107] Regarding lowering the LOD_{size} values, instrument sensitivity should thus be increased, which can be achieved by carefully optimizing the instrumental conditions. Once NPs are introduced in plasma, solvent evaporation, analyte atomization, and ionization begins. As a result, spherical analyte ion clouds are formed, which diameter will increase due to diffusion as they progress downstream the plasma until they are finally sampled at the sampler orifice. The size of the ion clouds at the sampling point (i.e., at the sampler orifice) directly determines the number of detected analyte ions and, as such, should be maintained as compact as possible for improved detection efficiency of ICP-MS. Simultaneously, efficient ionization of the NPs should be achieved.[108–110]

The instrumental parameters used affect the analyte ionization degree and diffusion losses. Plasma RF-power affects the plasma temperature and, as such, should generally be maintained as high as possible to ensure efficient ionization. However, the obtained signal intensity is also shown to depend on the relative distance between the beginning of analyte atomization and the ion sampling position. This is known to be affected by both the sampling depth position and the nebulizer gas flow rate, which influence analyte residence time in plasma. If the distance is too large, diffusion losses will be significant, resulting in a decrease in the signal intensity. On the other hand, shifting the atomization downstream plasma by either increasing the nebulizer gas flow value or decreasing the sampling depth position may decrease the ionization degree, especially for larger particles.[108–110]

4.3.2 Dissolved analyte interference

The obtained raw intensities in SP-ICP-MS contain contributions from individual NP events and the background signal caused by instrumental noise and dissolved analyte. The discrimination between the signals originating from the analyte, either in dissolved or NP form, is performed by applying a certain threshold value, typically determined using an iterative "mean+3σ" calculation.

The threshold thus divides the observed intensities into two groups: those originating from individual NPs (intensities>threshold) and those calculated as dissolved analyte (intensities<threshold). In ideal cases, the background signal contribution is low, thus allowing the calculation of the threshold solely based on instrumental noise alone.[5,6] In the cases of real samples, however, samples may contain elevated concentrations of dissolved analyte. This is often the case with, e.g., environmental or toxicological samples or samples containing easily soluble NPs (such as ZnO). In these cases, the coexisting dissolved analyte increases the background signal and, thus, can severely interfere with the detection of NP events by increasing the LOD_{size} values.[68,97,111–113] This phenomenon is known as dissolved analyte interference.

The increased size limit of detection caused by coexisting dissolved analyte may lead to only partial capture of the NP size distribution and, thus, biased determination of NPs' size and concentration. Recently, we demonstrated that even relatively low concentrations of coexisting AgD (≥0.1 µg kg^{-1}) could interfere, especially with the detection of small 30 nm Ag NPs, leading to a severe underestimation of particle concentration (up to -93%) and overestimation of particle size (up to +80%).[II, III]

From a realistic risk assessment point of view, accurate characterization and quantification of NPs is essential, as the behavior and effects of NPs are known to be size- and concentration-dependent.[40] As such, the interfering effect of dissolved analyte in SP-ICP-MS can be considered one the most important remaining challenges to solve.

4.3.3 Other factors affecting the quality of results

In addition to the factors discussed in the previous sections, the accuracy of SP-ICP-MS results is also affected by other factors. Some of the remaining challenges to be addressed are briefly discussed here.

In addition to sample preparation (**Table 1**), the effect of the sample matrix should also be considered in the analysis stage, as differences between sample and calibration standard matrices may induce matrix effects. These may cause either signal enhancement or suppression, thus leading to over- or underestimation of the analyte content.[85,114] Sodium, for example, is a commonly known element causing matrix effects, which was previously[I] shown to cause up to a 50% decrease in the intensity of Au compared to ultrapure water.

Most SP-ICP-MS measurements use a conventional sample introduction system consisting of a pneumatic nebulizer and a spray chamber. With these systems, only a small portion of the aspirated sample reaches the plasma (generally ≤15%), while the majority is transported to waste.[115] Knowing this value (i.e., transport efficiency) is essential for obtaining reliable results. The value directly affects the accuracy of particle concentration determination and particle sizing if dissolved standards are used for calibration (Eqs. 1 and 4, respectively).[8] Any underestimation of this value would lead to an underestimation of particle size and an overestimation of particle concentration.[116] Although different methods can be used to determine this value

experimentally, they have often been shown to give differing results.[5,99,116] Despite the vast amount of discussion on the matter, there is still no general agreement on which method should be preferred. To complicate the issue even further, the transport of NPs in the sample introduction system might also depend on NP size[68,99] or surface[68,116] and be affected by the sample matrix as well.[8,85,II] As such, the transport of NPs in samples and standards might differ, leading to biased results.

Proper calibration of the instrument is essential for obtaining accurate results. The simplest way to obtain the particle size of unknown samples is to calibrate the instrument with NP standards with an accurately known mass or size. However, as discussed in paragraph 4.1, this availability is restricted to only some elements (mainly Au, Ag, and Pt). In addition, these are often not sufficiently well characterized. Instead, the particle size information provided by the supplier is typically based on the measurement of a very limited number of particles (≤100), which is insufficient for reliable determination. Further verification of the NP standards is often required in the laboratory before use. Often, deviation from the information provided by the supplier is found.[65,99,117,II] For example, we observed up to a 9% difference in NP size and a 22% difference in mass concentration for the commercial Ag and Au NPs used in this study (see paragraph 6.3).

Given the scarce commercial NP standards for most elements, calibration is often performed using dissolved standards. However, this approach requires the determination of an element mass entering plasma in a given dwell time (Eq. 4), for which the transport efficiency needs to be accurately known. In addition, ICP-MS responses for the analyte, either in dissolved or NP form, should be identical. However, this might not always be the case. Whereas acids are often added to dissolved standards to increase their stability, NP dispersions are often prepared in water, leading to possible matrix interferences.[8]

Considering the discussion above, well-characterized certified reference materials, such as those provided by the National Institute of Standards and Technology (NIST), could help to solve some of the remaining challenges of SP-ICP-MS analyses. Such standard materials with carefully determined NP size and concentration values are urgently needed for method development, validation, and quality control purposes. However, the availability of these materials is scarce and limited to pristine NPs of just a few elements, while no matrix reference materials currently exist. In addition, currently, no reference materials with certified values for particle concentration are available, which would be crucial for accurate particle concentration determination.[V]

5 IMPROVING THE ACCURACY OF SP-ICP-MS ANALYSES

5.1 Sensitivity improvement by instrumental parameter optimization

Instrument sensitivity and LOD_{size} values can be improved by carefully optimizing the instrumental parameters. Even though the importance of instrumental parameter optimization is well-recognized in solution ICP-MS,[118,119] only a few studies exist on the effect of instrumental conditions in SP-ICP-MS. Ho *et al.*[120] focused on studying the effect of sampling depth value on the intensity of Au and Zr in dissolved or NP form. Similar optimal sampling depth values were obtained both for dissolved gold and relatively small Au NPs (≤150 nm). However, due to the longer vaporization time required, the larger 250 nm Au and 80 nm ZrO_2 NPs' optimum sampling depth shifted to larger values than the dissolved analyte. Kalomista *et al.*[121] optimized the sampling depth value for measuring Au and Ag NPs. The ion signal was significantly enhanced at the optimal sampling depth value of 4 mm, which translated into a 25-30% reduction in the LOD_{size} values. As such, significant improvement in the ion signal can be achieved by optimization of sampling depth. However, as the effect of instrumental parameters is clearly dependent on each other in a complex way,[108,109] to obtain truly optimal conditions, the interaction effect between the parameters should be considered. This can be achieved by using a design of experiments (DoE) approach, which is a systematic approach used for planning and performing experiments to obtain valid and objective conclusions. Instead of changing the parameter (i.e., factor) value one at a time and monitoring the response, the values of all factors are varied simultaneously, allowing the assessment of potential interaction effects between the variables.[122,123]

Among DoE approaches, response surface methodology (RSM) is one of the most relevant multivariate techniques used in analytical optimization. It involves

statistical and mathematical techniques based on the fit of a polynomial equation to the obtained experimental data, allowing the prediction of the response at any point in the experimental field. In addition, a graphical presentation of the response in accordance with the factors can be obtained, which allows a careful evaluation of the factors' effects on the response.[124]

Utilizing RSM methodology first requires identifying the independent variables (i.e., factors) that significantly affect the response. After selecting the factors for the experiment, the maximum and minimum values define the experimental region to be studied. The experiments then take place according to the selected experimental design, which defines the specific set of experiments to be performed. A second-order model, such as a general or three-level factorial design, is used if the response is expected to present any curvature. After that, a polynomial equation is fitted to the experimental data, which relates the obtained response to the factors. The generalized second-order model equation can be expressed as follows (Eq. 5):

$$y = \beta_0 + \sum_{i=1}^{k} \beta_i x_i + \sum_{i=1}^{k} \beta_{ii} {x_i}^2 + \sum_{1 \le i \le j}^{k} \beta_{ij} x_i x_j + \varepsilon \qquad (5)$$

where y is the response, k is the number of variables, x represents the variables, β_0 is the constant term, β_i is the coefficient of the linear parameter, β_{ii} is the coefficient of the quadratic parameter, β_{ij} is the coefficient of the interaction parameters, and ε is the observed error in the response.[124]

The model's ability to describe the experimental results (i.e., the quality of the model) is then evaluated using statistical methods. Finally, the optimum values for each factor can be solved and further verified by the experimental results.[124]

5.2 Improving accuracy by dissolved element removal

Detecting NP events is challenging in SP-ICP-MS in the presence of a high background signal. The following chapters discuss different means to improve the accuracy of NPs' detection and determination in the presence of an elevated background signal.

5.2.1 The effect of data acquisition parameters and data processing

The dwell time used is an important parameter to consider for detecting NP events, especially in the presence of a high background signal. Although modern instruments allow using dwell times down to 10 µs, values in the millisecond range (e.g., 2-10 ms) are still frequently applied.[10] As NPs are ionized in plasma, they will generate an ion signal with a ca. 400-500 µs duration.[125] As such, depending on the dwell time used, NP events can be recorded either as one-

reading signals, i.e., as spikes (with dwell time in the millisecond range) or as transient signals (with dwell time in the microsecond range, ≤200 µs). In the former case, a relatively large contribution of the signal intensity comes from the background signal, thus limiting the smallest detectable NP size. As the intensity of the background signal is affected by the dwell time used and the intensity of the NP spike is not, using shorter dwell times will allow smaller NPs to be detected.[87]

Compared to millisecond dwell times, using shorter dwell times in the microsecond range available in modern instruments has improved the detection of the smaller NPs. As dwell times shorter than the ion signal duration are used, the background signal contribution is split between different dwells. Thus, the only contribution of the background signal to the NP event comes from beneath the NP signals.[87] When using high data-acquisition frequencies, the accuracy of NP event identification in the presence of a high background signal can be improved further by using more sophisticated data processing methods to separate NP events from the baseline. Cornelis and Hassellöv[126] demonstrated a deconvolution method using Polygaussian probability mass functions for improved separation of the NP signals in the presence of high dissolved analyte levels. Mozhayeva *et al.*[127] suggested using a data processing method based on Poisson statistics to determine threshold values used for identifying NP events. However, these data processing methods are currently unavailable in commercial software, thus requiring laborious manual data processing.

5.2.2 Sample dilution

As the background signal's magnitude depends on the dissolved analyte concentration,[6] sample dilution is by far the simplest alternative for minimizing the dissolved analyte interference. Ideally, samples should be diluted to reduce the dissolved concentration near or below the method detection limit (MDL), as even low concentrations of dissolved analyte can interfere with the detection of the smallest NP events (e.g., ≥0.1 µg L^{-1} for 30 nm Ag NPs[II,III]). Schwertfeger *et al.*[97] proposed a simple method for reducing the interfering effect of the dissolved analyte, which is based on a serial dilution of the samples. At first, samples are diluted only if necessary to capture dissolved concentration in the calibration range. After this, particle concentration is determined from "optimally diluted" samples, where the dissolved analyte concentration is reduced to <MDL. A second dilution is then performed to verify the obtained results by further diluting the samples 2-fold.

However, although sample dilution offers a simple and effective means for eliminating dissolved analyte interference, it suffers from some drawbacks. First, sample dilution also affects the sample's particle concentration and, thus, may prove problematic for environmental samples with low particle concentration (e.g., <10 ng L^{-1} Ag NPs in surface waters[105,106,128]). Although sampling times may be extended to capture sufficient NP events for statistically significant determination,[97,IV] total analysis time can increase significantly.[IV] Second, sample

dilution may increase the risk of NP instability in highly diluted suspensions, leading to biased results.[129–131]

5.2.3 Extraction methods

Solid-phase and liquid-liquid extraction (LLE) are mature and routinely used sample preparation techniques, utilizing the different partitioning of analyte species between two phases.[132] Both techniques can be applied for analyte preconcentration or separating sample constituents before analysis. In recent years, these techniques have also been applied to analyze NPs from various matrices using the SP-ICP-MS technique. Considering SP-ICP-MS analysis, the main purpose of these techniques has been the discrimination of NPs from their ionic counterparts while preserving the original NP properties.

LLE methods, such as CPE, utilize analyte partitioning between two immiscible phases. Several authors have demonstrated the applicability of CPE in determining Ag and Au NPs with the SP-ICP-MS technique over the years.[78,94,133,134] In CPE, a non-ionic surfactant (such as Triton X-114) is added to an aqueous sample solution over the critical micellar concentration. Heating the mixture above the cloud point temperature allows the formation of hydrophobic surfactant micelles, which can capture NPs from the sample matrix and thus allow the separation of NPs from their ionic counterparts. Separation of the two phases can then be achieved simply by decanting or centrifugation.[78] As CPE allows the preconcentration of NPs in a small volume, it can be seen as highly beneficial in analyzing, e.g., environmental samples with low particle concentration. However, the technique still requires additional development, as the NP extraction efficiency is shown to be affected by particle surface and other compounds present. As reported by Hadri *et al.*,[134] low extraction efficiencies (<30%) were obtained for PVP-stabilized NPs and in the presence of humic substances. In addition, some dissolved analyte can still be coextracted with NPs into the surfactant-rich phase, thus leading to only partial elimination of the background signal.[78]

Compared to LLE, SPE offers some significant benefits, such as the wide range and availability of materials. Numerous papers[96,112,113,135,136,II] have demonstrated the applicability of SPE materials for separating NPs and their ionic counterparts, followed by determination with SP-ICP-MS. In these studies, the main purpose has been the removal of the dissolved analyte, thus allowing more accurate NP determination. Luo *et al.*[96] applied in-lab synthesized magnetic sorbent for adsorbing ionic silver in environmental waters. The sorbent containing the silver ions could then be easily recovered by an external magnet, allowing more accurate sizing of Ag NPs. However, as the method resulted in only partial removal of dissolved ions (81-98%) and some Ag NPs (<30%) were coextracted, additional development is needed.

Among the commercially available SPE materials, "Chelex 100" has been frequently applied in analyzing Ag,[113,135,II] ZnO,[111,112] and La_2O_3[136] NPs for removing the dissolved element in various matrices. For example, Hadioui *et al.*[113] demonstrated the first online coupling of Chelex 100 resin with SP-ICP-MS,

allowing efficient removal of AgD and, thus, more accurately determinating Ag NP size. However, total analysis time can be increased considerably for the lengthy washing and regeneration steps needed to ensure the resin's proper functioning.[113,135] Recently, we presented a simple sample pretreatment method for the efficient removal of AgD in Ag NP dispersions based on the utilization of SPE materials.[II] Compared with the existing online systems, the proposed off-line procedure maximized samples throughput in ICP-MS by omitting the laborious washing and regeneration steps used in online systems.

5.2.4 3D printing

During the past decades, 3D printing or additive manufacturing has gained great interest in a wide range of applications in different fields. 3D printing allows the fabrication of three-dimensional objects based on a pre-designed model, thus serving as a means to produce custom-specified items with relative ease. The advances made in the field over the years have increased the performance of 3D printers and the range of compatible materials, which has led to developing numerous innovative applications. 3D printing has already been beneficiated in, e.g., bioprinting of tissues and organs, fabrication of optical lenses, or even metallic components.[109,137–139]

With the increasing interest and development in the field, the 3D technique is expected to bring many benefits to analytical chemistry. For its ability to produce complex objects with high precision, 3D printing has been used, e.g., for improving chromatographic efficiency by preparing innovative non-linear columns (e.g., spiral, serpentine) or bed materials, and for preparing low-cost parts used e.g., in spectroscopic instruments.[137] In addition to fabricating custom labware and complex items, 3D printing can be beneficiated in preparing objects with actual functionalities. This has enabled the development of many innovative solutions for preparing catalysts[140,141] and extracting and preconcentrating elements. For example, Kulomäki *et al.*[142,143] developed a method for efficiently preconcentrating mercury using 3D printed scavengers, thus allowing its accurate quantification in natural waters. 3D printed scavengers can also be used to remove pharmaceuticals from wastewater, as demonstrated by Frimodig *et al.*[144]

Despite its potential, utilizing 3D printing in NMs' determination is still rare. Su *et. al.*[145] used 3D printed knotted reactors to differentiate ionic silver and Ag NPs from wastewater samples by carefully adjusting the sample acidity. It was shown that selectively extracting AgD is achieved at pH 12, whereas both analyte forms can be retained at pH 11. The retained AgD and Ag NPs were then detached with 1% HNO_3, followed by the quantification of total silver concentration with ICP-MS. The concentration of Ag NPs was then calculated as Ag_{total}-$Ag_{dissolved}$. However, no information can be obtained from NP size using this method.

Despite its scarce beneficiation in SP-ICP-MS analyses, 3D printing has much to offer. We recently demonstrated a novel sample pretreatment procedure for efficiently removing AgD in Ag NP dispersions using functional 3D printed

scavengers.[III] Selective laser sintering (SLS) enabled the incorporation of SPE material into highly porous 3D printed scavengers, which allowed rapid and highly efficient AgD removal while preserving the original properties of Ag NPs.

6 EXPERIMENTAL

6.1 SP-ICP-MS measurements

The SP-ICP-MS measurements of silver and gold were performed with a NexION 350D ICP-MS operating in a time-resolved analysis mode (**Table 2**). The instrument's general performance was checked daily before the measurements using a multielement tuning solution and adjusted if found necessary. Raw data were processed using a commercial Syngistix Nano Application Module (v. 2.5) software, which automatically separates NP events from the baseline (dissolved) signal by applying a threshold value determined with an iterative "mean+3σ" calculation.[146] All measurements performed for papers II and III were carried out using an ESI 4DX autosampler, whereas a manual sample introduction was used for paper I.

TABLE 2 Instrumental parameters used for the SP-ICP-MS measurements of gold and silver.

Parameter	Gold (Au)	Silver (Ag)
ICP RF-power (W)	1200–1600	1600
Nebulizer gas flow (L min^{-1})	0.90–1.06	0.92–0.95
Plasma gas flow rate (L min^{-1})	18	18
Auxiliary gas flow rate (L min^{-1})	1.2	1.2
Spray chamber	Baffled Cyclonic, Glass (cooled to 2 °C)	Baffled Cyclonic, Glass (cooled to 2 °C)
Nebulizer	ESI PFA Concentric	ESI PFA Concentric
Injector	1.8 mm i.d. Sapphire	1.8 mm i.d. Sapphire
Sampling depth (mm)	9–12	11
Dwell time	100 µs	100 µs
Sampling time (s)	30–60	30–120
Transport efficiency (%)	7.48–7.53	6.1–8.7
Sample uptake rate (g min^{-1})	0.284–0.291	0.263–0.314
Isotope monitored	^{197}Au	^{107}Ag
Density (g mL^{-1})	19.3	10.49

All aqueous solutions used in this study were prepared using ultrapure (UP) water with a resistivity of 18.2 MΩ·cm. The sample uptake rate (Q_{sam}, g min^{-1}) was determined daily, at least in duplicate, by quantifying the uptake rate of water after 3 min of aspiration and regularly monitored during measurements. Transport efficiency (η_n) was determined daily according to Eq. 2 at least in triplicate using the particle frequency method presented by Pace *et al.*[5] Dispersions containing ca. 10^5 particles g^{-1} of 50 and 100 nm PEG-COOH-stabilized Au NPs in UP water designed for SP-ICP-MS calibration were used for their stability.

AgD calibration standards (0.1-2 µg kg^{-1}) were prepared from a standard stock solution of silver by dilution with a 0.5 mM solution of sodium thiosulfate (STS). 40, 50, and 80 nm citrate-stabilized Ag NPs were used for the particle calibration of silver. Before measurements, the matrix of all sample and calibration standard solutions was adjusted to 0.5 mM STS to minimize any matrix differences.

The particle calibration of gold was performed using 30, 50, and 80 nm PEG-COOH-stabilized Au NPs, which were diluted to a particle concentration of approximately 10^5 part. g^{-1} before use.

All solutions used in this study were diluted gravimetrically using new high-density polyethylene bottles and polypropylene (PP) centrifuge tubes. All samples and calibration standards used in the experiments were diluted daily right before the measurements.

6.2 ICP-MS measurements

Some of the gold and silver measurements were performed using a NexION 350D ICP-MS operating in solution (standard) mode (**Table 3**). Calibration standards of silver ranging from 1 to 100 µg kg^{-1} were prepared from a standard stock solution of silver by dilution with a thiourea solution (0.1% thiourea (w/v), 2.25% HCl (v/v) and 0.75% HNO_3 (v/v)). The calibration standards of gold (0.1-5 µg kg^{-1}) were diluted from a stock solution of gold with a solution composed of 2.25% HCl (v/v) and 0.75% HNO_3 (v/v).

TABLE 3 Instrumental parameters used for ICP-MS measurements of gold and silver.

Parameter	Gold (Au)	Silver (Ag)
ICP RF-power (W)	1200–1600	1600
Nebulizer gas flow (L min^{-1})	0.90–1.06	0.93–0.94
Plasma gas flow rate (L min^{-1})	18	18
Auxiliary gas flow rate (L min^{-1})	1.2	1.2
Spray chamber	Baffled Cyclonic, Glass (cooled to 2 °C)	Baffled Cyclonic, Glass (cooled to 2 °C)
Nebulizer	ESI PFA Concentric	ESI PFA Concentric
Injector	1.8 mm i.d. Sapphire	1.8 mm i.d. Sapphire
Sampling depth (mm)	9–12	11
Dwell time	50 ms	50 ms
Readings/sample	3	3
Isotope monitored	^{197}Au	^{107}Ag
Internal standard [1]	^{195}Pt	^{102}Ru

[1] Not used in the optimization measurements of gold

6.3 Verification measurements of the commercial NP dispersions

The particle concentrations and diameters of the commercial Au and Ag NP standard dispersions used in this study were verified in the laboratory before use (**Table 4**), as deviations from the information provided by the supplier have been previously reported.[65,99,117] The mass concentration (mg L^{-1}) of the commercial NP dispersions was determined with ICP-MS from acid-digested (aqua regia) samples at least in duplicate. The citrate-stabilized Au and Ag NPs' particle size was performed using TEM. ≥250 particles were considered for the calculation of average particle diameters. However, the TEM's rather high detection limit was found inadequate for verifying the PEG-COOH stabilized Au NPs for the low particle concentration of the dispersions (ca. 10^7 part. mL^{-1}). The particle size of these NPs was thus determined with SP-ICP-MS by using 30 and 50 nm citrate-stabilized Au NPs as a reference.

The mean particle sizes of the commercial NP standards were found to differ <10% from the values provided by the supplier (**Table 4**) and were used throughout the study. Although the mass concentration of the NP dispersions was generally found to be in good agreement (<10% different) with the values provided by the supplier, significantly lower (up to 21.5%) values were obtained for the 50 and 100 nm PEG-COOH stabilized Au NPs. The in-lab verified mass concentration values of the Au and Ag NP standards were used to calculate the particle concentration values (part. g^{-1}) used in papers II and III.

TABLE 4 Verification measurements of the commercial NP dispersions.

	Particle diameter (nm), mean ± standard deviation (1s)			**Mass concentration (mg L^{-1})**		
Particle[1]	Supplier	Measured	Difference (%)	Supplier	Measured	Difference (%)
20 nm Au NP (Citrate), NC	18.2±2.1	18.9±1.9	3.6	51	56	+9.3
30 nm Au NP (Citrate), NC	30±3	30±3	-1.5	52.5	51.9	-1.2
30 nm Au NP (PEG-COOH), PE	27.1±1.1	27.1±0.1	-0.1	0.002	0.002	+3.8
50 nm Au NP (PEG-COOH), PE	49.6±2.1	50.6±0.2	+2.0	0.0124	0.0100	-19.1
50 nm Au NP (Citrate), NC	52±5	53±7	+1.1	52	52	-0.1
100 nm Au NP (PEG-COOH), PE	99.4±3.0	96.4±0.3	-3.0	0.0993	0.0779	-21.5
30 nm Ag NP (Citrate), NC	29±3	28±4	-4.3	21	19	-8.1
40 nm Ag NP (Citrate), NC	41±5	45±5	+8.6	21	19	-7.5
50 nm Ag NP (Citrate), NC	52±6	51±6	-1.5	21	19	-9.1
80 nm Ag NP (Citrate), NC	77±9	83±11	+8.4	21	21	+0.8

[1] Supplier is given as follows: NC=NanoComposix (particle size determined with TEM), PE=PerkinElmer (particle size determined with SP-ICP-MS)

6.4 Optimization of SP-ICP-MS' instrumental parameters for gold

A DoE approach was used to optimize instrumental parameters for both dissolved and NP gold. For the experiments, solutions containing 1 μg kg^{-1} of dissolved gold and 50 nm PEG-COOH stabilized Au NPs (ca. 10^5 part. g^{-1}) were prepared in UP water. A general factorial design approach was used for designing the experiments for its ability to describe in detail the changes in the response variable in accordance with the studied variables. Nebulizer gas flow (A), plasma power (B), and sampling depth (C) were chosen as the independent variables (i.e., factors), whereas gold intensity was the response variable measured. The factors and their levels used in the experiments are presented in **Table 5**. Minitab 19 software was used to analyze the experimental data and generate the surface plots.

TABLE 5 The factors and their levels used in the experiments.[I]

	Variables		
Levels	Plasma RF-power (W)	Sampling depth (mm)	Nebulizer gas flow (L min-1)
1	1200	9.0	0.90
2	1400	10.5	0.92
3	1600	12.0	0.94
4			0.96
5			0.98
6			1.00
7			1.02
8			1.04
9			1.06

Results obtained for 20 and 30 nm Au NPs using robust and optimal conditions were compared to study the effect of instrumental parameters' optimization on the accuracy of Au NP determination. For the robust settings, the ICP-MS instrument was tuned according to the instrument software's tuning protocols (i.e., maximum sensitivity with minimal interferences). For the measurements performed under optimal conditions, optimized instrumental parameters were used with the nebulizer gas flow adjusted to gain maximum $^{197}Au^+$ intensity.

6.5 Characterization of the water samples

This study used several water samples (UP, synthetic, waste, and environmental waters) with different physicochemical properties obtained from different locations in Southern Ostrobothnia and Central Finland. The concentration of

silver (both NP and AgD) in the water samples was quantified with SP-ICP-MS. The other major and minor elements were determined with ICP-OES. A more thorough characterization of the physicochemical properties was performed for the water samples used in paper II, of which more details can be found therein.

6.6 Application of SPE materials for AgD removal

6.6.1 Investigating the AgD interference

To investigate the effect of coexisting AgD on Ag NPs' determination, dispersions containing 30, 40, 50, or 80 nm Ag NPs (ca. 10^5 part. g^{-1}) were spiked with increasing amounts of AgD (0-1 μg kg^{-1}). All samples were prepared in triplicate and measured with SP-ICP-MS. To evaluate the interfering effect of AgD, particle mean size (d) and concentration (C_p) values obtained for samples spiked with AgD were compared to those obtained at a AgD concentration of 0 μg kg^{-1}.

6.6.2 Extraction experiments using SPE materials

Various commercially available SPE materials were evaluated for AgD removal in Ag NP dispersions. Details of the SPE materials used in the experiments can be found in paper II (in Table 2). Before use, all SPE materials were pretreated to remove the finest particles, which could block the ICP-MS instrument's sample introduction system. Some SPE materials were further converted to their sodium (Na^+) form to minimize pH changes in the sample solution during the separation process.

The applicability of the SPE materials for AgD removal in Ag NP dispersions was evaluated by assessing these materials' effect on sample properties. The experiments were generally conducted as follows: Solutions containing 30 or 50 nm Ag NPs (ca. 10^5 part. g^{-1}) and/or 0-1 μg kg^{-1} of AgD were prepared in different water matrices. 10±1 mL of the sample solution was poured into 15 mL PP tubes containing 40-50 mg of SPE materials. All samples were then manually mixed for 5 min, after which the SPE materials were separated with centrifugation. Finally, the supernatant liquid was carefully separated by pipetting. Reference samples (i.e., samples analyzed without pretreatment) were similarly prepared as above but without the addition of SPE materials. All samples were prepared at least in duplicate and measured with SP-ICP-MS as described in Chapter 6.1.

SPE materials' effect on sample properties was evaluated according to Eqs. 6 and 7, where *EE*-% is the SPE material's AgD extraction efficiency, C_{Ag} is the concentration of AgD (μg kg^{-1}), and C_p is the particle concentration (part. g^{-1}) in reference sample (Ref.) and in the sample treated with SPE material (Sample):

$$EE - \% = \frac{C_{Ag(Ref.)} - C_{Ag(Sample)}}{C_{Ag(Ref.)}} \cdot 100\% \quad (6)$$

$$C_p\ recovery(\%) = \frac{C_{p(Sample)}}{C_{p(Ref.)}} \cdot 100\% \quad (7)$$

Furthermore, the particle size distribution histograms and the mean size values obtained for samples treated with SPE materials were compared to those obtained for reference samples.

6.7 Application of functional 3D printed scavengers

6.7.1 Preparation and characterization of 3D printed scavengers

The cylinder-shaped 3D scavengers used in paper III were designed to fit into 10 mL syringes and printed with a Sharebot SnowWhite SLS 3D printer. The printing parameters (i.e., laser speed and temperature) were adjusted to obtain highly porous yet durable 3D scavengers, which allow the sample solution to flow through the objects.

For the experiments performed in paper III, two types of 3D scavengers were prepared. First, for the selection of the most suitable supporting material used for printing, bare 3D scavengers constituting solely of the supporting material were prepared using polyamide-12 (PA-12), thermoplastic polyurethane (TPU), and polystyrene (PS). Second, after the selection of the materials, the final 3D scavengers were prepared using PS and SPE material SiliaBond Tosic acid (TA), which were manually mixed in a mass ratio of 1:10 before printing (10 m-%). After printing, all 3D scavengers were pretreated to remove any residual impurities and unsintered powder, after which they were placed in 10 mL syringes (1 scavenger/syringe).

Scanning electron microscopy with backscatter electron detection (BSD-SEM) was used for the structural characterization of the 3D TA scavengers. To improve imaging, samples were sputter coated with gold.

6.7.2 Evaluation of the 3D printed scavengers' effects on analyte properties

For the evaluation of the 3D scavengers' effect on analyte properties, dispersions containing 30 or 50 nm Ag NPs (ca. 10^5 part. g^{-1}) and/or AgD (0.2 or 1 µg kg^{-1}) were prepared. All samples were analyzed as such and after passing through the 3D scavengers at least in duplicate. Generally, 10 mL of sample solution was passed through one 3D scavenger using a syringe piston with a flow rate of ca. 10 mL min^{-1}, and the outflowing solution containing Ag NPs was collected into a 15 mL PP tube. Any sample residues were then removed by rinsing, after which UP water was passed through the 3D scavengers as blank samples to estimate

possible carryover. The AgD retained within the 3D TA scavenger was then eluted using a 0.5 mM STS solution (V=10 mL). The determination of Ag NPs and AgD concentration of the samples was then carried out with SP-ICP-MS, as described in Chapter 6.1.

3D scavengers' effect on Ag NP properties was estimated according to Eq. 8, where C_p is the obtained particle concentration (part. g^{-1}) for samples before (i) and after (f) passing through the 3D scavengers:

$$C_p\, recovery\ (\%) = \frac{C_{p(f)}}{C_{p(i)}} \cdot 100\% \quad (8)$$

In addition, the particle size distribution histograms and the mean particle sizes obtained for samples before and after passing through the 3D scavengers were compared.

The 3D scavengers' AgD extraction efficiency was calculated using Eqs. 9 or 10, where C_{Ag} is the concentration of AgD (µg kg^{-1}) before (i) and after (f) passing through the 3D TA scavenger. AgD's limit of quantification (LOQ) of 0.02 µg kg^{-1} was considered in the calculations as follows:

$C_{Ag(f)}$ > LOQ:

$$EE - \% = \frac{C_{Ag(i)} - C_{Ag(f)}}{C_{Ag(i)}} \cdot 100\% \quad (9)$$

$C_{Ag(f)}$ < LOQ:

$$EE - \% \geq \frac{C_{Ag(i)} - LOQ}{C_{Ag(i)}} \cdot 100\% \quad (10)$$

The desorption efficiency of AgD (DE-%) was determined using Eqs. 11 or 12, where $C_{Ag(e)}$ is the AgD concentration in the elution solution (in µg kg^{-1}), and V_e and V_i are the volumes of the elution and sample solutions (in kg), respectively:

$C_{Ag(f)}$ > LOQ:

$$DE - \% = \frac{C_{Ag(e)} \cdot V_e}{(C_{Ag(i)} - C_{Ag(f)}) \cdot V_i} \cdot 100\% \quad (11)$$

$C_{Ag(f)}$ < LOQ:

$$DE - \% \geq \frac{C_{Ag(e)} \cdot V_e}{(C_{Ag(i)} - 0) \cdot V_i} \cdot 100\% \quad (12)$$

7 RESULTS AND DISCUSSION

This chapter summarizes the main results and findings obtained from the three publications included in the thesis. Paper I focused on improving the detection of Au NPs by instrumental parameter optimization. In contrast, papers II and III focused on improving the accuracy of Ag NP characterization and quantification by AgD removal using SPE materials.

7.1 Optimization of SP-ICP-MS instrumental parameters for gold

7.1.1 Fitting of the second-order model

First, a second-order polynomial model was fitted to the experimental data according to Eq. 5 (paragraph 5.1) for dissolved and nanoparticulate gold. Then, a backward elimination method available on the Minitab 19 software was used to automatically remove the statistically insignificant terms with P-values >0.05 (95% confidence level).

The statistical significance of the final regression models, main variables, and their interactions was evaluated based on analysis of variance (ANOVA, not shown). Large F-values and P-values <0.05 were obtained for both models, indicating that the models are significant and can explain the observed variation in the response. The obtained adjusted R^2- and predicted R^2-values were >92% for nanoparticulate and dissolved gold, indicating a good fit between the model and experimental data.

For both forms of the analyte, the main and quadratic effects of the main variables (A, B, C, A^2, B^2, C^2) as well as the two-way interaction effects A*B and A*C were found to have a significant effect on the response (the intensity of gold) at the 95% confidence level. The final predictive equations obtained for nanoparticulate and dissolved gold were as follows (in uncoded units):

Nanoparticulate gold:

$$y\,(counts) = -3217 + 9411A - 1.899B - 13.2C - 7604A^2 - 0.000192B^2 - 10.071C^2 + 2.5117AB + 198.3AC \quad (13)$$

Dissolved gold:

$$y\,(counts) = 1745603 + 5070025A - 998.6B + 12810C - 4090912A^2 - 0.1255B^2 - 5422C^2 + 1417.0AB + 94268AC \quad (14)$$

7.1.2 The effect of the variables on the intensity of gold

To study the instrumental parameters' (A, B, C) effect on the intensity of gold in more detail, response surface plots were drawn based on Eqs. 13 and 14 (**Fig. 2**).

The detailed analysis of the effects of the variables can be found on paper I, and is only briefly discussed here.

As the response surface plots obtained for nanoparticulate and dissolved gold are compared (**Fig. 2**), a high resemblance is observed. This indicates similar behavior of the two analyte forms in plasma in accordance with the instrumental parameters used. The instrumental parameter values clearly significantly affect the obtained response (the intensity of gold) for both forms of the analyte. This results from the changes in plasma characteristics, affecting the overall degree of analyte ionization and the transport of ions in plasma and, thus, the obtained intensity value.[109,110,118,119,147–151] The interaction effects of the main variables (*A*B* and *A*C*) are visible in **Fig. 2**, and the effect of adjusting the value of one variable depends largely on the value of the other variable. As an example, although decreasing the sampling depth at low nebulizer gas flows (ca. ≤1 mL min^{-1}) leads to an intensity increase, the opposite is true for high nebulizer gas flows values (**Fig. 2 c and d**). As such, variables should be optimized using the DoE approach instead of one factor at a time if the maximum intensity is expected.

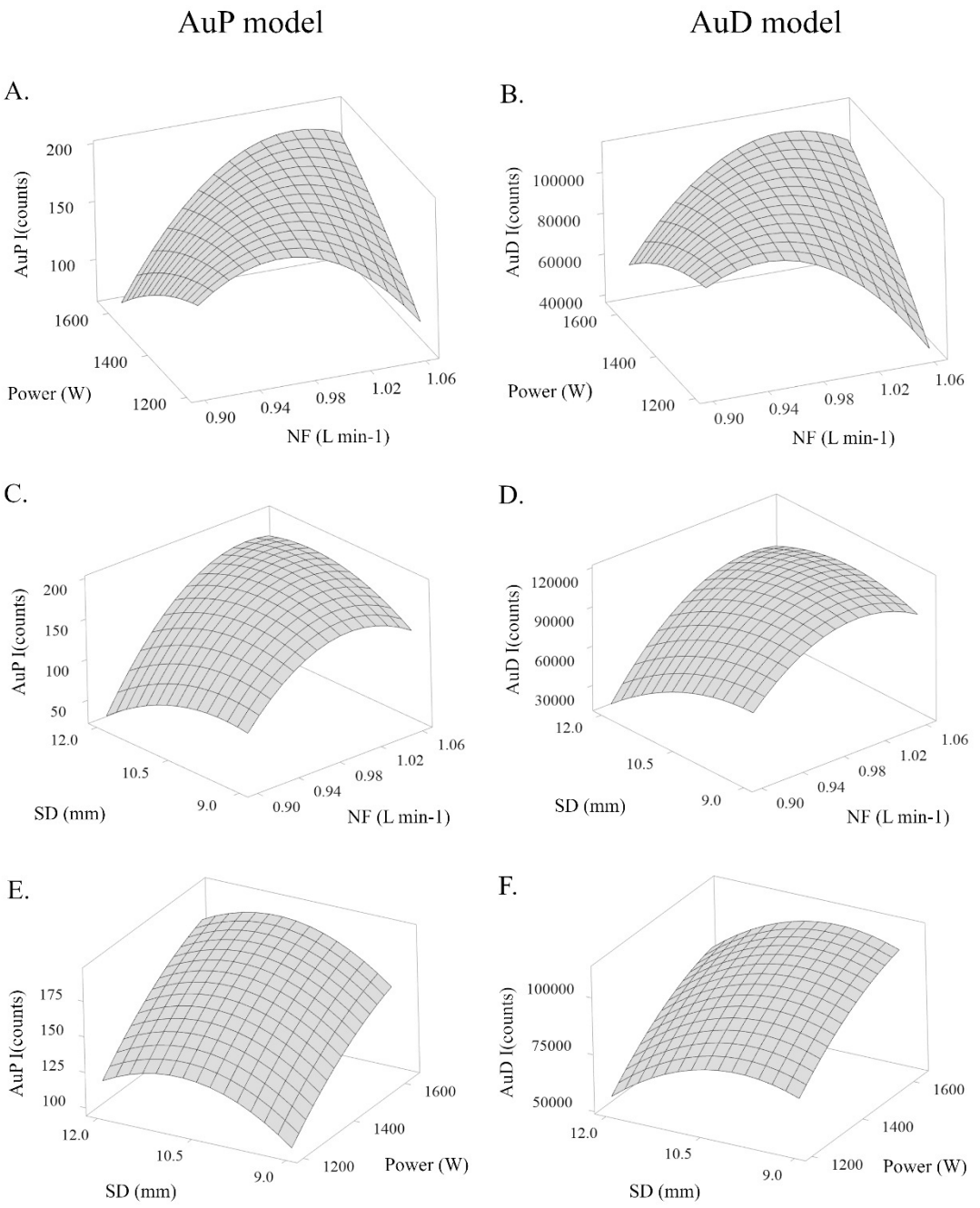

FIGURE 2 Variations in the intensity of nanoparticulate (AuP) and dissolved (AuD) gold (counts) with respect to: A, B) Nebulizer gas flow (NF, L min^{-1}) and RF-power (power, W); C, D) Nebulizer gas flow (L min^{-1}) and sampling depth (SD, mm) and E, F) RF-power (W) and sampling depth (mm). Reproduced with kind permission from Elsevier.[I]

7.1.3 Optimized instrumental parameter values

The predicted optimal instrumental conditions were solved using Minitab 19 software as follows (for nanoparticulate/dissolved gold): A 1.03/1.01 L min^{-1}, B 1600W, and C 11.0/10.0 mm. As minor differences were observed in the predicted optimal conditions for different analyte forms, additional experiments were conducted to confirm the optimal sampling depth values. In these experiments, the nanoparticulate and dissolved gold intensity was determined at different sampling depth positions (9, 10, 11, and 12 mm) with plasma power and nebulizer gas flow set to their optimal values (1600W and nebulizer flow optimized for a given sampling depth position). The highest intensities for both dissolved and nanoparticulate gold were obtained using 11.0 mm as the sampling depth. For dissolved gold, the differences in the obtained intensity at sampling depth positions of 10 and 11 mm were negligible (<5%). This could explain the differences in the predicted optimal conditions obtained for the two analyte forms. However, the optimal sampling depth range is narrower for nanoparticulate than for dissolved gold. Decreasing the sampling depth value <11 resulted in up to a 10% decrease in the intensity, presumably due to the longer time required for complete vaporization and ionization of the particles.[109,110,150,152,153]

Compared to robust conditions, optimization of instrumental parameter values increased the nebulizer gas flow value. This contrasts with the findings of Kálomista *et al.*,[121] who found the optimum sampling depth value to be 4 mm. However, as only the sampling depth value was optimized, the interaction effects of variables could not be considered. Although significant improvement in the intensity can be achieved by adjusting the instrumental parameters one at a time, for obtaining maximum intensity values, parameters should be jointly optimized using the DoE approach. This is because of the significant interaction effects of the main variables, i.e., the optimal setting of each variable is dependent on the other two variables.[123,154]

7.1.4 The effect of optimization on the accuracy of NP determination

Results for 20 and 30 nm Au NPs obtained under optimal and robust conditions were compared to study the effect of instrumental parameter optimization on Au NP determination. A significant (+70%) increase in instrument sensitivity was achieved by instrumental parameter optimization as compared to robust conditions, translating into a 15% decrease in the LOD_{size}. The increased sensitivity allowed the detection of smaller NPs, thus achieving more accurate sizing and counting of the 20 nm Au NPs (**Table 6**). However, low particle concentration recoveries (<30%) were still obtained under both conditions. This is most likely due to the challenges of determining NPs near the LOD_{size}, as also observed by other authors.[155] Excellent recoveries (101%) were obtained for the 30 nm Au NPs under both conditions, indicating that experimental results obtained for <30 nm NPs should be interpreted with caution.

TABLE 6 Instrumental conditions' effect on the determination of 20 and 30 nm Au NPs, given as a mean ± standard deviation (1s) of three replicates.

	LOD_{size} (nm)	Mean size (nm)		C_p recovery (%)	
		20 nm Au NP (Citrate)	30 nm Au NP (PEG-COOH)	20 nm Au NP (Citrate)	30 nm Au NP (PEG-COOH)
Optimal conditions[1]	13	21±1	28±1	27±2	101±4
Robust conditions[2]	15	22±1	27±1	23±3	101±5

[1] A 1.02 L min^{-1}, B 1600 W, C 11 mm

[2] A 0.93 L min^{-1}, B 1600 W, C 11 mm

7.2 Improving the accuracy of Ag NPs' determination with SPE material pretreatment

7.2.1 The interfering effect of coexisting AgD

Fig. 3 demonstrates the effect of coexisting AgD (0-1 µg kg^{-1}) on determining 30, 40, 50, and 80 nm Ag NPs. Elevated concentrations of AgD increase the background (dissolved) signal, which can overlap individual NP signals. In these cases, only NP events large enough to be distinguishable from the background signal are detected, leading to only a partial capture of NP size distribution and, thus, biased NP determination. Since the intensity of NP events depends directly on their size, coexisting AgD interferes foremost with the determination of the smallest NPs by increasing the LOD_{size}[100,113] (**Fig.3**). Whereas the determination of the larger 50 and 80 nm Ag NPs is not affected by AgD concentration up to 1 µg kg^{-1}, the detection of 30 nm and 40 nm Ag NPs clearly interferes with AgD concentrations ≥0.1 µg kg^{-1}. This results in a biased determination of NP size (up to +80% increase) and particle concentration (up to -93% decrease).

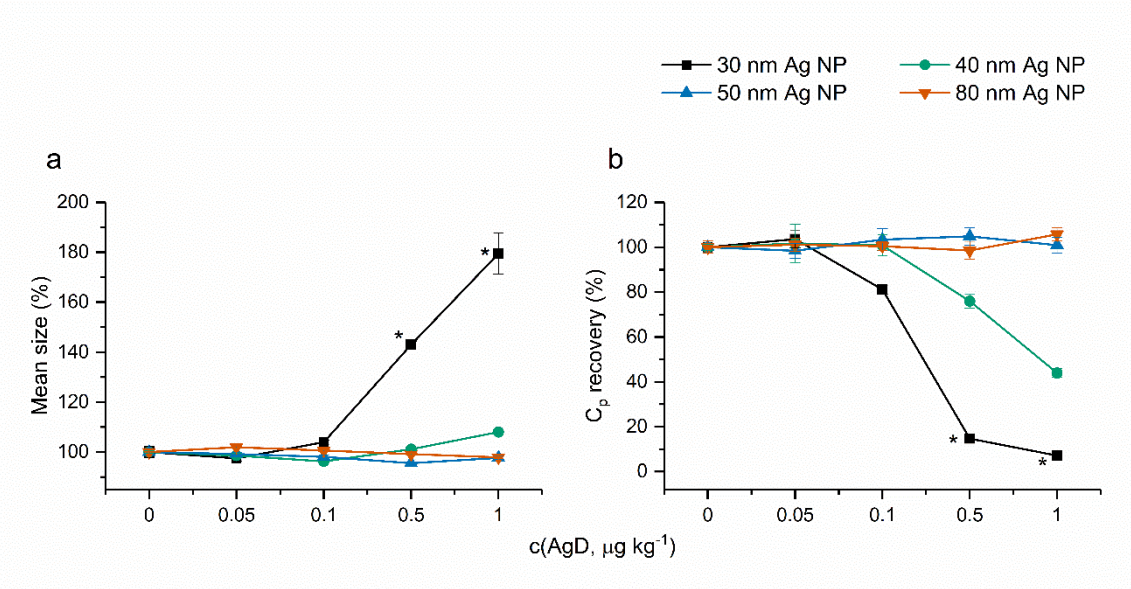

FIGURE 3 Experimental results obtained for Ag NP mean size (a) and concentration (b) in the presence of coexisting AgD. Results highlighted with an asterisk calculated based on insufficient number of NP events for reliable determination (<100). Reproduced with kind permission from Elsevier.[II]

7.2.2 SPE materials' effect on analyte properties

Various SPE materials obtained from commercial vendors were evaluated for AgD removal in Ag NP dispersions by assessing their effect on analyte properties. First, these materials' effect on Ag NP properties (particle size and concentration) was evaluated in different water matrices (UP, spring, lake, and brook water, **Fig. 4**). Pretreatment of samples with SPE materials TP 214, SM DEAM, and SM Tri was observed to cause significant NP losses (up to -64%) or decrease in particle size, indicating possible particle dissolution. Therefore, these materials were excluded. The remaining SPE materials (Chelex 100, C115HMR, SB TA, SM DMT, and SM Thiol), however, were found able to preserve the original NP properties. Similar results for particle size and concentration were obtained for samples treated with these materials as compared to those analyzed as such. No significant changes were observed in the particle size distribution histograms obtained for these samples (data not shown), further proving the lack of significant interactions between the SPE materials and Ag NPs.

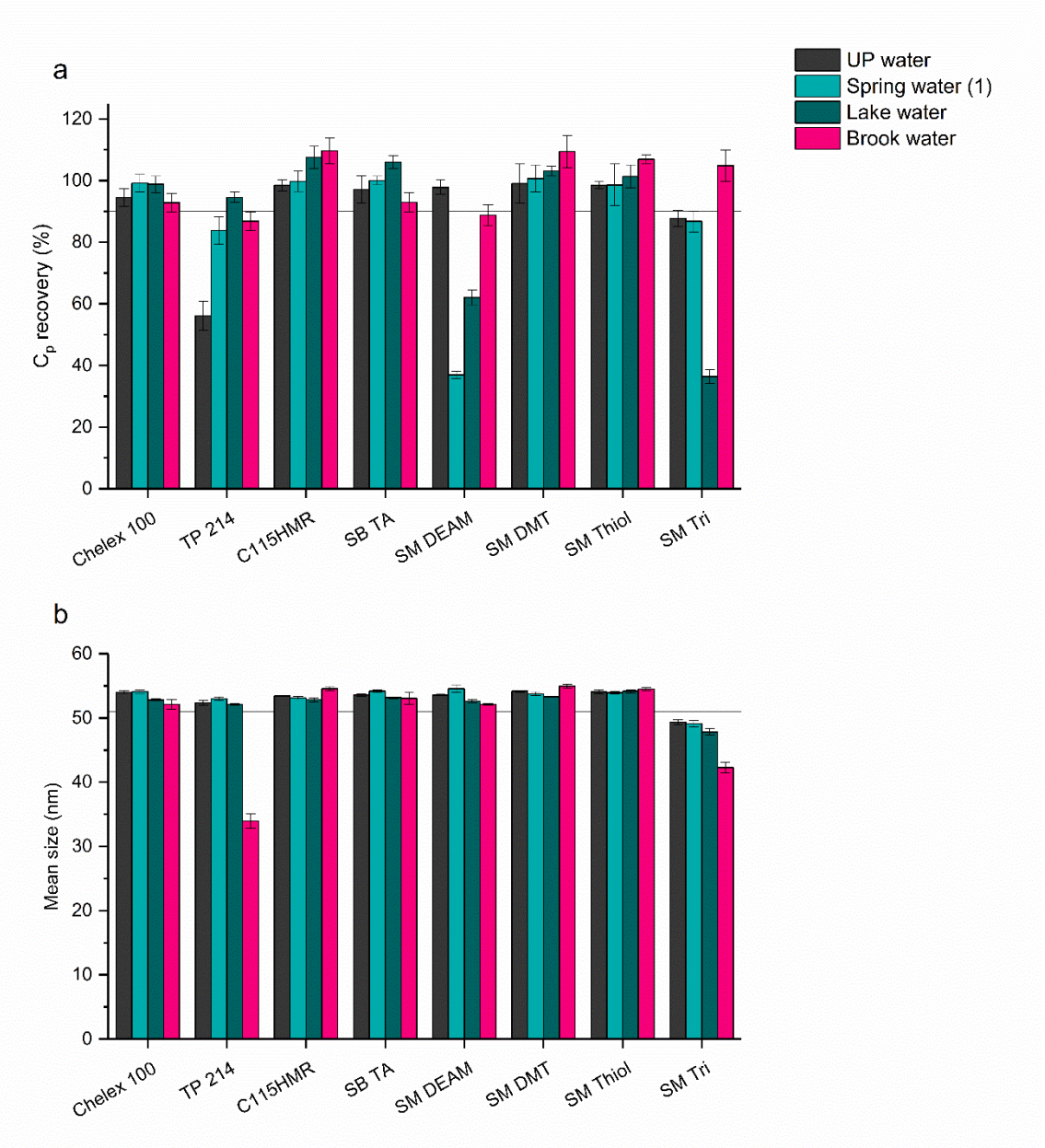

FIGURE 4 SPE materials' effect on 50 nm AgNPs' properties in different matrices. The black reference line in Figs. 4 a and b indicates the 90% C_p recovery and the verified mean size of the 50 Ag NPs (51 nm), respectively. Reproduced with kind permission from Elsevier.[II]

Once the materials that maintained original Ag NP properties were identified, their ability to remove AgD was further studied. As a sample matrix affects the efficiency of the SPE process,[111,112,156,157] experiments were performed in several water matrices with different physicochemical properties. As the obtained results in colorless and dark-colored waters (**Fig. 5 a and b**, respectively) are compared, the sample matrix's effect on AgD extraction efficiency can be clearly seen. Whereas up to 97% extraction efficiencies are obtained in colorless waters without humic substances (DOC <5 mg L^{-1}), the SPE materials' ability to extract AgD clearly decreases in dark-colored waters. The most likely explanation for

this is the competitive binding of silver ions into humic substances' functional groups. [158]

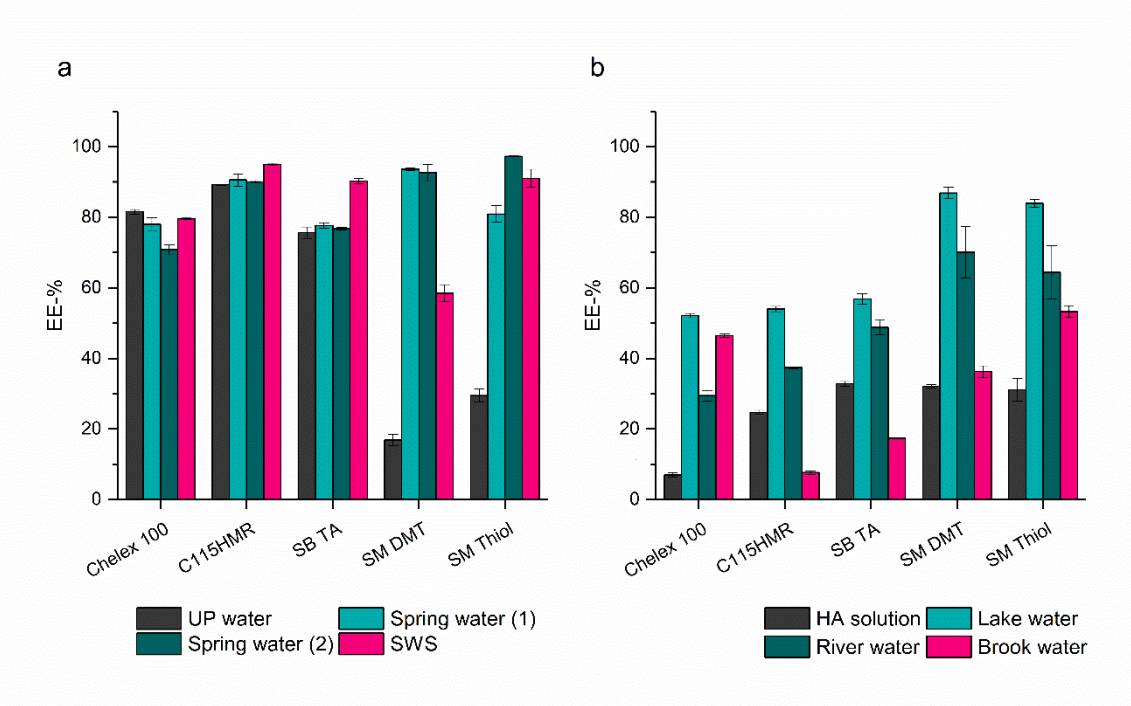

FIGURE 5 SPE materials' AgD extraction efficiencies (EE-%) in colorless (a) and dark-colored waters (b). Reproduced with kind permission from Elsevier.[II]

The sample matrix should thus be carefully considered when choosing the SPE materials for AgD removal in Ag NP dispersions. Based on the obtained results, ion-exchange materials Chelex 100, C115HMR, and SB TA are generally more efficient in colorless waters with 89-95% AgD extraction efficiencies. However, SPE materials SM DMT and SM Thiol with thiol groups should be preferred in dark-colored waters with higher amounts of humic substances. This is most likely due to the strong affinity of silver towards sulfur groups.

Based on the obtained results, C115HMR and SM Thiol were chosen as the final SPE materials used for dissolved removal in Ag NP dispersions for their negligible effects on Ag NP properties and high AgD extraction capabilities. Experiments were also performed with Chelex 100 for its frequent use in previous studies.[113,135]

7.2.3 The effect of the pretreatment method on Ag NP determination

The effect of the proposed sample pretreatment method on Ag NPs' determination was evaluated by comparing the obtained results for samples analyzed as such and after pretreatment with the chosen SPE materials. 30 nm Ag NP dispersions containing 0-1 µg kg^{-1} of AgD prepared in colorless and dark-colored waters were treated with the chosen SPE materials C115HMR, Chelex 100, and SM Thiol, as described in paragraph 6.6.2.

As seen in **Fig. 6**, as samples are analyzed as such, AgD severely interferes with the detection of the 30 nm Ag NPs, resulting in significantly biased NP determination. Increasing the AgD concentration causes a greater overlap between the signals originating from the analyte, either in nanoparticulate or dissolved form, leading to an NP size overestimation (up to +58%) and particle concentration underestimation (up to -90%). Pretreatment of samples with the SPE materials, however, removes a large portion of the AgD and thus minimizes its interfering effect. In colorless waters, SPE materials Chelex 100 and C115HMR remove AgD efficiently (up to 95%), allowing the accurate sizing and counting of the 30 nm Ag NPs. However, in river water with moderate amounts of humic substances (DOC 11 mg L^{-1}), SM Thiol is found more efficient in AgD removal and should be preferred. As a result of sample pretreatment, a highly accurate determination of Ag NP size (28±2 nm) and particle concentration (<21% different) was achieved over the whole concentration range studied.

As the obtained particle concentration values for the samples analyzed as such and after pretreatment with the SPE materials in UP water (**Fig. 6**) are inspected in detail, some peculiar differences can be observed. Significantly lower (up to -40%) particle recoveries are obtained for the analyzed samples compared to those pretreated with SPE materials. Similar behavior was not observed in other matrices, and no changes were observed in NP size, which could indicate particle dissolution. As such, this unexpected behavior is assumed to be due to the adsorption of Ag NPs into the sample introduction system's surfaces, as reported before.[47] SPE materials may reduce the interaction of the Ag NPs with solid surfaces, thus explaining the observed results.

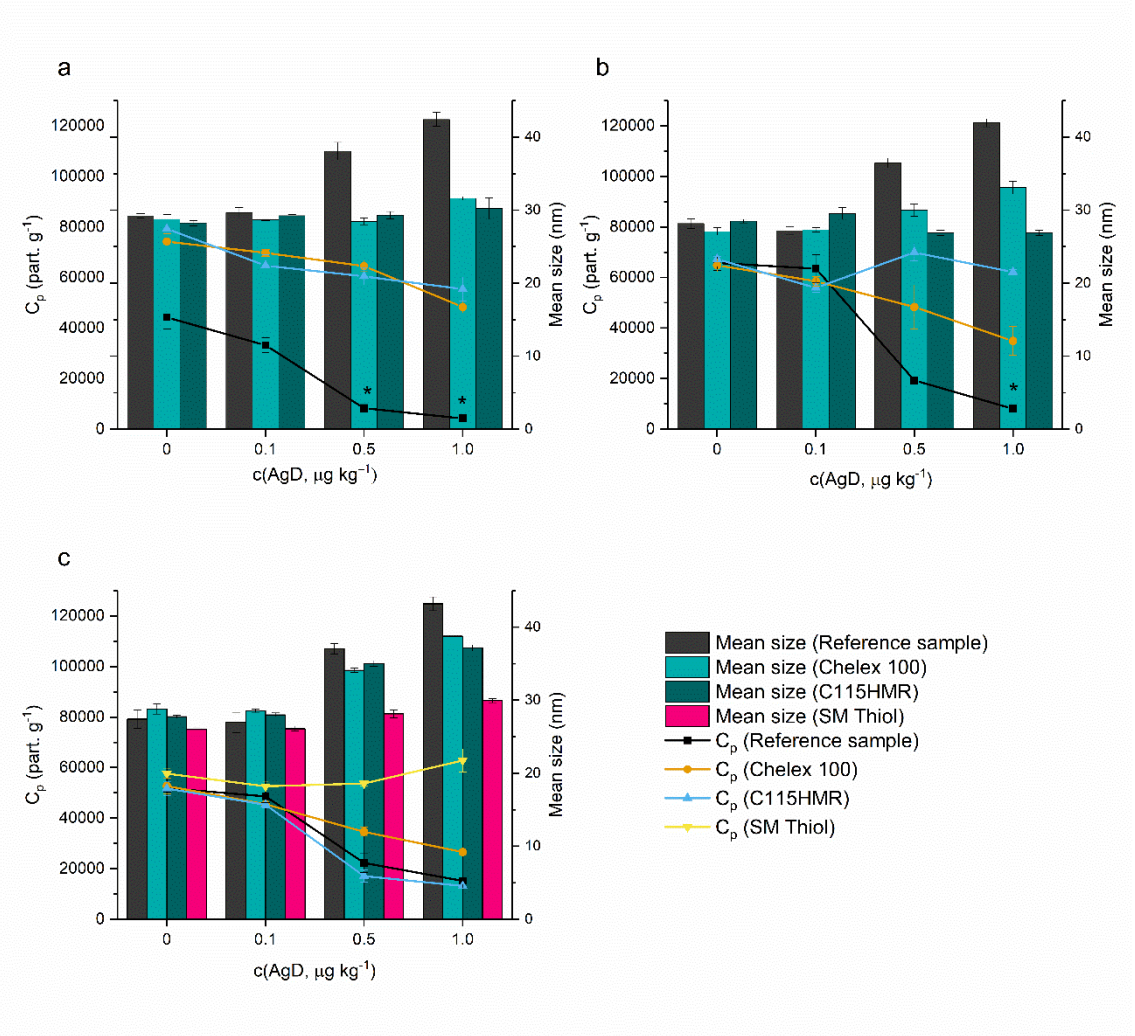

FIGURE 6 Selected SPE materials' effect on 30 nm Ag NPs' properties in UP water (a), spring water (2) (b), and river water (c). Results highlighted with an asterisk calculated based on insufficient number of NP events for reliable determination (<100). Reproduced with kind permission from Elsevier.[II]

7.3 Improving the accuracy of Ag NP determination with 3D printed functional scavengers

7.3.1 Preparation and characterization of 3D printed scavengers

For the preparation of functional 3D scavengers, a small amount of chemically active material is mixed with a polymer used for building the object's structure (i.e., used as a supporting matrix). Considering the applicability of 3D scavengers for the pretreatment of Ag NP dispersions, highly efficient AgD removal should be achieved while preserving the original Ag NP properties of the sample. As such, care was taken in selecting the materials used for constructing the 3D scavengers, and their effect on Ag NP properties was thoroughly investigated. Of the three polymer materials evaluated for supporting matrices (PA-12, TPU, and PS), PS was chosen for its negligible effects on NP properties. Based on the obtained results in publication II, TA was chosen as the chemically active component for its efficient AgD removal capability, availability, and lack of significant interactions with the Ag NPs.

The structural characterization of the final 3D TA scavengers constituting PS and TA was conducted using BSD-SEM. As shown in **Fig. 7**, the PS particles are only partially sintered together, forming a highly porous object with a large surface area. The TA particles are strongly bound onto the surface of the PS particles, thus decreasing the loss of capacity during use while remaining available for chemical reactions. The voids and cavities in the range of 30 – 70 µm within the object allow the sample solution to pass freely through the object while enabling an efficient interaction between the analyte and the chemically active TA material.

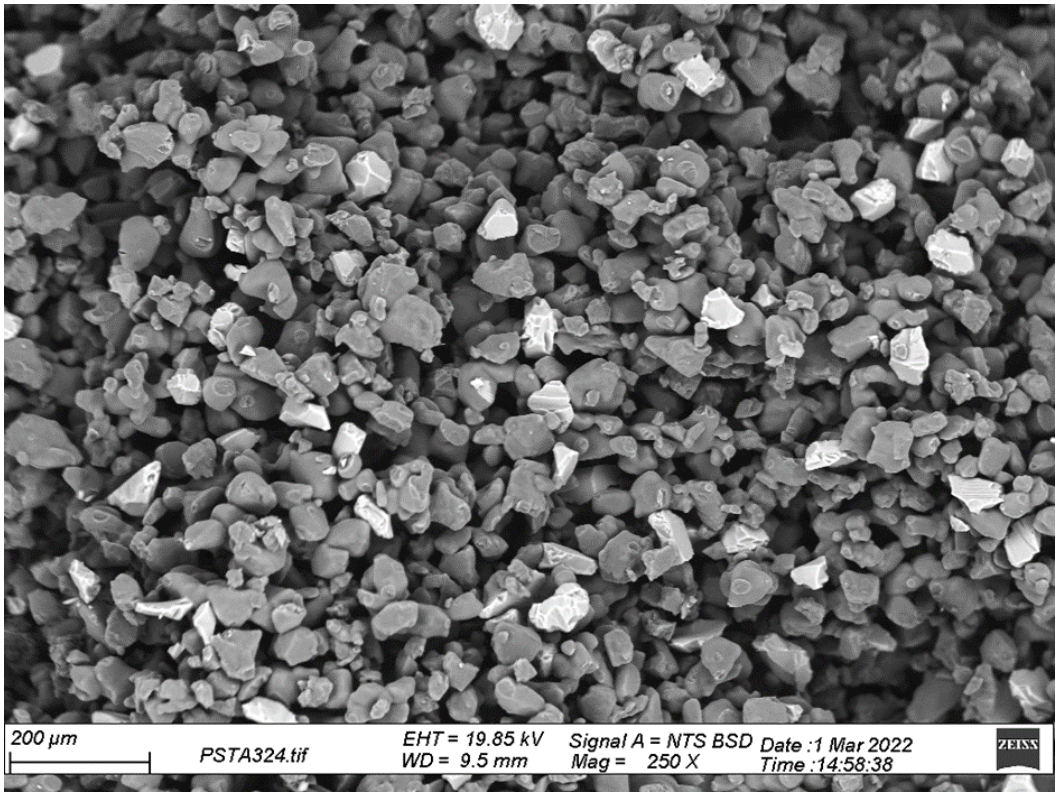

FIGURE 7 BSD-SEM image of 3D TA scavenger's break surface, showing TA particles dispersed evenly within the structure (shown in lighter grey). Reproduced with kind permission from Elsevier.[III]

7.3.2 The effect of 3D TA scavengers on sample properties

3D TA scavengers were evaluated for Ag NP dispersions pretreatment by evaluating their effect on original Ag NP properties and examining their AgD removal efficiency. As shown in **Fig. 8**, similar results for NP mean size and particle concentration were obtained for samples analyzed as such (**Fig. 8 a**) and after passing through the 3D TA scavengers (**Fig. 8 b**). The 3D TA scavengers were not found to affect the particle size distribution, confirming the lack of significant interactions between Ag NPs and the 3D TA scavengers.

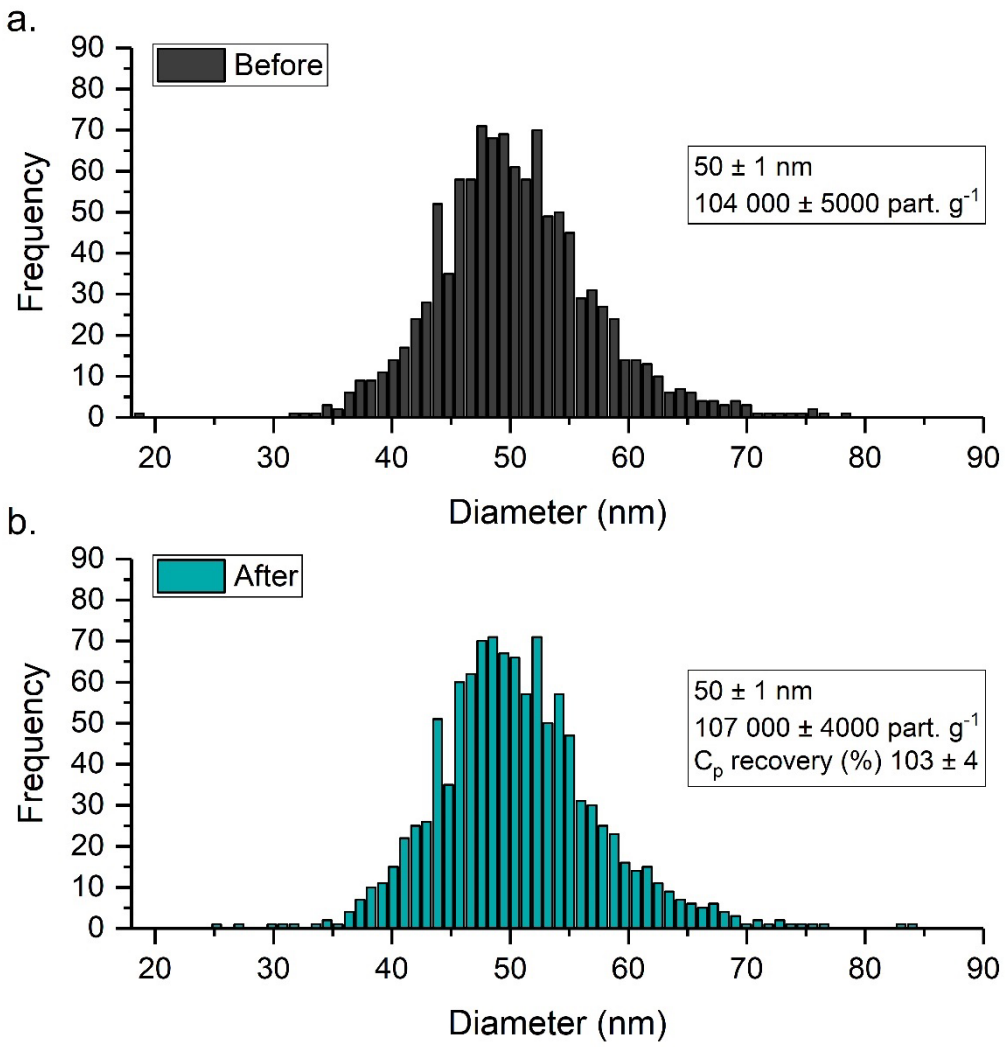

FIGURE 8 The experimental results obtained for 50 nm Ag NPs analyzed as such (a) and after passing through the 3D TA scavengers (b). Reproduced with kind permission from Elsevier.[III]

In the following stage of the experiments, 3D TA scavengers' ability to extract AgD was investigated in UP and spring water matrices. The 3D TA scavengers proved highly efficient in removing AgD in all matrices, and extraction efficiencies ≥89% were achieved. The competitive binding of common elements found in environmental waters (Ca, K, Mg, Na, Sr) was not found to significantly affect the 3D TA scavengers' ability to extract AgD, proving 3D scavengers' suitability for the pretreatment of natural water samples. Silver was not found in the blank samples passed through the 3D scavengers after samples, indicating an efficient retainment of the AgD in the 3D TA scavengers.

Next, the possibility of desorbing the adsorbed silver was studied with a 0.5 mM solution of STS. Independent of the sample matrix, desorption efficiencies of

≥75% were obtained. This indicates that 3D TA scavengers could also be used to preconcentrate AgD.

7.3.3 The effect of the pretreatment method on Ag NP determination

The proposed sample pretreatment method's efficiency for improving the accuracy of Ag NP determination was evaluated in UP and two spring water matrices. As Ag NPs in environmental samples are expected to be small (<30 nm),[68,105,106] experiments were performed using 30 nm Ag NPs spiked with 0.2 µg kg^{-1} of AgD to evaluate the 3D scavengers' performance under more realistic environmental conditions. The obtained results for samples pretreated with the 3D TA scavengers were compared to those analyzed as such. As the literature suggests using sample dilution to eliminate AgD interference,[97,159] the determination was also performed on 4-fold diluted samples for comparative purposes. Results are displayed in **Fig. 9**.

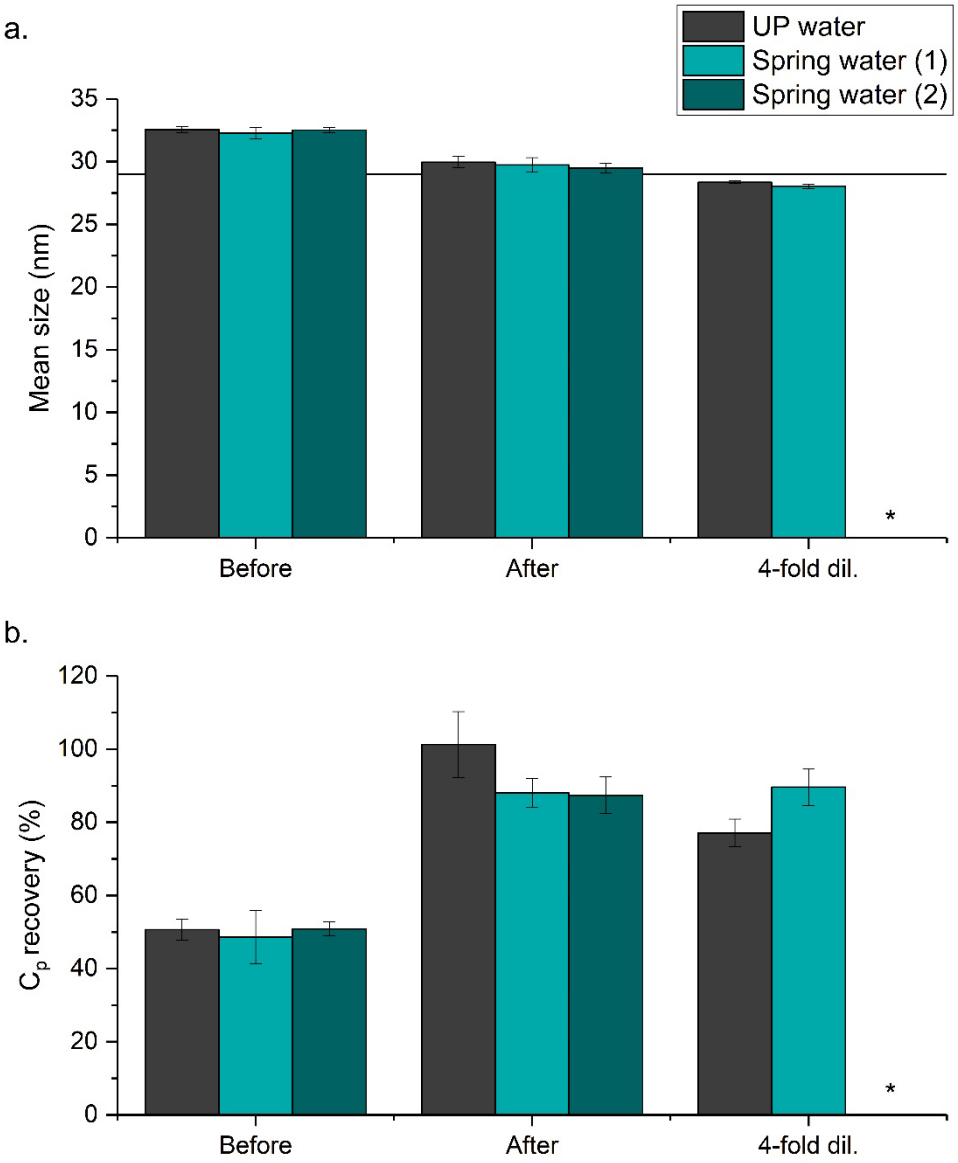

FIGURE 9 The experimental results obtained for 30 nm Ag NPs spiked with AgD, analysed before and after passing through the 3D TA scavengers, and after a 4-fold dilution. The black reference line indicates the diameter of the 30 nm Ag NPs (29±3 nm as given by the supplier) used in the experiments. The results obtained for the 4-fold diluted spring water (2) sample are not shown due to the occurrence of false positives. Reproduced with kind permission from Elsevier.[III]

As seen in **Fig. 9**, coexisting AgD interferes with the determination of 30 nm Ag NPs even at 0.2 µg kg^{-1} concentration independent of the sample matrix. The high background signal caused by coexisting AgD prevents the detection of the smallest NP events entirely and shifts the size distribution to larger sizes. This results in significantly biased NP sizing (up to +12%) and concentration

determination (up to -51%). Pretreatment of the samples with the 3D TA scavengers eliminates the interfering effect of AgD by highly efficient AgD removal (≥89%, AgD concentrations <LOQ). As such, a much more accurate determination of the 30 nm Ag NPs is obtained (**Fig. 9**). In addition, the retained AgD was eluted with satisfactory results (≥75%).

Considering UP and spring water (1) samples, highly similar values were obtained for 4-fold diluted samples and samples pretreated with the 3D TA scavengers (**Fig. 9**), further confirming the suitability of the pretreatment method for Ag NP dispersions. However, an anomalously high number of low-intensity events were observed in the 4-fold diluted spring water (2) sample's size distribution histogram (data not shown). As these events are most likely false positives causing biased results, these results were discarded (a more detailed discussion can be found in paper III). Nevertheless, the interfering effect of coexisting AgD can be eliminated with 3D TA scavengers extremely fast (ca. 1 min/sample) in all matrices while preserving the original Ag NP properties. This results in a more accurate determination of Ag NP size (<4% different) and particle concentration (<13% different). As such, compared to sample dilution, sample pretreatment with functional 3D scavengers offers a simpler and more efficient alternative for AgD removal.

8 CONCLUDING REMARKS

Although nanomaterials (NMs) have become inseparable from our everyday lives, their environmental and human health effects are not yet fully understood. An impartial evaluation of the benefits and the potential environmental and human health risks is vital to ensure NMs' sustainable production and use in various applications. This will require sophisticated analytical techniques able to accurately determine the properties of these materials, even in complex environmental sample matrices. As a contribution to available techniques for reliable NM characterization, this dissertation thesis aimed to improve the accuracy of NPs' determination with the SP-ICP-MS technique.

First, instrumental parameters (plasma RF-power, nebulizer gas flow, and sampling depth) were optimized using a DoE approach for both dissolved and NP gold. The purpose was to improve the detection of Au NPs by decreasing the size limit of detection (LOD_{size}), thus allowing more accurate sizing and counting of the Au NPs. Significant interaction effects between the main variables were noticed, highlighting the importance of DoE approaches in optimization. The results showed similar optimal conditions for nanoparticulate and dissolved gold, indicating similar behavior of the two analyte forms in plasma. Significant (70%) enhancement in instrument sensitivity and a 15% decrease in LOD_{size} values were achieved through optimization of instrumental conditions, which allowed more accurate determination of Au NPs near the LOD_{size} compared to frequently used robust conditions.

In the following stages of the study, the interfering effect of AgD on the determination of Ag NPs was studied. AgD concentrations of ≥0.1 µg kg^{-1} were shown to severely interfere with the detection of 30 and 40 nm Ag NPs, thus leading to a significant bias in Ag NP sizing (up to +58%) and concentration determination (up to -90%). Two simple sample pretreatment procedures utilizing solid phase extraction (SPE) materials for efficiently removing AgD were developed, thus allowing more accurate Ag NP determination. First, the applicability of several commercially available SPE materials was evaluated for AgD removal in Ag NP dispersions in several environmental water matrices. SPE materials' AgD extraction efficiency depended on the sample matrix and, thus,

different SPE materials were recommended for colorless and dark-colored waters. The developed sample pretreatment method efficiently removed the dissolved analyte, allowing a more accurate determination of NP size and concentration of the 30 nm Ag NPs.

In the final stage of the study, an effective sample pretreatment procedure utilizing functional 3D printed scavengers for AgD removal was presented. 3D printing allowed the incorporation of an ion-exchange resin SiliaBond Tosic acid (TA) into highly porous 3D printed objects. The 3D TA scavengers were highly efficient in AgD removal while preserving the original Ag NP properties of the sample. Pretreatment of the samples using 3D TA scavengers eliminated the interfering effect of coexisting AgD and resulted in more accurate sizing (30±1 nm, <4% different) and counting (<13% different) of the 30 nm Ag NPs. Furthermore, the extracted AgD was efficiently (≥75%) recovered using a sodium thiosulfate solution, indicating the possibility of using 3D TA scavengers even for the preconcentration of AgD.

The results presented here show that although SP-ICP-MS is a versatile technique for the determination of NPs, the accuracy of the results depends on several factors. The detection of the smallest NPs can be improved by carefully optimizing instrumental conditions. In addition, the interfering effect of dissolved analyte can be minimized by applying SPE materials, thus allowing more accurate determination of NPs' size and concentration. However, to select the most suitable SPE material, the sample matrix must be considered. The results also revealed that functional 3D printed scavengers offer a simple, reusable, and highly efficient sample pretreatment procedure for AgD removal in Ag NP dispersions.

Overall, this dissertation thesis has increased the knowledge of the potential and existing limitations of SP-ICP-MS measurements. The increasingly important nanomaterials' determinations have been significantly promoted by presenting analytical methods suitable even for complex environmental water matrices, allowing a more accurate determination of their properties. The sample pretreatment methods presented in this work can also be potentially applied to various other analytes and sample matrices, which could be studied more in the future. In addition, more research on the interfering effect on the sample matrix should be performed. While using internal standards would improve the accuracy of the results, they might prove problematic to develop. Most importantly, certified reference materials are urgently needed for method development and validation purposes.

REFERENCES

1 S. A. Mazari, E. Ali, R. Abro, F. S. A. Khan, I. Ahmed, M. Ahmed, S. Nizamuddin, T. H. Siddiqui, N. Hossain, N. M. Mubarak and A. Shah, *J. Environ. Chem. Eng.*, 2021, **9**, 105028.

2 I. Khan, K. Saeed and I. Khan, *Arab. J. Chem.*, 2019, **12**, 908–931.

3 F. Laborda, E. Bolea, G. Cepriá, M. T. Gómez, M. S. Jiménez, J. Pérez-Arantegui and J. R. Castillo, *Anal. Chim. Acta*, 2016, **904**, 10–32.

4 S. Mourdikoudis, R. M. Pallares and N. T. K. Thanh, *Nanoscale*, 2018, **10**, 12871–12934.

5 H. E. Pace, N. J. Rogers, C. Jarolimek, V. A. Coleman, C. P. Higgins and J. F. Ranville, *Anal. Chem.*, 2011, **83**, 9361–9369.

6 F. Laborda, J. Jiménez-Lamana, E. Bolea and J. R. Castillo, *J. Anal. At. Spectrom.*, 2011, **26**, 1362–1371.

7 C. Degueldre and P.-Y. Favarger, *Colloids. Surf. A: Physicochem. Eng. Asp.*, 2003, **217**, 137–142.

8 M. D. Montaño, J. W. Olesik, A. G. Barber, K. Challis and J. F. Ranville, *Anal. Bioanal. Chem.*, 2016, **408**, 5053–5074.

9 E. Bolea, M. S. Jimenez, J. Perez-Arantegui, J. C. Vidal, M. Bakir, K. Ben-Jeddou, A. C. Gimenez-Ingalaturre, D. Ojeda, C. Trujillo and F. Laborda, *Anal. Methods*, 2021, **13**, 2742–2795.

10 D. Mozhayeva and C. Engelhard, *J. Anal. At. Spectrom.*, 2020, **35**, 1740–1783.

11 D. R. Boverhof, C. M. Bramante, J. H. Butala, S. F. Clancy, W. M. Lafranconi, J. West and S. C. Gordon, *Regul. Toxicol. Pharmacol.*, 2015, **73**, 137–150.

12 M. F. Hochella, D. W. Mogk, J. Ranville, I. C. Allen, G. W. Luther, L. C. Marr, B. P. McGrail, M. Murayama, N. P. Qafoku, K. M. Rosso, N. Sahai, P. A. Schroeder, P. Vikesland, P. Westerhoff and Y. Yang, *Science*, 2019, **363**, 8299.

13 W. Stöber, A. Fink and E. Bohn, *J. Colloid Interface Sci.*, 1968, **26**, 62–69.

14 A. Ioannou, G. Gohari, P. Papaphilippou, S. Panahirad, A. Akbari, M. R. Dadpour, T. Krasia-Christoforou and V. Fotopoulos, *Environ. Exp. Bot.*, 2020, **176**, 104048.

15 A. A. Yaqoob, T. Parveen, K. Umar and M. N. M. Ibrahim, *Water*, 2020, **12**, 495.

16 A. K. Hussein, *Renewable and Sustainable Energy Reviews*, 2015, **42**, 460–476.

17 M. Abd Elkodous, G. S. El-Sayyad, I. Y. Abdelrahman, H. S. El-Bastawisy, A. E. Mohamed, F. M. Mosallam, H. A. Nasser, M. Gobara, A. Baraka, M. A. Elsayed and A. I. El-Batal, *Colloids Surf. B: Biointerfaces*, 2019, **180**, 411–428.

18 M. F. L. De Volder, S. H. Tawfick, R. H. Baughman and A. J. Hart, *Science*, 2013, **339**, 535–539.

19 K. P. Bautista-Gutierrez, A. L. Herrera-May, J. M. Santamaría-López, A. Honorato-Moreno and S. A. Zamora-Castro, *Materials*, 2019, **12**, 3548.

20 X. F. Zhang, Z. G. Liu, W. Shen and S. Gurunathan, *Int. J. Mol. Sci.*, 2016, **17**, 1534.
21 L. Wei, J. Lu, H. Xu, A. Patel, Z.-S. Chen and G. Chen, *Drug Discov. Today*, 2015, **20**, 595–601.
22 S. M. Imani, L. Ladouceur, T. Marshall, R. Maclachlan, L. Soleymani and T. F. Didar, *ACS Nano*, 2020, **14**, 12341–12369.
23 E. A. J. Bleeker, S. Evertz, R. E. Geertsma, W. J. G. M. Peijnenburg, J. Westra and S. W. P. Wijnhoven, *Assessing health & environmental risks of nanoparticles*, National Institute for Public Health and the Environment, Bilthoven, The Netherlands, 2015.
24 J. Zhao, M. Lin, Z. Wang, X. Cao and B. Xing, *Crit. Rev. Environ. Sci. Technol.*, 2021, **51**, 1443–1478.
25 Z. Ferdous and A. Nemmar, *Int. J. Mol. Sci.*, 2020, **21**, 2375.
26 E. Kabir, V. Kumar, K. H. Kim, A. C. K. Yip and J. R. Sohn, *J. Environ. Manage.*, 2018, **225**, 261–271.
27 J. R. Lead, G. E. Batley, P. J. J. Alvarez, M. N. Croteau, R. D. Handy, M. J. McLaughlin, J. D. Judy and K. Schirmer, *Environ. Toxicol. Chem.*, 2018, **37**, 2029–2063.
28 J. Du, J. Tang, S. Xu, J. Ge, Y. Dong, H. Li and M. Jin, *Regul. Toxicol. Pharmacol.*, 2018, **98**, 231–239.
29 S. Jahan, I. B. Yusoff, Y. B. Alias and A. F. B. A. Bakar, *Toxicol. Rep.*, 2017, 4, 211–220.
30 R. Ding, P. Yang, Y. Yang, Z. Yang, L. Luo, H. Li and Q. Wang, *Food Add. Contam.: A*, 2018, **35**, 2052–2061.
31 A. Mackevica, M. E. Olsson and S. F. Hansen, *J. Hazard Mater.*, 2017, **322**, 270–275.
32 A. Mackevica, M. E. Olsson and S. F. Hansen, *J. Nanopart. Res.*, 2018, **20**, 1–11.
33 K. L. Garner, S. Suh and A. A. Keller, *Environ. Sci. Technol.*, 2017, **51**, 5541–5551.
34 Y. Dan, W. Zhang, R. Xue, X. Ma, C. Stephan and H. Shi, *Environ. Sci. Technol.*, 2015, **49**, 3007–3014.
35 H. K. Sung, E. Jo, E. Kim, S.-K. Yoo, J.-W. Lee, P.-J. Kim, Y. Kim and I.-C. Eom, *Chemosphere*, 2018, **209**, 815–822.
36 F. Gallocchio, G. Biancotto, V. Cibin, C. Losasso, S. Belluco, R. Peters, G. Van Bemmel, C. Cascio, S. Weigel, P. Tromp, F. Gobbo, S. Catania and A. Ricci, *J. Agric. Food Chem.*, 2017, **65**, 3767–3774.
37 J. Jiménez-Lamana, J. Wojcieszek, M. Jakubiak, M. Asztemborska and J. Szpunar, *J. Anal. At. Spectrom.*, 2016, **31**, 2321–2329.
38 B. Xiao, Y. Zhang, X. Wang, M. Chen, B. Sun, T. Zhang and L. Zhu, *Environ. Sci. Nano*, 2019, **6**, 3431–3441.
39 J. Wojcieszek, J. Jiménez-Lamana, K. Bierla, M. Asztemborska, L. Ruzik, M. Jarosz and J. Szpunar, *J. Anal. At. Spectrom.*, 2019, **34**, 683–693.
40 A. Sukhanova, S. Bozrova, P. Sokolov, M. Berestovoy, A. Karaulov and I. Nabiev, *Nanoscale Res. Lett.*, 2018, 13.

41 A. Cox, P. Venkatachalam, S. Sahi and N. Sharma, *Plant Physiol. Biochem.*, 2016, 107, 147–163.
42 M. Shakeel, F. Jabeen, S. Shabbir, M. S. Asghar, M. S. Khan and A. S. Chaudhry, *Biol. Trace Elem. Res.*, 2016, 172, 1–36.
43 S. Bettini, E. Boutet-Robinet, C. Cartier, C. Coméra, E. Gaultier, J. Dupuy, N. Naud, S. Taché, P. Grysan, S. Reguer, N. Thieriet, M. Réfrégiers, D. Thiaudière, J. P. Cravedi, M. Carrière, J. N. Audinot, F. H. Pierre, L. Guzylack-Piriou and E. Houdeau, *Sci. Rep.*, 2017, **7**, 40373.
44 C. Beer, R. Foldbjerg, Y. Hayashi, D. S. Sutherland and H. Autrup, *Toxicol. Lett.*, 2012, **208**, 286–292.
45 Y. Choi, H.-A. Kim, K.-W. Kim and B.-T. Lee, *J. Environ. Sci.*, 2018, **66**, 50–60.
46 S. López-Sanz, N. R. Fariñas, R. S. Vargas, R. del C. R. Martín-Doimeadios and A. Ríos, *Talanta*, 2017, **164**, 451–457.
47 R. Sekine, K. Khurana, K. Vasilev, E. Lombi and E. Donner, *Nanotoxicology*, 2015, **9**, 1005–1012.
48 J. Zhang, W. Guo, Q. Li, Z. Wang and S. Liu, *Environ. Sci. Nano*, 2018, 5, 2482–2499.
49 Q. Abbas, B. Yousaf, Amina, M. U. Ali, M. A. M. Munir, A. El-Naggar, J. Rinklebe and M. Naushad, *Environ. Int.*, 2020, **138**, 105646.
50 R. J. Williams, S. Harrison, V. Keller, J. Kuenen, S. Lofts, A. Praetorius, C. Svendsen, L. C. Vermeulen and J. van Wijnen, *Curr. Opin. Environ. Sustain.*, 2019, **36**, 105–115.
51 Y. Li, J. Zhao, E. Shang, X. Xia, J. Niu and J. Crittenden, *Environ. Sci. Technol.*, 2018, **52**, 4842–4849.
52 S. A. Johari, M. Sarkheil, M. B. Tayemeh and S. Veisi, *Chemosphere*, 2018, **209**, 156–162.
53 R. A. D. Lish, S. A. Johari, M. Sarkheil and I. J. Yu, *Environ. Pollut.*, 2019, **255**, 113358.
54 A. Albanese, P. S. Tang and W. C. W. Chan, *Annu. Rev. Biomed. Eng.*, 2012, **14**, 1–16.
55 J. Jiménez-Lamana and V. I. Slaveykova, *Sci. Total Environ.*, 2016, **573**, 946–953.
56 L. M. Furtado, B. C. Norman, M. A. Xenopoulos, P. C. Frost, C. D. Metcalfe and H. Hintelmann, *Environ. Sci. Technol.*, 2015, **49**, 8441–8450.
57 A. Wimmer, A. Urstoeger, N. C. Funck, F. P. Adler, L. Lenz, M. Doeblinger and M. Schuster, *Water Res.*, 2020, **171**, 115399.
58 L. Q. Chen, L. Fang, J. Ling, C. Z. Ding, B. Kang and C. Z. Huang, *Chem. Res. Toxicol.*, 2015, **28**, 501–509.
59 J. Dobias and R. Bernier-Latmani, *Environ. Sci. Technol.*, 2013, **47**, 4140–4146.
60 S. Lekamge, A. F. Miranda, A. Abraham, V. Li, R. Shukla, V. Bansal and D. Nugegoda, *Front. Environ. Sci.*, 2018, **6**, 152.
61 P. Linkov, M. Artemyev, A. E. Efimov and I. Nabiev, *Nanoscale*, 2013, 5, 8781–8798.

62 A. Bour, F. Mouchet, J. Silvestre, L. Gauthier and E. Pinelli, *J. Hazard Mater.*, 2015, **283**, 764–777.
63 D. J. Spurgeon, E. Lahive and C. L. Schultz, *Small*, 2020, **16**, 2000618.
64 S. López-Sanz, F. J. Guzmán Bernardo, R. C. Rodríguez Martín-Doimeadios and Á. Ríos, *Anal. Chim. Acta*, 2019, **1059**, 1–15.
65 A. R. Montoro Bustos, K. P. Purushotham, A. Possolo, N. Farkas, A. E. Vladár, K. E. Murphy and M. R. Winchester, *Anal. Chem.*, 2018, **90**, 14376–14386.
66 S. Motellier, N. Pelissier and J. G. Mattei, *J. Anal. At. Spectrom.*, 2017, **32**, 1348–1358.
67 Y. Chang, Y. Shih, C.-H. Su and H.-C. Ho, *J. Hazard Mater.*, 2017, **322**, 95–104.
68 K. Newman, C. Metcalfe, J. Martin, H. Hintelmann, P. Shaw and A. Donard, *J. Anal. At. Spectrom.*, 2016, **31**, 2069–2077.
69 E. J. Petersen, A. R. Montoro Bustos, B. Toman, M. E. Johnson, M. Ellefson, G. C. Caceres, A. L. Neuer, Q. Chan, J. W. Kemling, B. Mader, K. Murphy and M. Roesslein, *Environ. Sci. Nano*, 2019, **6**, 2876–2896.
70 B. Meermann and V. Nischwitz, *J. Anal. At. Spectrom.*, 2018, **33**, 1432–1468.
71 J. Soto-Alvaredo, M. Montes-Bayón and J. Bettmer, *Anal. Chem.*, 2013, **85**, 1316–1321.
72 Y. Yang, L. Luo, H.-P. Li, Q. Wang, Z.-G. Yang, Z.-P. Qu and R. Ding, *Talanta*, 2018, **182**, 156–163.
73 C. A. Sötebier, S. M. Weidner, N. Jakubowski, U. Panne and J. Bettmer, *J. Chromatogr. A*, 2016, **1468**, 102–108.
74 S. K. Mwilu, E. Siska, R. B. Nasir Baig, R. S. Varma, E. Heithmar and K. R. Rogers, *Sci. Total Environ.*, 2014, **472**, 316–323.
75 A. García-Figueroa, F. Pena-Pereira, I. Lavilla and C. Bendicho, *Talanta*, 2019, **193**, 176–183.
76 T. Tolessa, X.-X. Zhou, M. Amde and J.-F. Liu, *Talanta*, 2017, **169**, 91–97.
77 X. Zhang, Y. Zhang, X. Zhang, S. Li and Y. Huang, *J. Hazard Mater.*, 2017, **337**, 1–9.
78 L. Torrent, F. Laborda, E. Marguí, M. Hidalgo and M. Iglesias, *Anal. Bioanal. Chem.*, 2019, **411**, 5317–5329.
79 L. Li, G. Hartmann, M. Döblinger and M. Schuster, *Environ. Sci. Technol.*, 2013, **47**, 7317–7323.
80 G. Hartmann, C. Hutterer and M. Schuster, *J. Anal. At. Spectrom.*, 2013, **28**, 567–572.
81 C. Degueldre and P.-Y. Favarger, *Anal. Chim. Acta*, 2006, **555**, 263–268.
82 C. Degueldre and P.-Y. Favarger, *Talanta*, 2004, **62**, 1051–1054.
83 C. Degueldre and P.-Y. Favarger, *Anal. Chim. Acta*, 2004, **518**, 137–142.
84 C. Degueldre, P.-Y. Favarger, R. Rossé and S. Wold, *Talanta*, 2006, **68**, 623–628.
85 R. Peters, Z. Herrera-Rivera, A. Undas, M. Van Der Lee, H. Marvin, H. Bouwmeester and S. Weigel, *J. Anal. At. Spectrom.*, 2015, **30**, 1274–1285.
86 P. Shaw and A. Donard, *J. Anal. At. Spectrom.*, 2016, **31**, 1234–1242.

87 F. Laborda, A. C. Gimenez-Ingalaturre, E. Bolea and J. R. Castillo, *Spectrochim. Acta B*, 2020, **169**, 105883.
88 S. Cuello-Nuñez, I. Abad-Álvaro, D. Bartczak, M. E. Del Castillo Busto, D. A. Ramsay, F. Pellegrino and H. Goenaga-Infante, *J. Anal. At. Spectrom.*, 2020, **35**, 1832–1839.
89 K. Flores, R. S. Turley, C. Valdes, Y. Ye, J. Cantu, J. A. Hernandez-Viezcas, J. G. Parsons and J. L. Gardea-Torresdey, *Appl. Spectrosc. Rev.*, 2021, **56**, 1–26.
90 D. M. Schwertfeger, J. R. Velicogna, A. H. Jesmer, S. Saatcioglu, H. McShane, R. P. Scroggins and J. I. Princz, *Anal. Chem.*, 2017, **89**, 2505–2513.
91 Y. Yang, C.-L. Long, H.-P. Li, Q. Wang and Z.-G. Yang, *Sci. Total Environ.*, 2016, **563–564**, 996–1007.
92 L. Li, Q. Wang, Y. Yang, L. Luo, R. Ding, Z.-G. Yang and H.-P. Li, *Anal. Chem.*, 2019, **91**, 9442–9450.
93 D. M. Mitrano, E. K. Lesher, A. Bednar, J. Monserud, C. P. Higgins and J. F. Ranville, *Environ. Toxicol. Chem.*, 2012, **31**, 115–121.
94 A. Wimmer, A. Urstoeger, T. Hinke, M. Aust, P. J. Altmann and M. Schuster, *Anal. Chim. Acta*, 2021, **1150**, 238198.
95 A. Georgantzopoulou, P. Almeida Carvalho, C. Vogelsang, M. Tilahun, K. Ndungu, A. M. Booth, K. V. Thomas and A. Macken, *Environ. Sci. Technol.*, 2018, **52**, 9431–9441.
96 L. Luo, Y. Yang, H. Li, R. Ding, Q. Wang and Z. Yang, *Sci. Total Environ.*, 2018, **612**, 1215–1222.
97 D. M. Schwertfeger, J. R. Velicogna, A. H. Jesmer, R. P. Scroggins and J. I. Princz, *Anal. Chem.*, 2016, **88**, 9908–9914.
98 J. Noireaux, R. Grall, M. Hullo, S. Chevillard, C. Oster, E. Brun, C. Sicard-Roselli, K. Loeschner and P. Fisicaro, *Separations*, 2019, **6**, 6010003.
99 V. Geertsen, E. Barruet, F. Gobeaux, J. L. Lacour and O. Taché, *Anal. Chem.*, 2018, **90**, 9742–9750.
100 H. E. Pace, N. J. Rogers, C. Jarolimek, V. A. Coleman, E. P. Gray, C. P. Higgins and J. F. Ranville, *Environ. Sci. Technol.*, 2012, **46**, 12272–12280.
101 H.-A. Kim, B.-T. Lee, S.-Y. Na, K.-W. Kim, J. F. Ranville, S.-O. Kim, E. Jo and I.-C. Eom, *Chemosphere*, 2017, **171**, 468–475.
102 A. R. Montoro Bustos, E. J. Petersen, A. Possolo and M. R. Winchester, *Anal. Chem.*, 2015, **87**, 8809–8817.
103 F. Laborda, J. Jiménez-Lamana, E. Bolea and J. R. Castillo, *J. Anal. At. Spectrom.*, 2013, **28**, 1220–1232.
104 S. Lee, X. Bi, R. B. Reed, J. F. Ranville, P. Herckes and P. Westerhoff, *Environ. Sci. Technol.*, 2014, **48**, 10291–10300.
105 L. Li, M. Stoiber, A. Wimmer, Z. Xu, C. Lindenblatt, B. Helmreich and M. Schuster, *Environ. Sci. Technol.*, 2016, **50**, 6327–6333.
106 A. Wimmer, R. Ritsema, M. Schuster and P. Krystek, *Sci. Total Environ.*, 2019, **663**, 154–161.
107 F. Laborda, E. Bolea and J. Jiménez-Lamana, *Anal. Chem.*, 2014, **86**, 2270–2278.

108 K. Niemax, *Spectrochim. Acta B.*, 2012, **76**, 65–69.
109 A. Murtazin, S. Groh and K. Niemax, *Spectrochim. Acta B*, 2012, **67**, 3–16.
110 J. W. Olesik and P. J. Gray, *J. Anal. At. Spectrom.*, 2012, **27**, 1143–1155.
111 M. Hadioui, V. Merdzan and K. J. Wilkinson, *Environ. Sci. Technol.*, 2015, **49**, 6141–6148.
112 L. Fréchette-Viens, M. Hadioui and K. J. Wilkinson, *Talanta*, 2019, **200**, 156–162.
113 M. Hadioui, C. Peyrot and K. J. Wilkinson, *Anal. Chem.*, 2014, **86**, 4668–4674.
114 M. Loula, A. Kaňa and O. Mestek, *Talanta*, 2019, **202**, 565–571.
115 O. Geiss, I. Bianchi, G. Bucher, E. Verleysen, F. Brassinne, J. Mast, K. Loeschner, L. Givelet, F. Cubadda, F. Ferraris, A. Raggi, F. Iacoponi, R. Peters, A. Undas, A. Müller, A. K. Meinhardt, B. Hetzer, V. Gräf, A. R. Montoro Bustos and J. Barrero-Moreno, *Nanomaterials*, 2022, **12**, 725.
116 J. Liu, K. E. Murphy, M. R. Winchester and V. A. Hackley, *Anal. Bioanal. Chem.*, 2017, **409**, 6027–6039.
117 R. C. Merrifield, C. Stephan and J. R. Lead, *Talanta*, 2017, **162**, 130–134.
118 M. Aghaei, H. Lindner and A. Bogaerts, *Spectrochim. Acta B*, 2012, **76**, 56–64.
119 M. Vaughan, G. Horlick and S. H. Tan, *J. Anal. At. Spectrom.*, 1987, **2**, 765–772.
120 K. S. Ho, W. W. Lee and W. T. Chan, *J. Anal. At. Spectrom.*, 2015, **30**, 2066–2073.
121 I. Kálomista, A. Kéri and G. Galbács, *Talanta*, 2017, **172**, 147–154.
122 R. Leardi, *Anal. Chim. Acta*, 2009, **652**, 161–172.
123 S. A. Weissman and N. G. Anderson, *Org. Process Res. Dev.*, 2015, **19**, 1605–1633.
124 M. A. Bezerra, R. E. Santelli, E. P. Oliveira, L. S. Villar and L. A. Escaleira, *Talanta*, 2008, **76,** 965–977.
125 I. Abad-Álvaro, E. Peña-Vázquez, E. Bolea, P. Bermejo-Barrera, J. R. Castillo and F. Laborda, *Anal. Bioanal. Chem.*, 2016, **408**, 5089–5097.
126 G. Cornelis and M. Hassellöv, *J. Anal. At. Spectrom.*, 2014, **29**, 134–144.
127 D. Mozhayeva and C. Engelhard, *J. Anal. At. Spectrom.*, 2019, **34**, 1571–1580.
128 R. J. B. Peters, G. van Bemmel, N. B. L. Milani, G. C. T. den Hertog, A. K. Undas, M. van der Lee and H. Bouwmeester, *Sci. Total Environ.*, 2018, **621**, 210–218.
129 M. Tejamaya, I. Römer, R. C. Merrifield and J. R. Lead, *Environ. Sci. Technol.*, 2012, **46**, 7011–7017.
130 NIST Special Publication 1200-21, *Characterization of nanoparticle suspensions using single particle inductively coupled plasma mass spectrometry,* U.S. Department of Commerce, 2015.
131 J. Wan, Y. Kim, M. J. Mulvihill and T. K. Tokunaga, *Environ. Toxicol. Chem.*, 2018, **37**, 1301–1308.
132 M. Faraji, Y. Yamini and M. Gholami, *Chromatographia*, 2019, **82**, 1207–1249.
133 I. López-García, Y. Vicente-Martínez and M. Hernández-Córdoba, *Spectrochim. Acta B.*, 2014, **101**, 93–97.

134 H. El Hadri and V. A. Hackley, *Environ. Sci. Nano*, 2017, **4**, 105–116.
135 P. Cervantes-Avilés, Y. Huang and A. A. Keller, *Water Res.*, 2019, **166**, 115072.
136 L. Fréchette-Viens, M. Hadioui and K. J. Wilkinson, *Talanta*, 2017, **163**, 121–126.
137 H. Agrawaal and J. E. Thompson, *Talanta Open*, 2021, **3**, 100036.
138 U. Kalsoom, P. N. Nesterenko and B. Paull, *TrAC - Trends Anal. Chem.*, 2018, **105**, 492–502.
139 B. Gross, S. Y. Lockwood and D. M. Spence, *Anal. Chem.*, 2017, **89**, 57–70.
140 E. Lahtinen, E. Kukkonen, V. Kinnunen, M. Lahtinen, K. Kinnunen, S. Suvanto, A. Vaïsänen and M. Haukka, *ACS Omega*, 2019, **4**, 16891–16898.
141 E. Lahtinen, L. Turunen, M. M. Hänninen, K. Kolari, H. M. Tuononen and M. Haukka, *ACS Omega*, 2019, **4**, 12012–12017.
142 S. Kulomäki, E. Lahtinen, S. Perämäki and A. Väisänen, *Talanta*, 2022, **240**, 123163.
143 S. Kulomäki, E. Lahtinen, S. Perämäki and A. Väisänen, *Anal. Chim. Acta*, 2019, **1092**, 24–31.
144 J. Frimodig, A. Autio, E. Lahtinen and M. Haukka, *3D Print. Addit. Manuf.*, 2022, DOI: https://doi.org/10.1089/3dp.2021.0063.
145 C. K. Su, M. H. Hsieh and Y. C. Sun, *Anal. Chim. Acta*, 2016, **914**, 110–116.
146 US Patent US9754774B2, *Systems and methods for automated analysis of output in single particle inductively coupled plasma mass spectrometry and similar data sets*, United States Patent and Trademark Office, 2017.
147 W. W. Lee and W. T. Chan, *J. Anal. At. Spectrom.*, 2015, **30**, 1245–1254.
148 S. Kaneco, T. Nomizu, T. Tanaka, N. Mizutani and H. Kawaguchi, *Anal. Sci.*, 1995, **11**, 835–840.
149 G. Zhu and R. F. Browner, *Appl. Spectros.c*, 1987, **41**, 349–359.
150 A. Bogaerts and M. Aghaei, *J. Anal. At. Spectrom.*, 2017, **32**, 233–261.
151 H. Lindner, A. Murtazin, S. Groh, K. Niemax and A. Bogaerts, *Anal. Chem.*, 2011, **83**, 9260–9266.
152 C. C. Garcia, A. Murtazin, S. Groh, V. Horvatic and K. Niemax, *J. Anal. At. Spectrom.*, 2010, **25**, 645–653.
153 J. Fuchs, M. Aghaei, T. D. Schachel, M. Sperling, A. Bogaerts and U. Karst, *Anal. Chem.*, 2018, **90**, 10271–10278.
154 D. C. Montgomery, *Design and Analysis of Experiments*, Wiley, 4th edn., 1996.
155 O. Mestek, M. Loula, A. Kaňa and M. Vosmanská, *Talanta*, 2020, **210**, 120665.
156 L. Li and K. Leopold, *Anal. Chem.*, 2012, **84**, 4340–4349.
157 Bio-Rad Laboratories, *Chelex® 100 and Chelex 20 Chelating Ion Exchange Resin Instruction Manual*, Bio-Rad Laboratories, 2017.
158 Edward Tipping, *Cation Binding by Humic Substances*, Cambridge University Press, New York, 1st ed., 2002.
159 G. Kajner, A. Kéri, Á. Bélteki, S. Valkai, A. Dér, Z. Geretovszky and G. Galbács, *Lab Chip*, 2022, **22**, 2766–2776.

ORIGINAL PAPERS

I

OPTIMIZATION OF INSTRUMENTAL PARAMETERS FOR IMPROVING SENSITIVITY OF SINGLE PARTICLE INDUCTIVELY-COUPLED PLASMA MASS SPECTROMETRY ANALYSIS OF GOLD

by

Virva Kinnunen, Siiri Perämäki & Rose Matilainen 2021

Spectrochimica Acta Part B: Atomic Spectroscopy vol 177, 106104

DOI: 10.1016/j.sab.2021.106104

Spectrochimica Acta Part B: Atomic Spectroscopy 177 (2021) 106104

Contents lists available at ScienceDirect

Spectrochimica Acta Part B: Atomic Spectroscopy

journal homepage: www.elsevier.com/locate/sab

Optimization of instrumental parameters for improving sensitivity of single particle inductively-coupled plasma mass spectrometry analysis of gold

Virva Kinnunen *, Siiri Perämäki, Rose Matilainen

Department of Chemistry, Chemistry in Circular Economy, University of Jyväskylä, P.O. Box 35, FI-40014 Jyväskylä, Finland

ARTICLE INFO

Keywords:
SpICP-MS
Instrumental parameters
Nanoparticles
Optimization
Matrix effect

ABSTRACT

Single particle inductively-coupled plasma mass spectrometry (spICP-MS) is a promising technique for analysis of engineered nanoparticles, whose utilization has increased substantially over the past years. Optimization of instrumental conditions is, however, crucial to improve the sensitivity and precision of nanoparticle (NP) detection. In this study, the influence of ICP-MS instrumental parameters (nebulizer gas flow, plasma radiofrequency-power and sampling depth) on the signal intensity of gold in spICP-MS was evaluated using dispersions of Au NPs and a solution of dissolved gold. The interaction effects of the main factors were found to have a significant effect on the signal intensity, proving that factor values should be jointly optimized instead of one at a time, if maximum ion signal is expected. Optimization of instrumental parameter values was performed for both analyte forms and found to be in a good agreement, indicating a similar behavior of the particles in plasma compared with the dissolved analyte. However, some differences in the behavior of the two analyte forms as regard to sampling depth position was observed. Particle size or the presence of complex sample matrix was not found to influence the optimal instrumental parameter values, however, a significant signal depression for gold was observed (up to 50%) in matrices containing high levels of sodium. Compared to frequently used 'robust conditions', a 70% increase in the ion signal intensity of gold and a 15% decrease in the particle size detection limit was achieved with instrumental parameter optimization. As such, instrumental parameter optimization for sensitive NP analysis can be seen as highly beneficial procedure.

1. Introduction

The remarkable advancements made in the field of nanotechnology have incorporated engineered nanomaterials (ENMs) into our everyday lives. The unique and tunable properties of ENMs have enabled the development of exciting new innovations, which are changing our way to diagnose and treat diseases, produce and store energy and cultivate our lands [1–3]. However, the increasing production of nano-enhanced products has raised concerns about the potential negative effects of these materials on the environment and human health [4–8].

In order to understand the potential impact of nanomaterials on to the environment and human health, it is crucial to characterize these materials carefully. As engineered nanoparticles are produced in various sizes, shapes and with different elemental compositions and surface functionalities, all of which might influence their behavior and effects in the environment [5,6,9,10], characterization of nanoparticles (NPs) can be done in numerous ways. However, as nanomaterial definition is based on size [11], the determination of NP size and number size distribution can be seen as one of the most important parameters to be determined. Several methods are available for NP size characterization, such as microscopic (transmission and scanning electron microscopy (TEM, SEM)), fractionation (hydrodynamic chromatography (HDC) and field-flow fractionation (FFF)) and ensemble methods (dynamic light scattering (DLS) and small-angle X-ray scattering (SAXS)). However, many of the current methods are not well suited for environmental samples [12–15]. The challenge with many currently used methods is that they lack the method sensitivity required for analysis of environmental samples with low NP concentration or may require tedious sample preparation steps, which might lead to sample alteration [13–16].

Single particle inductively-coupled plasma mass spectrometry (spICP-MS) is considered as one of the most promising methods for the determination of NPs, as it is able to overcome many limitations faced with other techniques [17–20]. Compared to other techniques, spICP-MS holds some advantages for NP analysis in environmental samples. Thanks to its sensitivity, spICP-MS enables the measurement of NP size,

* Corresponding author.
E-mail address: virva.v-t.kinnunen@jyu.fi (V. Kinnunen).

https://doi.org/10.1016/j.sab.2021.106104
Received 29 October 2020; Received in revised form 22 January 2021; Accepted 22 January 2021
Available online 30 January 2021

number size distribution, particle number concentration and ionic content at realistic environmental concentrations [17]. In addition, water samples can be analyzed without any sample preparation, which minimizes the risk of altering the state of the NPs. Compared with e.g. microscopic techniques, spICP-MS can provide information of relatively high number of particles in a short period of time (e.g. ≤60s). However, even though particle concentration detection limits in spICP-MS-technique are low (e.g. 100 p/mL) [21], particle size detection limits (LOD_{size}) are often >10 nm for monoisotopic NPs and > 100 nm for oxides [22]. Considering that in the European Commission Recommendation (2011/696/EU) the term 'nanomaterial' is defined as a material containing particles having at least one external dimension in the size range 1–100 nm [11], improving the LOD_{size} can be considered as one of the most important aspects in developing this technique.

The smallest detectable particle size in spICP-MS is determined by the smallest pulse height that can be distinguished from the background and depends mostly on the detection efficiency of the instrument. As such, in terms of lowering the LOD_{size}, improving the ionization conditions and the ion sampling efficiency is crucial. As particles are introduced into the ICP as single droplets, a process of droplet solvation, particle vaporization, atomization and ionization begins [17,23]. As a result, an ion cloud is formed, which diameter will increase as it progresses in the plasma central channel before it is sampled at the sampler orifice. The intensity of the NP signal depends on the relative distance of the ion sampling position (sampler orifice) and the point, where particles start to vaporize. If the signal is measured too early, when vaporization is not complete, the signal will be low. On the other hand, if the signal is measured too late, diffusion losses will be significant, resulting in a decrease in the signal intensity [23–25]. As such, an optimum ion sampling position exists, where ionization has reached its maximum and diffusion losses do not play an effect.

Ionization degree and diffusion losses are affected by particle residence time in the plasma, which is known to be influenced by instrumental parameters, such as nebulizer gas flow, plasma radiofrequency (RF)-power, injector inner diameter (injector i.d.) and sampling depth [23–31]. The optimum value of these parameters depends on a number of factors, including e.g. ionization potential of the element and the boiling point of the corresponding oxide, the size of the introduced droplets and particles and the sample matrix [23,26,29–33]. As such, optimization of instrumental parameters for precise and sensitive NP analysis is crucial. Even though the importance of optimizing instrumental parameters in solution ICP-MS is well-known [32,34–37], the effect of instrumental conditions in spICP-MS are far less studied. In ICP-MS measurements, instrument software's pre-programmed tuning protocols are frequently used for parameter adjustment, which aim to maximize ion signal while minimizing interferences (i.e. 'robust' operation conditions). However, as these protocols are not designed for NP analysis, the adjusted parameters can differ significantly from the optimal values. To the best of our knowledge, only a few articles have focused on studying the effects of instrumental parameters on spICP-MS results. Ho et al. [29] studied the effect of sampling depth values to the intensity of Au and ZrO_2 NPs. Similar optimal sampling depth values were found for dissolved Au and relatively small Au NPs (≤150 nm), however the longer vaporization time of 250 nm Au and 80 nm ZrO_2 NPs resulted in a shift in the optimal sampling depth value as compared to the dissolved analyte. Recently, Kálomista et al. [28] reported that the LOD_{size} for Au and Ag NPs could be significantly improved (25–30%) compared with robust conditions by sampling depth optimization.

As highlighted by Mozhayeva and Engelhard in a recently published review article [38], optimization of instrumental parameters is crucial in order to improve the sensitivity and precision of NP detection. The most critical parameters to optimize are plasma RF-power, sampling depth and nebulizer gas flow, as these are known to affect the ion signal significantly. In addition, the possible effect of the sample matrix and particle size to the optimum conditions should be considered [23,26,29–33]. The traditional optimization method is called as one factor at a time (OFAT) approach, where the optimum value for each factor is determined by varying the value of each factor one at a time [39]. Even though relatively simple to perform, OFAT approach can produce misleading results as it cannot consider any interaction between factors [40]. However, in spICP-MS the effects of instrumental parameters are known to depend on other parameter values (i.e. interaction effects) [25,26], which should be taken into account in optimization studies. This can be achieved by using a design of experiments (DoE) approach, in which the values of factors are varied together allowing one to estimate possible interaction effects between the factors [39,40].

To the best of our knowledge, publications addressing the effects and mutual interactions of plasma RF-power, sampling depth and nebulizer gas flow on spICP-MS analysis do not exist. Hence, the objective of this paper was to optimize these ICP-MS instrumental conditions using a DoE approach. Since gold is one of the most common analytes in spICP-MS, it was selected as the analyte of interest and instrumental parameters for both particulate and dissolved gold were optimized, enabling the comparison between the two. The influence of these parameters on the intensity of particulate and dissolved gold was evaluated in order to assess if dissolved gold could be used in instrument parameter optimization for spICP-MS analysis. The obtained optimum instrumental conditions, as well as the effect on the LOD_{size}, were compared with the robust conditions. Additionally, the possible effect of particle size and sample matrix on optimum instrumental parameter values was evaluated.

2. Experimental

2.1. Materials and methods

2.1.1. Optimization and verification measurements

For optimization measurements, ultra-uniform PEG Carboxyl-stabilized Au NPs with nominal diameter of 50 nm and a solution of dissolved (ionic) gold were used. Au NPs were purchased from PerkinElmer Inc. (Massachusetts, USA) and diluted to a particle concentration of approximately 10^5 particles/g with ultrapure water (resistivity of 18.2 MΩ·cm, PURELAB Ultra, ELGA LabWater, Buckinghamshire, UK). Dissolved gold solution was prepared from a standard stock solution of 100 μg mL^{-1} Au in 2% HCl (Pure Plus, PerkinElmer Inc.) by dilution in ultrapure water to a concentration of 1 μg kg^{-1} and its stability was routinely checked during measurements. Even though dissolved standard solutions are often acidified to improve the analyte stability in the solution [41,42], only ultrapure water was used in all cases for sample dilutions. This allowed the evaluation of the possible differences in the behavior of the two analyte forms, without the risk of incorporating any matrix-induced effects.

For verification of the LOD_{size} under robust and optimal conditions, 20 nm citrate-stabilized (NanoComposix, San Diego, CA, USA) and 30 nm PEG Carboxyl-stabilized (PerkinElmer, Inc.) Au NPs were used. The particle frequency method described by Pace et al. [18] was used to determine the transport efficiency (TE-%) in triplicate using a diluted 50 nm Au NP suspension (PerkinElmer Inc.). All nano-dispersions were diluted to a particle concentration of approximately 10^5 particles/g with ultrapure water. The sample uptake rate was measured in duplicate by weighing the water uptake after 3 min aspiration, and its value was regularly checked during the measurements.

In order to evaluate the possible effects of particle size or sample matrix to the optimal instrumental parameter values, PEG Carboxyl-stabilized Au NPs with nominal diameters of 30, 50 and 100 nm and a solution of dissolved gold (PerkinElmer Inc.) were used. All nano-dispersions were diluted to a particle concentration of approximately 10^5 particles/g and dissolved gold to a concentration 1 μg kg^{-1} with either ultrapure water, 1 mM sodium citrate solution (Sodium Citrate Tribasic Dihydrate from Sigma Aldrich, Darmstad, Germany) or outgoing wastewater. Wastewater was obtained from a municipal wastewater treatment plant located in Central Finland and filtrated with Whatman grade 41 filtration paper before use to remove any solid

material, that might cause blockage of the sample introduction system. Elemental composition of the wastewater used in the experiments was determined with inductively-coupled plasma optical emission spectrometer (PerkinElmer Optima 8300DV ICP-OES) and is presented in Table S1 (Appendix).

All solutions used in the experiments were diluted gravimetrically using new 50 mL polypropylene centrifuge tubes (VWR International) fresh on a daily basis prior to the experiments.

2.1.2. Particle size verification measurements

The certified sizes of the Au NPs used in the experiments were verified in our laboratory (Table S2, Appendix), as at times the standard particle diameters have shown to deviate from the information provided by the manufacturer [12,41,43,44]. Even though microscopic techniques (SEM, TEM) are the common routes used for particle size verification [41,45], the high method detection limit of these techniques made verification of the standard particles with low particle concentration (≈10^7 particles/mL) impossible. As such, the particle diameters of the PEG Carboxyl-stabilized Au NPs used in the experiments were verified with spICP-MS technique by using citrate-stabilized Au NPs with nominal diameters of 30 and 50 nm (NanoComposix) as a reference. The diameter of these particles was verified with TEM (JEM-1400HC, JEOL, MA, USA) and found to be in good agreement with the values provided by the manufacturer (Table S2, Appendix). The mean particle sizes of the PEG Carboxyl-stabilized Au NPs was found to differ ≤3% from the certified values provided by the manufacturer and were use throughout the study.

2.2. Equipment and softwares

A NexION350 D ICP-MS (PerkinElmer Inc., MA, USA) was used in all measurements. Analyses of the NP samples were performed operating the spectrometer in a time-resolved analysis mode using a dwell time of 100 μs, whereas solution mode was used for measurements of the dissolved analyte. General instrumental parameters are shown in Table 1. All data processing was performed using the Syngistix Nano Application Module (v. 2.5) and Microsoft Excel. The isotope ^{197}Au was measured. Minitab 19 software (Minitab, PA, USA) was used for analyzing the experimental data, solving the optimal instrumental parameters and generation of the surface plots.

For measurements performed under 'robust' conditions, a NexION Setup Solution (1 μg L^{-1} Be, Ce, Fe, In, Li, Mg, Pb, and U in 1% HNO_3, Pure Plus, PerkinElmer) was used to adjust the equipment according to instrument software's tuning protocols (maximum sensitivity with CeO^+/Ce^+-level <2.5%) and to check the overall performance. For measurements performed under 'optimal' conditions, the value of nebulizer gas flow was optimized to gain maximum ^{197}Au intensity. Due to the slight day-to-day variations of the instrument condition, the value of nebulizer gas flow was adjusted on a daily basis.

Table 1
Instrumental parameters used in solution ICP-MS and spICP-MS.

	Value[1]	
Parameter	ICP-MS, solution mode	spICP-MS
ICP RF-power (W)	1200–1600 (1000–1600)	1200–1600
Nebulizer gas flow (L min^{-1})	0.90–1.06 (0.80–1.18)	0.90–1.06
Plasma gas flow rate (L min^{-1})	16	16
Auxiliary gas flow rate (L min^{-1})	1.2	1.2
Spray chamber	Baffled Cyclonic, Glass (cooled to 2 °C)	Baffled Cyclonic, Glass (cooled to 2 °C)
Nebulizer	ESI PFA Concentric	ESI PFA Concentric
Injector	1.8 mm i.d. Sapphire	1.8 mm i.d. Sapphire
Sampling depth (mm)	9–12 (9–14)	9–12
Dwell time	50 ms	100 μs
Sampling time (s)		30–60
Transport efficiency (%)		7.48–7.53
Sample uptake rate (g min^{-1})		0.284–0.291

[1] Values shown in brackets used in initial optimization measurements (see Section 3.1).

2.3. Experimental design

The influence of ICP-MS instrumental parameters on the intensity of ^{197}Au was investigated using a DoE approach. Experiments were designed using a general factorial design (GFD), which allows the studied factors to have various, independent levels [39]. Nebulizer gas flow (*A*), plasma RF-power (*B*) and sampling depth (*C*) were chosen as the independent variables and the intensity of gold (^{197}Au) was the response variable (*Y*) measured.

The variables and their levels used for generating the regression models are shown in Table S3 (Appendix). All measurements were performed in a randomized order, except for nebulizer gas flow, to minimize the effect of any uncontrolled factors [46]. Due to a high number of measurements, nebulizer gas flow values were changed from low to high values in all cases in order to save time. Two replicates divided into two blocks were measured in order to increase the precision of the final predictive model. In addition, one experimental point was measured at the beginning and at the end of the 1st and 2nd block, in order to estimate the possible effect of instrumental drift on the response. A total of $2 \times 9 \times 3 \times 3 + 2 = 164$ measurements were performed in this study for both particulate and dissolved gold. The detailed experimental plan and the obtained results are shown in Tables S4 and S5 (Appendix) for particulate and dissolved gold, respectively.

2.4. Statistical analysis

Minitab 19 software was used to analyze the experimental data according to the response surface analysis and to generate surface plots. A second-order polynomial equation was fitted to the experimental data, which is used to express the relationship between the response and the variables. The generalized second-order model has the following form (1):

$$y = \beta_0 + \sum_{i=1}^{k} \beta_i x_i + \sum_{i=1}^{k} \beta_{ii} x_i^2 + \sum \sum_{i<j}^{k} \beta_{ij} x_i x_j + \varepsilon \quad (1)$$

where y is the response (intensity of ^{197}Au), k is the number of variables, x represents the variables, β_0 is the constant term, β_i is the coefficient of the linear parameter, β_{ii} is the coefficient of the quadratic parameter, β_{ij} is the coefficient of the interaction parameters and ε is observed error in the response [39]. Minitab 19 software's response optimization feature was used to solve the optimal instrumental parameters for maximum ^{197}Au response for both particulate and dissolved gold.

3. Results and discussion

3.1. Initial optimization experiments

In the beginning of the study, initial optimization experiments of ICP-MS instrumental conditions were carried out using a solution of dissolved gold (1 μg kg^{-1}). To investigate the influence of ICP-MS instrumental parameters on ^{197}Au intensity, a wide experimental domain was at first monitored (Table 1): plasma RF-power values 1000–1600 W, nebulizer gas flow values 0.80–1.18 L min^{-1} and sampling depth values 9–14 mm, resulting in 400 measurements. During the initial optimization experiments, two main observations were made. First, complex interaction effects between the main factors (nebulizer gas flow, plasma RF-power and sampling depth) were noticed. Secondly, the signal intensity proved to be low at high sampling depth values (>12 mm) and at low plasma RF-value (1000 W). Consequently, a GFD was

chosen to design the experiments using the factor values shown in Table S3 (Appendix). Even though the use of response surface methods with a limited number of measurements are generally more popular approaches in optimization studies, in this case they were found inadequate in describing the changes in the response variable. As in GFD all levels of each factor are combined with all levels of other factors studied, it provides a more detailed description of the change in the response variable in accordance with the variables studied.

3.2. Fitting a second-order polynomial equation and model adequacy checking

To relate the measured intensity to the variables, a second-order polynomial model was fitted to the data according to Eq. (1). In order to improve the model for operating conditions, the statistically insignificant terms were automatically removed using a backward elimination process available in Minitab 19 software. This procedure automatically excludes certain terms from the regression model, which are not found to have statistically significant impact on the response at the chosen 95% confidence level (i.e., variables with P-values <0.05). For both forms of the analyte, the interaction effect of plasma power (*B*) and sampling depth (*C*) was found statistically insignificant at the 95% confidence level. In addition, no statistically significant difference was found between the two blocks, indicating that the results obtained for the two replicates were in good agreement. As such, these variables were removed from the final regression models.

The significance of the final fitted regression models, main factors and their interactions was evaluated on the basis of analysis of variance (ANOVA), which are presented in Tables S6 and S7 (Appendix) for particulate and dissolved gold, respectively. The statistical significance of the different terms was evaluated using the corresponding P-values, with 95% confidence level as the chosen significance level (P = 0.05). The resulting models have large F-values (287.68 for particulate and 335.05 for dissolved gold) and P-values < 0.05, indicating that the models are able to explain the observed variation in the response and can be used to optimize the conditions. In the final models, the main and quadratic effects of the studied variables (nebulizer gas flow (*A*), plasma RF-power (*B*) and sampling depth (*C*) and A^2, B^2 and C^2) were found to have significant effects on the response (intensity of ^{197}Au) for both particulate and dissolved gold. Of the two-level interaction terms, the interaction effect of nebulizer gas flow and plasma RF-power (*A**B*) and nebulizer gas flow and sampling depth (*A**C*) were found statistically significant at the 95% confidence level.

For testing the goodness of fit of the regression equations, the R-values were evaluated. For both of the models, R^2-and adjusted R^2-values are >93% indicating a good agreement between experimental and predicted values. The models' ability to predict the responses for the new observations accurately can be estimated on the basis of R^2(pred.)-value, which in this case were high for both models; >92%. The P-value for the lack-of-fit is >0.05, indicating that the proposed models are able to specify the relationship between the response and the variables correctly. Model assumption checks and the main effects plots for both models are presented in Figs. S1–S4 (Appendix).

The final predictive equations obtained for the particulate and dissolved gold in uncoded units were obtained as follows:

Particulate gold:

$$Y(counts) = -3217 + 9411A - 1.899B - 13.2C - 7604A^2 - 0.000192B^2 - 10.071C^2 + 2.5117A*B + 198.3A*C \quad (2)$$

Dissolved gold:

$$Y(counts) = 1\,745\,603 + 5\,070\,025A - 998.6B + 12\,810C - 4\,090\,912A^2 - 0.1255B^2 - 5422C^2 + 1417.0A*B + 94\,268A*C \quad (3)$$

where Y is the intensity of ^{197}Au (in counts), A is the nebulizer gas flow (L min^{-1}), B is the plasma RF-power (W) and C is the sampling depth (mm).

3.3. Effect of instrumental parameters on Au intensity

The obtained second-order polynomial equations presented in the previous section (Eqs. (2) and (3)) were used for generating response surface plots (Fig. 1A–F), which can be used to investigate the effect of instrumental parameters on the response. In each surface plot, the value of one variable is kept fixed at a constant value, allowing one to consider the effects of the other two variables. In order to evaluate the behavior of the two analyte forms under optimal instrumental conditions, in each surface plot the value of the 3rd variable was kept fixed at its predicted optimal value (as determined in Section 3.4).

In Fig. 1A and B the effect of nebulizer gas flow and plasma RF-power on the measured intensity of particulate and dissolved gold is presented. In order to evaluate the behavior of the two analyte forms under the optimal instrumental conditions (as determined in Section 3.4), the value of sampling depth is kept fixed at its predicted optimal value (11.0/10.0 mm for particulate and dissolved gold, respectively). High similarity in the surface plots can be seen, indicating a similar behavior of both forms of the analyte as the factor values are changed. Clearly, the interaction effect of these two variables has a major effect on the intensity value of gold and the overall effect of changing one factor value is highly dependent on the value of the other variable. As expected, the measured intensity generally increases when using higher power values due to higher ionization efficiency of the analyte [27,34–36,47]. However, due to a significant interaction effect of the two variables, the optimal value of nebulizer gas flow depends on the applied power (and vice versa). As plasma power is increased, the optimal flow shifts to larger values due to changes in plasma characteristics [36,47]. The value of nebulizer gas flow is known to influence analyte transport through plasma and the axial plasma temperature, thus affecting the analyte residence time in the plasma. As the value of nebulizer gas flow is increased, the maximum temperature of the plasma central channel decreases and the atomization position will shift downstream the plasma closer to the sampler cone orifice [26,36,47,48]. If a low nebulizer gas flow value is used, increasing the plasma RF-power will cause the sample to ionize immediately after entering the plasma, i.e., at a position distant from the sampler orifice resulting to diffusion losses and a decrease in signal intensity [23,24,26,30,47]. For both forms of the analyte, at the given sampling depth value, the maximum intensity values can be found at plasma RF-power 1600 W and nebulizer gas flow value of 1.01–1.03 L min^{-1}.

The interaction effect of nebulizer gas flow and sampling depth can be investigated from Fig. 1C and D for particulate and dissolved gold, respectively. In both cases, plasma RF-power is held constant at its predicted optimal value of 1600 W. For both forms of the analyte, a general increase in the intensity is observed as larger values of nebulizer gas flow are used, with optimal area found at flow rates >1 L min. Even though decreasing the sampling depth position generally results in an increase in the intensity at low nebulizer gas flow values (≈<1 L min^{-1}), at higher gas flow rates the optimal value of sampling depth is shifted to larger values. This is because as the value of nebulizer gas flow is increased, the ionization degree of the analyte decreases as the interaction time of the analyte with the hot plasma decreases [23,26,36,47]. As a consequence, in order to compensate the temperature drop caused by a larger volume of gas injected, longer residence time (i.e. sampling depth) is needed for complete vaporization and ionization [23,25,26,30]. For both forms of the analyte, highest intensity values are found at nebulizer gas flow values >1 L min^{-1} and at sampling depth

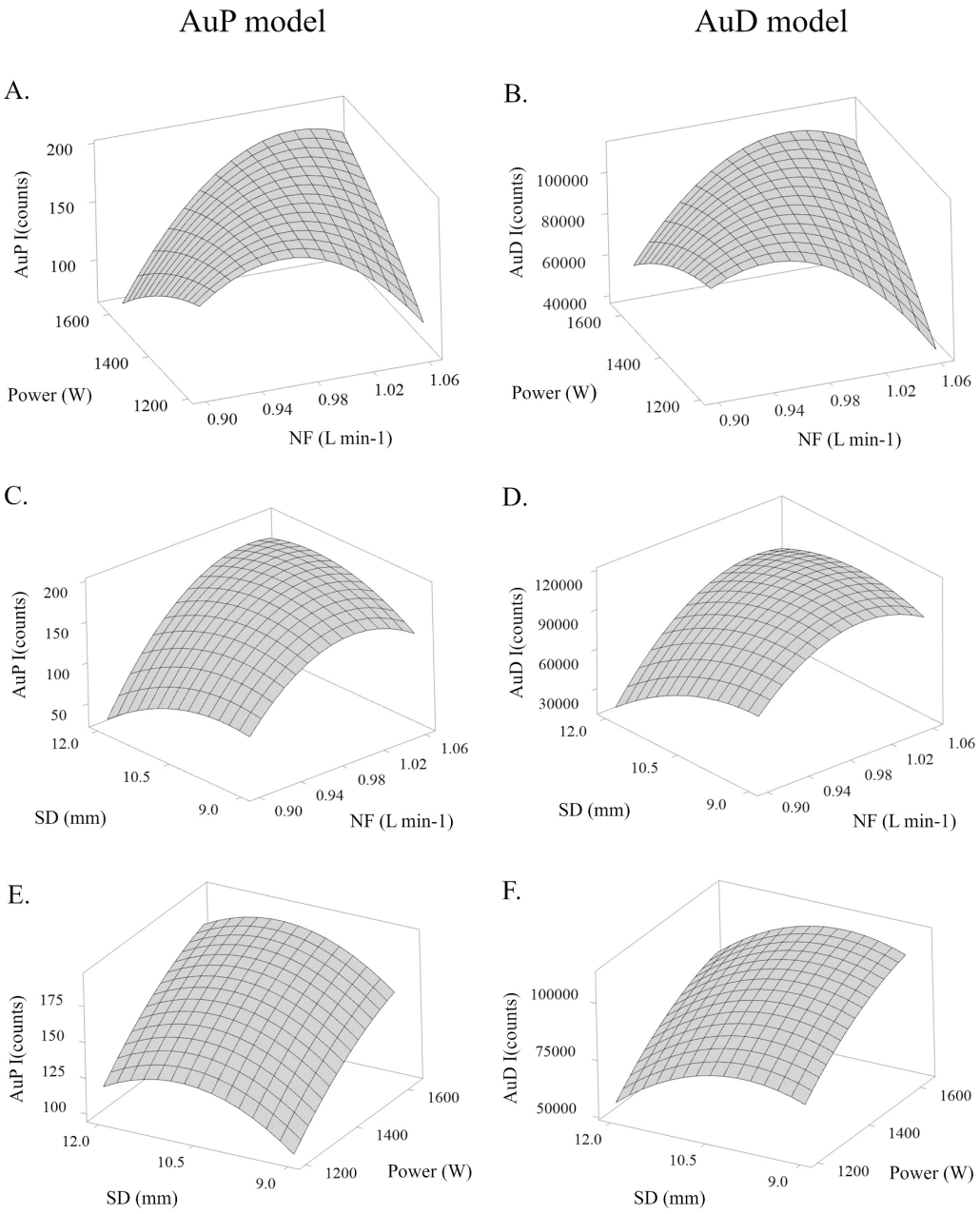

Fig. 1. Response surface plots showing the individual and interaction effects of A, B) Nebulizer gas flow (NF, L min^{-1}) and RF-power (power, W); C, D) Nebulizer gas flow (L min^{-1}) and sampling depth (SD, mm) and E, F) RF-power (W) and sampling depth (mm) on the measured intensity of gold. In each surface plot, one variable is kept constant as follows (for particulate/dissolved gold): Nebulizer gas flow 1.03/1.01 L min^{-1}, RF-power 1600 W and sampling depth 11.0/10.0 mm. Response surface plots for particulate gold (AuP) are shown on the left, and for dissolved gold (AuD) on the right side of the figure. (For interpretation of the references to colour in this figure legend, the reader is referred to the web version of this article.)

values 10–11 mm.

When comparing the response surface plots drawn for particulate and dissolved gold (Fig. 1C and D), high similarity in the graphs can be seen. However, some minor differences as regard to the effect of the sampling depth position can be observed. For dissolved gold, at the vicinity of maximum intensity area (Fig. 1D, at nebulizer gas flow rates $\geq$1 L min^{-1}), only minor differences in the intensity are observed at sampling depth range 9–11 mm. However, a decrease in intensity is observed for particulate gold as the value of sampling depth is decreased <10 mm. It seems that the intensity of particulate gold is somewhat more dependent on the effect of these two variables. As discussed before, increasing the nebulizer gas flow value has the effect of decreasing plasma temperature and increasing analyte velocity through plasma, thus shifting the point of atomization closer to sampler cone orifice [26,36,48]. As particles are expected to require longer time for complete vaporization and atomization [23,26,33,47,49], larger sampling depth

values might be required for efficient ionization. In addition, as sampling depth is increased, the temperature of the plasma has shown to increase [29,31], leading to an increase in the ionization degree.

The difference in the behavior of the two analyte forms as regard to the sampling depth position can be more clearly seen in Fig. 1E and F, where the interaction effect of plasma RF-power and sampling depth is presented. The value of nebulizer gas flow is kept fixed at its predicted optimum value (at 1.03/1.01 L min^{-1} for particulate and dissolved gold, respectively). For both forms of the analyte, increasing plasma RF-power results to a significant increase in the intensity value independent on the applied sampling depth position. However, the value of sampling depth position has clearly different effect on the intensity of the two analyte forms. Whereas for dissolved gold decreasing the sampling depth value generally results in an increase in the intensity value, for particulate gold the intensity is observed to decrease. In contrast to dissolved gold, the highest intensity values for particulate gold are found at slightly larger sampling depth values (11 mm as contrast to 10 mm). This might be because of the longer residence time needed for complete vaporization and atomization of the particles, as discussed previously. However, as can be seen in Fig. 1F, only minor differences are observed in the intensity of dissolved gold at the sampling depth range 9–11 mm.

Based on the obtained results, the interaction effects of the main variables clearly have a significant effect on the intensity of gold for particulate and dissolved gold. As the overall effect of adjusting instrumental parameter values is dependent on other parameter values, careful optimization of factors is crucial if maximum ion signal is expected. For both forms of the analyte, the highest intensity values can be achieved by using high plasma RF-power (1600 W) and sampling depth value of 10–11 mm. For a given plasma RF-power and sampling depth value, a narrow area of optimal nebulizer gas flow value is found, as already noticed for solution ICP-MS [34,35]. Deviation from the optimal values could result in a loss of intensity and thus increase in the LOD_{size}.

When comparing the response surfaces generated for particulate and dissolved gold, high similarity between the graphs can be seen. However, regarding the sampling depth position, some minor differences in the behavior of particulate and dissolved gold was observed. As the vaporization and ionization of the particles require somewhat longer times as compared to the dissolved analyte [23,26,33,47,49], the optimal sampling depth value for Au NPs was found at slightly higher values (11 mm as compared to 10 mm). However, as seen in Fig. 1D and F, adjusting the sampling depth position at the range of 9–11 mm was not found to impact the intensity of dissolved gold to a large extend. As such, the predicted optimal instrumental parameters can be expected to be similar for Au NPs and dissolved gold with some minor differences in the optimal sampling depth positions.

3.4. Optimization of instrumental parameters

The predicted optimal instrumental parameters for the measurement of particulate and dissolved gold were solved with Minitab 19 software's response optimizer feature, which automatically solves the optimal set of parameter values producing the maximum responses of Eqs. (2) and (3) (see Section 3.2). The predicted optimal instrumental parameter values were as follows (for particulate/dissolved gold): nebulizer gas flow value 1.03/1.01 L min^{-1}, plasma RF-power 1600 W and sampling depth 11.0/10.0 mm. In order to verify the optimal instrumental conditions, the intensities of both particulate and dissolved gold were measured under the predicted optimal conditions and the obtained experimental intensities were compared with the predicted values (Table S8, Appendix). Even though the optimization and verification measurements were performed on different days and as such were susceptible to the day-to-day variation in the general intensity level, the obtained values were observed to differ <9% from the predicted values. In addition, as the measured intensities fell under the 95% prediction interval (represents the range of values where a single new observation is likely to fall with 95% confidence), the acquired regression models can be concluded to be reasonably accurate for predicting the ^{197}Au intensity with optimized instrumental parameters for both forms of the analyte.

As regard to the predicted optimal values of sampling depth and nebulizer gas flow rate, slight differences are found for particulate and dissolved gold. However, as discussed before and seen on Fig. 1D and F, at plasma power 1600 W, the predicted differences in the intensity of dissolved gold at the sampling depth range of 9–11 mm are expected to be small and thus could be attributed to the uncertainty of the regression model. As such, an additional experiment was performed in order to verify the optimal values for sampling depth and nebulizer gas flow and to evaluate the effect of the different experimental conditions. The intensity of particulate and dissolved gold was thus measured at sampling depth positions 9–12 mm (with an increment of 1 mm) with plasma power set to its optimal value of 1600 W. As already discussed in Section 3.3 and seen in Fig. 1 C and D, the optimal value of nebulizer gas flow is highly dependent on the applied sampling depth position. As such, in order to find the maximum intensity at different conditions, the value of nebulizer gas flow was separately optimized for every sampling depth position. Measurements were performed in triplicate in a randomized order to minimize the effect of any uncontrollable factors on the results. The detailed experimental plan and the obtained results are presented in Tables S9 and S10 (Appendix), respectively, and displayed in Fig. 2.

As can be seen in Fig. 2, for both forms of the analyte the highest intensity values are obtained at sampling depth position of 11.0 mm. As the sampling depth position is altered from the optimum value, the intensity value is observed to decrease up to 10%. However, especially for dissolved gold, the differences in the intensities between sampling depth positions 10 and 11 mm are found to be extremely small (<5%), which could explain the observed differences in the predicted optimal instrumental parameter values for the two analyte forms. For particulate gold however, as already seen in Fig. 1C, the optimal sampling depth value range is more narrow and decreasing the SD value <11 mm results up to a 10% decrease in the intensity.

When comparing to robust conditions (i.e. conditions where nebulizer gas flow was adjusted to gain maximum ^{115}In sensitivity and $CeO^+/$

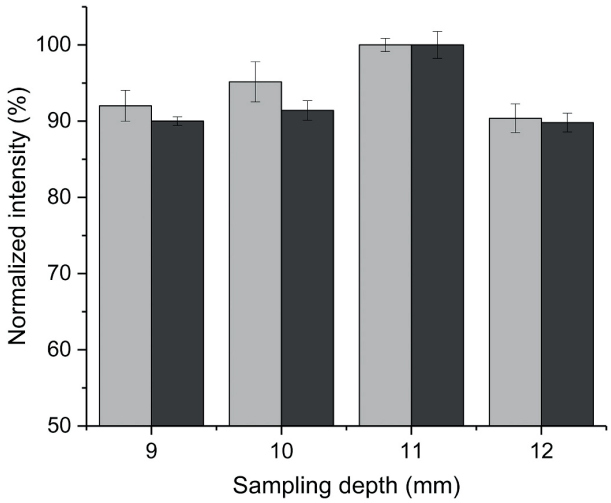

Fig. 2. The obtained maximum intensity of particulate (dark grey bars) and dissolved (light grey bars) gold at different sampling depth positions, presented as mean of three replicate measurements ± relative standard deviation (σ_r). At each sampling depth position, the measured intensity is presented as normalized intensity (%) against the obtained highest intensity value over the entire region, which for both forms of the analyte is obtained at sampling depth value of 11.0 mm. (For interpretation of the references to colour in this figure legend, the reader is referred to the web version of this article.)

Ce^+ <2.5%), the optimization of instrumental parameters resulted in an increase in the nebulizer gas flow value. One should note that as the instrumental parameter values are changed, interferences arising from oxides and double-charged ions should be considered. For some analytes, such as Ti and Fe, these plasma- and/or sample matrix-based interferences can have a severe impact on the accuracy of the results, and the use of collision or reaction gases (e.g. He, NH_3) for interference elimination might be needed [50,51]. However, in the case of analysis of Au NPs from environmental samples, the influence of these interferences (mainly $^{181}Ta^{16}O^+$) can be seen as insignificant. Decreasing sampling depth value from the robust setting (11 mm) was not found to improve the ion signal. This is somewhat in contrast to results obtained by Kálomista et al. [28], who found that NP signal can be significantly improved by sampling depth optimization (from 10 mm to 4 mm). The differences in the findings could arise from differences in instrumental configurations (e.g. sample introduction system) or, more likely, from the chosen optimization method. When optimization of sampling depth is performed by keeping all other instrumental parameter values fixed at a constant value, the interaction effects of the factors cannot be considered. Using this approach, the intensity of both forms of the analyte was found to increase as the value of sampling depth was decreased [28]. This is consistent with our findings at low nebulizer gas flow values (<1 L min^{-1}, see Fig. 1 C and D). However, due to interaction effects of the factors observed in this study, the true maximum intensity values were found at higher nebulizer gas flow (>1 L min^{-1}) and sampling depth values.

3.5. Effect of optimization on instrument sensitivity and on size detection limits

As discussed in Section 1, LOD_{size} (calculated as the particle size equivalent of three times the standard deviation of the blank of the particle calibration plot [17,18,52]) could be significantly improved by careful optimization of instrumental parameters. In order to evaluate the effect of instrumental parameter optimization to instrument sensitivity and LOD_{size}, particle calibration in the range 0–100 nm under optimized and robust conditions was performed and presented in Fig. S5 (Appendix). Under the optimized instrumental conditions, a significant (70%) increase in the instrument sensitivity was observed as compared to robust conditions, which translates in to a 16% decrease in the theoretical size detection limit, $LOD_{size(Theor.)}$ (from 10.4 nm to 8.7 nm). It should however be noted, that instrument software's Nano Application module was used to automatically calculate the $LOD_{size(Theor.)}$, where the smallest observed pulse intensity originating from particles is converted to particle mass and diameter using a calibration curve. The threshold limit used to discriminate the particle signals from the background signal is determined using an iterative 'mean+3σ' computation [53]. However, as the theoretical $LOD_{size(Theor.)}$ is calculated based on the measured intensities of the calibration blank, highly optimistic values are often obtained and at times some manual adjustment is required. During the measurements under this study, intensity values ≤2 counts with mean of ≈ 0 counts were obtained for the calibration blanks, resulting to a particle threshold of just 1 count. As such, particle intensity threshold limit was manually increased to 3 counts, converting to adjusted $LOD_{size(Adj.)}$ values of 13 and 15 nm under optimal and robust conditions, respectively.

In order to verify the estimated LOD_{size} values obtained under the different instrumental conditions, Au NPs with nominal diameter of 20 nm was measured in triplicate under optimal and robust conditions. The in-lab verified diameter of this particle is 18.9±1.9 (Table S2, Appendix), i.e., practically at the LOD_{size}. The obtained particle size frequency distribution for one of the replicates under optimal and robust conditions is presented in Fig. 3. For comparison purposes, measurements were performed also for 30 nm PEG-Carboxyl-stabilized Au NP. The obtained experimental results for the NPs under different conditions were compared as regard to particle concentration yield and particle size

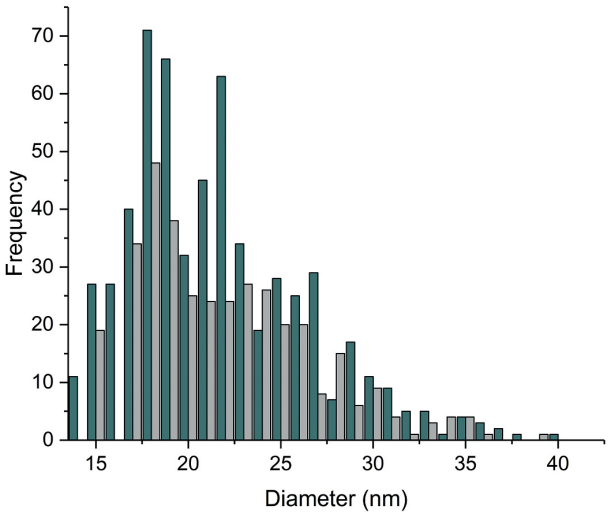

Fig. 3. Obtained particle size frequency distribution graph for 20 nm Au NP under optimal (green bars) and robust (grey bars) conditions. Instrumental parameters were set as follows (for optimal/robust conditions): Plasma RF-power 1600 W/1600 W; nebulizer gas flow 1.02/0.93 L min^{-1} and plasma sampling depth 11/11 mm. (For interpretation of the references to colour in this figure legend, the reader is referred to the web version of this article.)

and presented in Table S11 (Appendix). Under optimal instrumental conditions, the determined particle diameter was closer to the expected value and a 20% increase in the particle concentration yield was observed as compared to robust conditions. The higher particle concentration yield achieved under the optimal instrumental conditions results from the significantly increased sensitivity, allowing more particles to be detected over the background signal. However, under both conditions particle concentration yields <30% were obtained. When comparing the obtained results for the 30 nm Au NP under optimal and robust conditions, no significant differences are observed and particle concentration yields of 101% were achieved. This indicates that the experimental results obtained for particles <30 nm should be interpreted with caution, as low particle concentration recoveries might occur.

Clearly, the determination of small particles near the LOD_{size} is challenging and estimation of the particle concentration near this value should be done with caution. Even though optimization of instrumental parameters resulted in a significant increase in instrument sensitivity and thus in decrease in the LOD_{size}, low particle concentration yields were achieved for the 20 nm Au NPs under both conditions. The determination of particle concentration of particles with diameters close to the LOD_{size} is problematic, as the LOD_{size} cannot be interpreted as straightforward as in solution mode ICP-MS (i.e., concentrations >LOD visible and <LOD unvisible). The same observation was made recently by Mastek et al. [54], who reported particle concentration yields as low as 5% for particles with diameters close to the LOD_{size}. The reason why small particles near the LOD_{size} behave in such unexpected manner, remained unclear. According to some authors [41,52,54,55], particle size or surface could affect the transport efficiency value, which could in part explain the observed results. However, in this paper, these factors were not studied further. More research concerning the detection of small particles and the factors affecting the accuracy of the results is clearly needed.

3.6. Effect of particle size and matrix

As already discussed in Section 1, the sample matrix and sample mass could lead to differences in the optimal instrumental conditions. This is

because these are shown to affect the plasma characteristics and the required particle residence time in the plasma [33,56,57]. As larger particles require more time for complete atomization, under certain instrumental conditions incomplete ionization could occur, especially if low sampling depth values are used. This could cause the measured intensity to be lower than expected and thus lead to non-linear calibration curves [23,25,30,31]. In addition, the sample matrix could affect the position, where analyte atomization begins, by cooling the plasma locally or by affecting the introduced droplet size. As the time needed for complete desolvation of larger droplets is found to be longer, they penetrate deeper into ICP and thus the point of the analyte atomization is shifted closer to the sampler orifice [26,56].

As such, the sample matrix and particle size could affect the optimal instrumental parameter values and the linearity of the particle calibration curve. To investigate the possible effect of particle size and sample matrix to the optimal sampling depth values, the intensity of particulate (30 nm and 100 nm) and dissolved gold was measured in several matrices at different sampling depth positions: ultrapure water, wastewater and 1 mM trisodium citrate solution (TSC). The elemental composition of the wastewater matrix used in the experiments is presented in Table S1 (Appendix). Measurements were performed using a nebulizer gas flow value optimized for sampling depth 11.0 mm at RF-power 1600 W. The results are presented in Fig. 4 A–C and in supplementary material (Table S12 and Fig. S6, Appendix).

As the results show, the signal behavior of particulate and dissolved gold is highly similar, as shown already in Section 3.3 and noticed by other research groups as well [28–30], indicating that optimal instrumental conditions are in fact the same for both forms of the analyte. Matrix is not found to affect the behavior of the two analyte forms in different extents, and in all cases the largest intensity values are found at sampling depth value 11.0 mm for both particulate and dissolved gold. In addition, the behavior of the different sized particles (30 and 100 nm) is highly similar and no differences are observed in the optimal sampling depth position. This indicates that vaporization even of the larger particles (100 nm) under the experimental conditions had reached its maximum in all of the studied matrices. Interestingly, even though no differences were observed in the behavior of different forms of the analyte as regard to the sampling depth position, some differences were found between the matrices. Whereas in ultrapure water and in TSC solution the intensity of both forms of the analyte is observed to decrease up to 50% as sampling depth is increased from 11 mm to 14 mm, only 40% decrease is observed in the wastewater matrix. This might be because the ionization of the various elements present in wastewater (Table S1, Appendix) consume plasma energy, shifting the position of atomization closer to the sampler cone orifice and thus minimizing the diffusion losses [26,56].

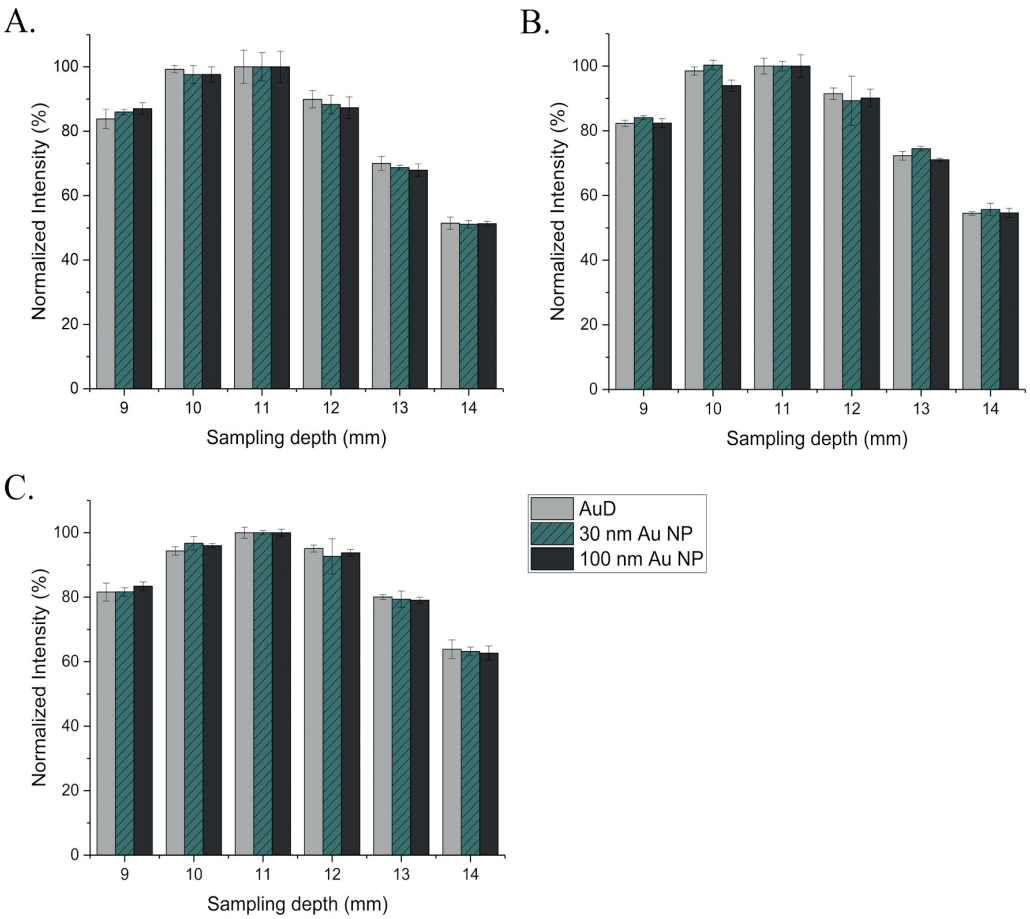

Fig. 4. The intensity of particulate (30 and 100 nm Au NP) and dissolved gold (AuD) in different matrices as a function of sampling depth, presented as mean of three replicate measurements ± relative standard deviation (σ_r). Results are normalized to the highest intensity value (100%). A) Ultrapure water, B) 1 mM Trisodium citrate solution and C) Wastewater. Light grey: Dissolved gold (AuD), green with diagonal lines: 30 nm Au NP and dark grey: 100 nm Au NP. Measuring parameters were set as follows (for particulate/dissolved gold): Plasma RF-power 1600 W/1600 W and nebulizer gas flow 1.02 L min^{-1}/1.01 L min^{-1}. (For interpretation of the references to colour in this figure legend, the reader is referred to the web version of this article.)

When comparing the obtained intensity values (Table S12 and Fig. S6, Appendix) in the different matrices, a significant signal depression in the wastewater and TSC matrices as compared to ultrapure water is observed. For both forms of the analyte, up to a 50% decrease in the intensities is observed in the wastewater matrix. In the TSC matrix, intensities were found to decrease up to 25% as compared to ultrapure water, however, only for particulate gold. The observed signal depression is most likely caused by the high level of sodium present in these matrices (70 mg L^{-1} in TSC solution and 180 mg L^{-1} in wastewater). Sodium is a known source of non-spectral interferences in spICP-MS-measurements, which' depressive effect is shown to increase with increasing concentration [58,59], consistent with our findings. As no significant signal depression was found for dissolved gold in TSC solution, it can be assumed, that the intensity of particulate gold is more affected by the matrix elements. It should be noted that differences in the sensitivities between particulate and dissolved analyte could lead to biased results, if dissolved calibration curve is used to determine particle size or transport efficiency. As such, the effect of sample matrix should be investigated in the early stages of method development process. Sample dilution or matrix matching between the sample and standard solutions can be used as a means to avoid systematic errors. However, is some cases these procedures cannot be applied or are found insufficient, as would be the case if the two analyte forms are affected by the matrix elements in different extends. Clearly, the matrix interferences are one of the remaining challenges in the spICP-MS-technique requiring more research in the future.

As discussed before, under certain instrumental conditions incomplete ionization or diffusion losses of the different-sized particles could occur. This could lead to non-linear particle calibration curves, as in spICP-MS particle calibration is based on a fact that measured intensity is directly proportional to the mass of an element [17]. As such, the effect of particle size on the linearity of the calibration curve under the optimized instrumental conditions in the range 0–100 nm was studied and presented in Fig. S5 (Appendix). As calibration was found to be linear over the studied range, it can be concluded, that for $\leq$100 nm particles vaporization has reached its maximum at the instrumental conditions used and no clear indication of diffusion losses of the smaller particles can be seen. However, larger particles ($\geq$100 nm) might not vaporize completely at the instrumental conditions used, which should be considered if large (>100 nm) particles are analyzed.

4. Conclusions

In this paper, the optimization of spICP-MS instrumental parameters was performed using a DoE approach for particulate and dissolved gold, enabling the evaluation of the behavior of the two analyte forms as the factor values are changed. The variables studied were nebulizer gas flow, plasma RF-power and sampling depth, as these are known to affect the ion signal most. Results show that significant interaction effects between the main factors exists and clearly have a major effect on the intensity of gold for both forms of the analyte. As the overall effect of a parameter is highly dependent on other parameter values, changing the value of one parameter can result in a loss of intensity, if the other variables are not re-optimized. As such, traditional OFAT approaches are not suitable for spICP-MS optimization, as they cannot estimate the interaction of the factors and thus can produce misleading results.

In order to assess the possible differences in the behavior of the two analyte forms, the effect of instrument parameter values on the intensity of particulate and dissolved gold was evaluated. High similarity in the behavior of both forms of analyte in accordance with the variables was noticed, indicating that dissolved analyte can in fact be used in method optimization. Compared with nano-dispersions, the possibility to use dissolved analyte offers some benefits, such as better stability of the standard solutions and faster measurements. However, as regard to the effect of sampling depth position, some minor differences in the behavior of the analyte forms was observed. For dissolved gold at the vicinity of optimal conditions (plasma RF-power 1600 W and nebulizer gas flow values >1 L min^{-1}) adjusting the value of sampling depth had only minor effects on the intensity. However, as a result of longer residence time needed for efficient atomization, the intensity of particulate gold was observed to decrease at lower sampling depth positions.

The optimal instrumental parameters were solved and verified for both forms of the analyte and were as follows: Plasma RF-power 1600 W, sampling depth 11.0 mm and nebulizer gas flow 1.01–1.03 L min^{-1}. Due to the slight day-to-day variation of the instrument condition (e.g. the cleanliness of the sample introduction system), the optimal nebulizer gas flow value should however be routinely checked and re-optimized if necessary. One should note that optimal instrumental parameter values are analyte and instrument-specific, and should be optimized in the early stages of a method development process. In addition, the possible interferences caused by oxide- and double charged ions should be considered, especially in the case of more challenging analytes such as Fe and Ti.

The influence of instrument parameter optimization on the LOD_{size} was evaluated. Compared with robust conditions often used, instrument sensitivity was improved by 70% and LOD_{size} by approximately 15% (from 15 nm to 13 nm). Even though more particles were detected under optimal conditions as a result of significantly increased sensitivity, particle concentration yields <30% were achieved for particles with diameter close to the LOD_{size}. Clearly, the determination of small particles near the LOD_{size} value is challenging and estimation of particle concentration needs to be made with caution. The same observation has been made by other authors as well, indicating that more research on determination of small particles near LOD_{size} is urgently needed.

Finally, the influence of solution matrix and particle size to the optimal instrumental parameter values was studied. Neither particle size nor sample matrix was observed to influence the optimal instrumental conditions, indicating that the behavior of both forms of analyte is highly similar and even the larger particles ionize completely under the instrumental conditions used. However, due to the high level of sodium (180 mg L^{-1}) present in the wastewater matrix, a significant signal depression (up to 50%) for both particulate and dissolved gold was observed in the wastewater matrix as compared to ultrapure water. Similarly, up to a 25% decrease in the intensity was observed in the TSC solution, however, only for particulate gold. It seems that particulate gold is more susceptible to matrix effects, as the intensity of dissolved gold was not affected in the TSC solution containing 70 mg L^{-1} of sodium. As sodium is a common element present in both biological and environmental samples, its effect on analyte sensitivity should be investigated and care should be taken to match the sample and standard solution matrices to avoid systematic errors.

Declaration of Competing Interest

The authors declare that they have no known competing financial interests or personal relationships that could have appeared to influence the work reported in this paper.

Acknowledgements

This work was supported by the University of Jyväskylä (Finland), Department of Chemistry. Sini Reuna and Joona Rajahalme are greatly appreciated for their helpful comments regarding the manuscript and discussions regarding the experimental results.

Appendix A. Supplementary data

Supplementary data to this article can be found online at https://doi.org/10.1016/j.sab.2021.106104.

References

[1] M.C. Roco, C.A. Mirkin, M.C. Hersam, Nanotechnology research directions for societal needs in 2020: summary of international study, J. Nanopart. Res. 13 (2011) 897–919, https://doi.org/10.1007/s11051-011-0275-5.

[2] European Chemicals Agency (ECHA), European Union Observatory for Nanomaterials, (n.d.). https://euon.echa.europa.eu/ (accessed February 7, 2020).

[3] Project on Emerging Nanotechnologies. Consumer Products Inventory. (n.d.) http://www.nanotechproject.org/cpi/, 2013s, (accessed April 7, 2020).

[4] E.A.J. Bleeker, S. Evertz, R.E. Geertsma, W.J.G. Peijnenburg, J. Westra, S.W. P. Wijnhoven, Assessing Health & Environmental Risks of Nanoparticles, Report No. 2014-0157, National Institute for Public Health and the Environment, Bilthoven, The Netherlands, 2015.

[5] J.R. Lead, G.E. Batley, P.J.J. Alvarez, M.N. Croteau, R.D. Handy, M.J. McLaughlin, J.D. Judy, K. Schirmer, Nanomaterials in the environment: behavior, fate, bioavailability, and effects—an updated review, Environ. Toxicol. Chem. 37 (2018) 2029–2063, https://doi.org/10.1002/etc.4147.

[6] E. Kabir, V. Kumar, K.H. Kim, A.C.K. Yip, J.R. Sohn, Environmental impacts of nanomaterials, J. Environ. Manag. 225 (2018) 261–271, https://doi.org/10.1016/j.jenvman.2018.07.087.

[7] K. Savolainen, H. Alenius, H. Norppa, L. Pylkkänen, T. Tuomi, G. Kasper, Risk assessment of engineered nanomaterials and nanotechnologies-a review, Toxicology 269 (2010) 92–104, https://doi.org/10.1016/j.tox.2010.01.013.

[8] K.L. Garner, S. Suh, A.A. Keller, Assessing the risk of engineered nanomaterials in the environment: development and application of the nanoFate model, Environ. Sci. Technol. 51 (2017) 5541–5551, https://doi.org/10.1021/acs.est.6b05279.

[9] A. Albanese, P.S. Tang, W.C.W. Chan, The effect of nanoparticle size, shape, and surface chemistry on biological systems, Annu. Rev. Biomed. Eng. 14 (2012) 1–16, https://doi.org/10.1146/annurev-bioeng-071811-150124.

[10] A.L. Dale, E.A. Casman, G.V. Lowry, J.R. Lead, E. Viparelli, M. Baalousha, Modeling nanomaterial environmental fate in aquatic systems, Environ. Sci. Technol. 49 (2015) 2587–2593, https://doi.org/10.1021/es505076w.

[11] The European Commission, Off. J. Eur. Union 696, 2011, pp. 38–40.

[12] A.R. Montoro Bustos, K.P. Purushotham, A. Possolo, N. Farkas, A.E. Vladár, K. E. Murphy, M.R. Winchester, Validation of single particle ICP-MS for routine measurements of nanoparticle size and number size distribution, Anal. Chem. 90 (2018) 14376–14386, https://doi.org/10.1021/acs.analchem.8b03871.

[13] Y.-J. Chang, Y.-H. Shih, C.-H. Su, H.-C. Ho, Comparison of three analytical methods to measure the size of silver nanoparticles in real environmental water and wastewater samples, J. Hazard. Mater. 322 (2017) 95–104, https://doi.org/10.1016/j.jhazmat.2016.03.030.

[14] K. Tiede, M. Hassellöv, E. Breitbarth, Q. Chaudhry, A.B.A. Boxall, Considerations for environmental fate and ecotoxicity testing to support environmental risk assessments for engineered nanoparticles, J. Chromatogr. A 1216 (2009) 503–509, https://doi.org/10.1016/j.chroma.2008.09.008.

[15] F. Laborda, E. Bolea, G. Cepriá, M.T. Gómez, M.S. Jiménez, J. Pérez-Arantegui, J. R. Castillo, Detection, characterization and quantification of inorganic engineered nanomaterials: a review of techniques and methodological approaches for the analysis of complex samples, Anal. Chim. Acta 904 (2016) 10–32, https://doi.org/10.1016/j.aca.2015.11.008.

[16] M. Hassellöv, J.W. Readman, J.F. Ranville, K. Tiede, Nanoparticle analysis and characterization methodologies in environmental risk assessment of engineered nanoparticles, Ecotoxicology. 17 (2008) 344–361, https://doi.org/10.1007/s10646-008-0225-x.

[17] F. Laborda, E. Bolea, J. Jiménez-Lamana, Single particle inductively coupled plasma mass spectrometry: a powerful tool for nanoanalysis, Anal. Chem. 86 (2014) 2270–2278, https://doi.org/10.1021/ac402980q.

[18] H.E. Pace, N.J. Rogers, C. Jarolimek, V.A. Coleman, C.P. Higgins, J.F. Ranville, Determining transport efficiency for the purpose of counting and sizing nanoparticles via single particle inductively coupled plasma mass spectrometry, Anal. Chem. 83 (2011) 9361–9369, https://doi.org/10.1021/ac201952t.

[19] D.M. Mitrano, E.K. Lesher, A. Bednar, J. Monserud, C.P. Higgins, J.F. Ranville, Detecting nanoparticulate silver using single-particle inductively coupled plasma-mass spectrometry, Environ. Toxicol. Chem. 31 (2012) 115–121, https://doi.org/10.1002/etc.719.

[20] F. Laborda, E. Bolea, J. Jiménez-Lamana, Single particle inductively coupled plasma mass spectrometry for the analysis of inorganic engineered nanoparticles in environmental samples, Trends Environ. Anal. Chem. 9 (2016) 15–23, https://doi.org/10.1016/j.teac.2016.02.001.

[21] F. Laborda, J. Jiménez-Lamana, E. Bolea, J.R. Castillo, Critical considerations for the determination of nanoparticle number concentrations, size and number size distributions by single particle ICP-MS, J. Anal. At. Spectrom. 28 (2013) 1220–1232, https://doi.org/10.1039/c3ja50100k.

[22] S. Lee, X. Bi, R.B. Reed, J.F. Ranville, P. Herckes, P. Westerhoff, Nanoparticle size detection limits by single particle ICP-MS for 40 elements, Environ. Sci. Technol. 48 (2014) 10291–10300, https://doi.org/10.1021/es502422v.

[23] J.W. Olesik, P.J. Gray, Considerations for measurement of individual nanoparticles or microparticles by ICP-MS: determination of the number of particles and the analyte mass in each particle, J. Anal. At. Spectrom. 27 (2012) 1143–1155, https://doi.org/10.1039/c2ja30073g.

[24] M.P. Dziewatkoski, L.B. Daniels, J.W. Olesik, Time-resolved inductively coupled plasma mass spectrometry measurements with individual, monodisperse drop sample introduction, Anal. Chem. 68 (1996) 1101–1109, https://doi.org/10.1021/ac951013b.

[25] K. Niemax, Considerations about the detection efficiency in inductively coupled plasma mass spectrometry, Spectrochim. Acta Part B At. Spectrosc. 76 (2012) 65–69, https://doi.org/10.1016/j.sab.2012.06.027.

[26] A. Murtazin, S. Groh, K. Niemax, Investigation of sample introduction- and plasma-related matrix effects in inductively coupled plasma spectrometry applying single analyte droplet and particle injection, Spectrochim. Acta Part B At. Spectrosc. 67 (2012) 3–16, https://doi.org/10.1016/j.sab.2011.12.003.

[27] S. Kaneco, T. Nomizu, T. Tanaka, N. Mizutani, H. Kawaguchi, Optimization of operating conditions in individual airborne particle analysis by inductively coupled plasma mass spectrometry, Anal. Sci. 11 (1995) 835–840, https://doi.org/10.2116/analsci.11.835.

[28] I. Kálomista, A. Kéri, G. Galbács, Optimization of plasma sampling depth and aerosol gas flow rates for single particle inductively coupled plasma mass spectrometry analysis 172, 2017, pp. 147–154, https://doi.org/10.1016/j.talanta.2017.05.051.

[29] K.S. Ho, W.W. Lee, W.T. Chan, Effects of ionization potential of an element and boiling point of the corresponding oxide on the sensitivity of ICP-MS, J. Anal. At. Spectrom. 30 (2015) 2066–2073, https://doi.org/10.1039/c5ja00137d.

[30] W.W. Lee, W.T. Chan, Calibration of single-particle inductively coupled plasma-mass spectrometry (SP-ICP-MS), J. Anal. At. Spectrom. 30 (2015) 1245–1254, https://doi.org/10.1039/c4ja00408f.

[31] K.S. Ho, K.O. Lui, K.H. Lee, W.T. Chan, Considerations of particle vaporization and analyte diffusion in single-particle inductively coupled plasma-mass spectrometry, Spectrochim. Acta Part B At. Spectrosc. 89 (2013) 30–39, https://doi.org/10.1016/j.sab.2013.08.012.

[32] F. Vanhaecke, R. Dams, C. Vandecasteele, "Zone model" as an explanation for signal behaviour and non-spectral interferences in inductively coupled plasma mass spectrometry, J. Anal. At. Spectrom. 8 (1993) 433–438, https://doi.org/10.1039/JA9930800433.

[33] C.C. Garcia, A. Murtazin, S. Groh, V. Horvatic, K. Niemax, Characterization of single Au and SiO2 nano- and microparticles by ICP-OES using monodisperse droplets of standard solutions for calibration, J. Anal. At. Spectrom. 25 (2010) 645–653, https://doi.org/10.1039/b921041e.

[34] M. Vaughan, G. Horlick, S.H. Tan, Effect of operating parameters on analyte signals in inductively coupled plasma mass spectrometry, J. Anal. At. Spectrom. 2 (1987) 765–772, https://doi.org/10.1039/JA9870200765.

[35] G. Zhu, R.F. Browner, Investigation of experimental parameters with a quadrupole ICP/MS, Appl. Spectrosc. 41 (1987) 349–359, https://doi.org/10.1366/0003702874448869.

[36] M. Aghaei, H. Lindner, A. Bogaerts, Optimization of operating parameters for inductively coupled plasma mass spectrometry: a computational study, Spectrochim. Acta Part B At. Spectrosc. 76 (2012) 56–64, https://doi.org/10.1016/j.sab.2012.06.006.

[37] A.L. Gray, J.G. Williams, System optimisation and the effect on polyatomic, oxide and doubly charged ion response of a commercial inductively coupled plasma mass spectrometry instrument, J. Anal. At. Spectrom. 2 (1987) 81–82, https://doi.org/10.1039/JA9870200081.

[38] D. Mozhayeva, C. Engelhard, A critical review of single particle inductively coupled plasma mass spectrometry – a step towards an ideal method for nanomaterial characterization, J. Anal. At. Spectrom. (2019), https://doi.org/10.1039/c9ja00206e.

[39] D.C. Montgomery, Design and Analysis of Experiments, 7th ed., Wiley, 2009.

[40] S.A. Weissman, N.G. Anderson, Design of Experiments (DoE) and Process Optimization. A Review of Recent Publications 19, Org. Process Res. Dev., 2015, pp. 1605–1633, https://doi.org/10.1021/op500169m.

[41] V. Geertsen, E. Barruet, F. Gobeaux, J.L. Lacour, O. Taché, Contribution to accurate spherical gold nanoparticle size determination by single-particle inductively coupled mass spectrometry: a comparison with small-angle X-ray scattering, Anal. Chem. 90 (2018) 9742–9750, https://doi.org/10.1021/acs.analchem.8b01167.

[42] M.D. Montaño, J.W. Olesik, A.G. Barber, K. Challis, J.F. Ranville, Single particle ICP-MS: advances toward routine analysis of nanomaterials, Anal. Bioanal. Chem. 408 (2016) 5053–5074, https://doi.org/10.1007/s00216-016-9676-8.

[43] J. Liu, K.E. Murphy, R.I. Maccuspie, M.R. Winchester, Capabilities of single particle inductively coupled plasma mass spectrometry for the size measurement of nanoparticles: a case study on gold nanoparticles, Anal. Chem. 86 (2014) 3405–3414, https://doi.org/10.1021/ac403775a.

[44] R.C. Merrifield, C. Stephan, J.R. Lead, Single-particle inductively coupled plasma mass spectroscopy analysis of size and number concentration in mixtures of monometallic and bimetallic (core-shell) nanoparticles, Talanta. 162 (2017) 130–134, https://doi.org/10.1016/j.talanta.2016.09.070.

[45] S. Gschwind, M.D.L. Aja Montes, D. Günther, Comparison of sp-ICP-MS and MDG-ICP-MS for the determination of particle number concentration, Anal. Bioanal. Chem. 407 (2015) 4035–4044, https://doi.org/10.1007/s00216-015-8620-7.

[46] M. Shivhare, G. McCreath, Practical considerations for DoE implementation in quality by design, Bioprocess Int. 8 (2010) 22–30.

[47] A. Bogaerts, M. Aghaei, Inductively coupled plasma-mass spectrometry: insights through computer modeling, J. Anal. At. Spectrom. 32 (2017) 233–261, https://doi.org/10.1039/c6ja00408c.

[48] H. Lindner, A. Murtazin, S. Groh, K. Niemax, A. Bogaerts, Simulation and experimental studies on plasma temperature, flow velocity, and injector diameter effects for an inductively coupled plasma, Anal. Chem. 83 (2011) 9260–9266, https://doi.org/10.1021/ac201699q.

[49] J. Fuchs, M. Aghaei, T.D. Schachel, M. Sperling, A. Bogaerts, U. Karst, Impact of the particle diameter on ion cloud formation from gold nanoparticles in ICPMS, Anal. Chem. 90 (2018) 10271–10278, https://doi.org/10.1021/acs.analchem.8b02007.

[50] S. Candás-Zapico, D.J. Kutscher, M. Montes-Bayón, J. Bettmer, Single particle analysis of TiO2 in candy products using triple quadrupole ICP-MS, Talanta. 180 (2018) 309–315, https://doi.org/10.1016/j.talanta.2017.12.041.
[51] J.G. Fernández, C. Sánchez-González, J. Bettmer, J. Llopis, N. Jakubowski, U. Panne, M. Montes-Bayón, Quantitative assessment of the metabolic products of iron oxide nanoparticles to be used as iron supplements in cell cultures, Anal. Chim. Acta 1039 (2018) 24–30, https://doi.org/10.1016/j.aca.2018.08.003.
[52] K. Newman, C. Metcalfe, J. Martin, H. Hintelmann, P. Shaw, A. Donard, Improved single particle ICP-MS characterization of silver nanoparticles at environmentally relevant concentrations, J. Anal. At. Spectrom. 31 (2016) 2069–2077. doi:https://doi.org/10.1039/c6ja00221h.
[53] S. Bazargan, R. Hill, H. Badiei, Systems and methods for automated analysis of output in single particle inductively coupled plasma mass spectrometry and similar data sets, US 9, 754,774 B2, 2017.
[54] O. Mestek, M. Loula, A. Kaňa, M. Vosmanská, Can ultrafast single-particle analysis using ICP-MS affect the detection limit? Case study: silver nanoparticles, Talanta. 210 (2020) 120665, https://doi.org/10.1016/j.talanta.2019.120665.
[55] J. Liu, K.E. Murphy, M.R. Winchester, V.A. Hackley, Overcoming challenges in single particle inductively coupled plasma mass spectrometry measurement of silver nanoparticles, Anal. Bioanal. Chem. 409 (2017) 6027–6039, https://doi.org/10.1007/s00216-017-0530-4.
[56] S. Groh, C.C. Garcia, A. Murtazin, V. Horvatic, K. Niemax, Local effects of atomizing analyte droplets on the plasma parameters of the inductively coupled plasma, Spectrochim. Acta Part B At. Spectrosc. 64 (2009) 247–254, https://doi.org/10.1016/j.sab.2009.02.008.
[57] M. Guillong, D. Günther, Effect of particle size distribution on ICP-induced elemental fractionation in laser ablation-inductively coupled plasma-mass spectrometry, J. Anal. At. Spectrom. 17 (2002) 831–837, https://doi.org/10.1039/b202988j.
[58] M. Loula, A. Kaňa, O. Mestek, Non-spectral interferences in single-particle ICP-MS analysis: an underestimated phenomenon, Talanta. 202 (2019) 565–571, https://doi.org/10.1016/j.talanta.2019.04.073.
[59] R. Peters, Z. Herrera-Rivera, A. Undas, M. Van Der Lee, H. Marvin, H. Bouwmeester, S. Weigel, Single particle ICP-MS combined with a data evaluation tool as a routine technique for the analysis of nanoparticles in complex matrices, J. Anal. At. Spectrom. 30 (2015) 1274–1285, https://doi.org/10.1039/c4ja00357h.

II

SOLID PHASE EXTRACTION MATERIALS AS A KEY FOR IMPROVING THE ACCURACY OF SILVER NANOPARTICLE CHARACTERIZATION WITH SINGLE-PARTICLE INDUCTIVELY COUPLED PLASMA MASS SPECTROMETRY IN NATURAL WATERS THROUGH DISSOLVED SILVER REMOVAL

by

Virva Kinnunen, Siiri Perämäki & Rose Matilainen 2022

Spectrochimica Acta Part B: Atomic Spectroscopy vol 193, 106431

DOI: 10.1016/j.sab.2022.106431

Spectrochimica Acta Part B: Atomic Spectroscopy 193 (2022) 106431

Contents lists available at ScienceDirect

Spectrochimica Acta Part B: Atomic Spectroscopy

journal homepage: www.elsevier.com/locate/sab

Solid phase extraction materials as a key for improving the accuracy of silver nanoparticle characterization with single-particle inductively coupled plasma mass spectrometry in natural waters through dissolved silver removal

Virva Kinnunen *, Siiri Perämäki, Rose Matilainen

Department of Chemistry, Chemistry in Circular Economy, University of Jyväskylä, P.O. Box 35, FI-40014 Jyväskylä, Finland

ARTICLE INFO

Keywords:
SpICP-MS
Silver nanoparticles
SPE materials
Dissolved silver interference

ABSTRACT

The accurate characterization of silver nanoparticles (Ag NPs) in environmental samples is crucial for understanding the potential impact of these materials on the environment and human health. Single-particle inductively coupled plasma mass spectrometry (spICP-MS) is one of the few techniques available for quantifying NPs at environmentally relevant concentrations. However, the spICP-MS detection of Ag NPs can be interfered with coexisting dissolved analyte causing high background signals, which mask NP signals leading to a significant bias in NP characterization. In this paper, a simple sample pre-treatment procedure for efficient removal of dissolved silver in natural waters is proposed using solid phase extraction (SPE) materials, allowing more accurate characterization of NPs in environmental water matrices. The applicability of eight commercially available SPE materials was evaluated based on their effects on sample Ag NP properties and dissolved silver extraction efficiency in environmental waters, which were shown to depend on sample matrix. The SPE materials found most efficient in dissolved silver extraction were further studied for improving the characterization of 30 nm Ag NPs in colorless and dark-colored waters. Whereas dissolved silver concentrations of $\leq$1 μg kg^{-1} were shown to lead to a significant bias in NP characterization (up to +58% increase in NP size and − 90% decrease in particle concentration), pre-treatment of the samples with SPE materials 'SiliaMetS Thiol' and 'Purolite C115HMR' minimized the effect of dissolved silver interference. As a result, highly more accurate NP sizing (28 ± 2 nm) and relatively stable particle concentration was obtained for 30 nm Ag NPs in environmental waters.

1. Introduction

Over the past decades, the human population has witnessed a widespread beneficiation of engineered nanomaterials in various fields and consumer products. Among metallic nanoparticles (NPs), silver NPs are one of the most frequently exploited due to their exceptional antimicrobial, anti-angiogenic and optical properties. Ag NPs are in fact widely utilized in textiles, water purification systems, health care products, cosmetics, and in medical diagnostics just to name a few [1–3]. The increased production and use of nano-enhanced products inevitably lead to their growing release into the environment, which has raised serious concerns about their potential adverse effects on the environment and human health [4–10]. Despite the vast amount of previous research focused on the matter, knowledge gaps in the risk assessment of NPs still exist due to a number of factors confounding the issue. In addition to the properties of the NPs themselves (such as size, shape, concentration, surface functionalization, etc.), the environmental behavior and toxicity of NPs are also affected by environmental conditions, such as pH, temperature, and other elements and compounds present [11–20]. Clearly, understanding the potential impact of NPs on the environment and human health requires careful characterization of these materials at environmentally relevant concentrations.

Single-particle inductively coupled plasma mass spectrometry (spICP-MS) is widely recognized as a powerful tool in the characterization of engineered NPs. As a highly sensitive technique, spICP-MS enables the simultaneous determination of NP size, size distribution, particle number concentration, and ionic (dissolved) content at realistic environmental concentrations [21–25]. In spICP-MS, a sufficiently

* Corresponding author.
E-mail address: virva.v-t.kinnunen@jyu.fi (V. Kinnunen).

https://doi.org/10.1016/j.sab.2022.106431
Received 4 February 2022; Received in revised form 25 March 2022; Accepted 21 April 2022
Available online 26 April 2022

dilute NP suspension is nebulized into the plasma, resulting in vaporization, atomization, and ionization of an analyte element. Whereas the ionization of the dissolved form of the element produces a steady-state signal, individual NPs generate a burst of ions producing a transient signal, i.e. "a spike". The discrimination between the signal originating either from the analyte in the dissolved or NP form is based on the separation of the pulse intensities originating from individual NPs over a certain threshold limit, which typically is determined using an iterative 'mean + 3σ' computation [21,24,26–29]. However, distinguishing the NP events from the background signal is not a trivial task, especially in the presence of a high level of dissolved analyte. In these cases, the high background signal might overlap the NP signals resulting in a calculated threshold value being larger than some or possibly all NP signals. As a result of only a partial detection of the NP size distribution, the obtained NP number and size information will be biased (overestimation of the NP size and underestimation of the particle concentration). The situation is particularly challenging for samples containing high concentrations of dissolved analyte and/or small NPs, e.g., for environmental samples [30–32]. For accurate characterization of the NPs, minimizing the dissolved analyte concentration in NP samples is crucial.

Differentiation of the NP events from the continuous background signal can be improved by careful selection of the data acquisition parameters used, especially in the presence of a high level of dissolved analyte. As compared to millisecond dwell times frequently used [25], faster data acquisition with dwell times in the microsecond range (e.g. ≤100 μs) allows smaller NPs to be detected [24,29,33]. Mathematical methods can be further used to improve the accuracy of NP event identification [34,35]. For instance, Mozhayeva et al. [34] developed a data deconvolution procedure using Poisson statistics for improved identification of NP events using microsecond time resolved signals. The dissolved analyte content in the sample can also be reduced physically, thus eliminating the need for mathematical discrimination techniques. A simple way to reduce dissolved (background) signal at spICP-MS is by sample dilution [30,36]. However, considering environmental samples with low NP concentrations [5,30,32,37,38], sampling times might need to be extended to ensure the capture of a sufficient number of NP events for reliable NP characterization. Over the past years, a variety of approaches for discrimination of metallic NPs and their corresponding ionic counterparts have been developed including e.g. filtration and centrifugation methods [39,40], cloud point extraction [18,41–43], chromatographic separation [44–46], field flow fractioning methods [47,48] and magnetic solid phase extraction [49–53]. Even though effective, these methods suffer from some pitfalls including e.g. time-consuming sample pre-treatment stages, the need for careful optimization of separation conditions, and long analysis times. In addition, not all aforementioned methods are directly compatible with spICP-MS or changes in the original sample properties might also occur during complex sample treatment processes (e.g. changes in NP size or concentration), which should be avoided.

The applicability of solid phase extraction (SPE) on the separation of metal ions and their corresponding NPs in various matrices has been demonstrated in numerous papers over the past years [31,39,54–57,59,60]. In this technique, the analyte either in NP or dissolved form can be selectively extracted from the sample solution by careful selection of the SPE material and possible surface functionalization of the NPs. Alternatively, both forms of the analyte can simultaneously be extracted and the separation of the two is achieved by differential desorption [54]. The first on-line coupling of spICP-MS with an ion-exchange column for the characterization of Ag NPs was presented by Hadioui et al. [31]. The dissolved signal was efficiently decreased using cationic Chelex 100 resin, allowing more accurate characterization of the NPs. Since then, Chelex 100 resin has been applied for the removal of dissolved analyte in the characterization of Ag, La_2O_3, and Zn NPs in various matrices [55,60–62]. However, lengthy washing and regeneration steps (up to 60 min) needed to ensure the proper functioning of the resin and to minimize carry-over between samples [31,62] cause a significant increase in the analysis time, especially in on-line systems.

Despite the previous studies focused on the matter, more research is still urgently needed on the applicability of SPE materials on dissolved silver removal from real environmental waters before spICP-MS analysis, which is currently still rare. As such, the aim of this work was to develop a simple sample pre-treatment procedure for spICP-MS allowing more accurate NP characterization by dissolved silver signal removal using SPE materials. The effect of eight commercial SPE materials (Chelex 100, Lewatit MonoPlus TP 214, Purolite C115HMR, SiliaBond Tosic Acid, SiliaMetS (SM) DEAM, SM DMT, SM Thiol and SM Triamine) on silver in both dissolved or NP form is thoroughly investigated in several water matrices (spring, lake, river, brook and ultrapure (UP) water and synthetic water sample (SWS)). The effect of competing elements, matrix components, and humic substances on the dissolved silver extraction efficiency of the SPE materials is investigated. Finally, the most suitable SPE materials were selected for efficient dissolved silver removal in different environmental water matrices, and their benefit on improving NP characterization is demonstrated.

2. Experimental

2.1. Materials

UP water (18.2 MΩ•cm) obtained from PURELAB Ultra water purification system (ELGA LabWater, Buckinghamshire, UK) was used for the preparation of aqueous solutions and sample dilutions. Single-element standard stock solutions of silver, yttrium, and ruthenium (1000 mg L^{-1}, pure grade) and multi-element standard solutions (29-Element and 12-Element Solution, 10 mg L^{-1}) used for calibration purposes and preparation of Ag sample solutions were obtained from PerkinElmer (MA, USA). Citrate-stabilized Ag NPs with nominal sizes of 30, 40, 50, and 80 nm (NanoComposix, San Diego, CA, USA) were used for the preparation of NP dispersions. The certified values of the standard particles used in the experiments were further verified in our laboratory (see Chapter 2.3). A dispersion containing ultra-uniform 50 nm PEG-Carboxyl-stabilized Au NPs specially designed for spICP-MS calibration was obtained from PerkinElmer and used for transport efficiency determination.

Sodium thiosulfate (STS, purum p.a., ≥98.0%) and thiourea (Reagent plus, >99.0%) were obtained from Sigma-Aldrich (Saint Louis, MO, USA) and used for adjusting solution matrix and elimination of the memory effects of silver in spICP-MS and ICP-MS (standard mode) measurements, respectively. High-purity nitric (HNO_3) and hydrochloric (HCl) acids (Analpure, Analytika spol. s r.o., Prague, Chech Republic) were used for adjusting the sample matrix for inductively coupled plasma optical emission spectrometry (ICP-OES)-measurements and for acid digestion of the commercial NP standards. Nitric acid (puriss p.a., ≥65%) and NaOH (≥97%) were obtained from Sigma-Aldrich and used for the pre-treatment of the SPE materials.

SWS used in some experiments was prepared from stock solutions (1000 mg L^{-1}) of the individual elements. The composition of the SWS (0.5 mg L^{-1} of Al, 10 mg L^{-1} of Ca and Na, 1.5 mg L^{-1} of Fe, 2 mg L^{-1} of K and Mg, 4 mg L^{-1} of S, 72 mg L^{-1} NO_3^- and 5 mg L^{-1} Cl^-) was designed to represent the elements and their levels commonly found in natural waters. $Al(NO_3)_3$•$9H_2O$ (ACS Grade), KCl (≥99%) and $Mg(NO_3)_2$•$6H_2O$ (98.0–102.0%) was obtained from J.T.Baker (NJ, USA), $FeCl_3$ •$6H_2O$ (99.0–102.0%) was obtained from VWR International, $NaNO_3$ (≥99.5%) was obtained from Sigma-Aldrich, $Ca(NO_3)_2$•$4H_2O$ (99.0–103.0%) was obtained from Merck (NJ, USA) and 1000 mg L^{-1} solution of S (in H_2O) was obtained from PerkinElmer. Only UP water was used for the preparation of the stock solutions to maintain the pH of the SWS as close to the environmental waters as possible. Humic acid (HA) solution was used as humic substances' source in selected experiments and prepared by dissolving 1 g of HA (virgin, Carl ROTH, Karlsruhe, Germany) in 1000 ml of UP water under constant stirring for 24 h. The undissolved

fraction of the material was removed by filtration (Whatman grade 41) and the filtrate was stored in the dark until use in HDPE-container. The soluble fraction of the material was determined by weighting the undissolved material and found to be approximately 20%.

2.2. spICP-MS measurements

All spICP-MS measurements were performed on a NexION350 D ICP-MS (PerkinElmer) operating in a single particle mode equipped with an ESI 4DX autosampler (Elemental Scientific, NE, USA). General instrumental parameters are shown in Table 1. At least duplicate readings were recorded of all samples to monitor any sample introduction errors. A commercial NexION Setup Solution (1 μg L^{-1} Be, Ce, Fe, In, Li, Mg, Pb, and U in 1% HNO_3, Pure Plus, PerkinElmer) was used to adjust the equipment according to instrument software's tuning protocols and to check the overall performance (i.e., maximum sensitivity with CeO^+/Ce^+-level < 2.5% and Ce^{++}/Ce <3%). All data processing was performed using the Syngistix Nano Application Module (v. 2.5), which automatically separates the NP events from the background (dissolved) signal using a threshold value determined using an iterative 'mean + 3σ' computation [63].

Transport efficiency was determined on daily basis at least in triplicate using the particle frequency method described by Pace et al. [28]. A dispersion containing 50 nm PEG-Carboxyl-stabilized Au NPs (PerkinElmer) diluted to a particle concentration of approximately 10^5 particles g^{-1} with UP water was used for its stability. The sample uptake rate was measured daily at least in duplicate by weighing the water uptake after 3 min aspiration, and its value was regularly checked during measurements.

Dissolved silver calibration standards ranging from 0.1 μg kg^{-1} to 2 μg kg^{-1} were prepared from a standard stock solution of silver (1000 mg L^{-1}). All calibration standards were diluted with a 0.5 mM solution of STS to ensure the solution stability of silver. Particle calibration was performed using citrate-stabilized Ag NPs with nominal sizes of 40, 50, and 80 nm (NanoComposix) after dilution to a particle concentration of approximately 10^5 particles g^{-1} with UP water. Before spICP-MS-measurements, an appropriate amount of 1000 mM STS solution was added to adjust the matrix of the NP standard solutions to 0.5 mM STS. The purpose of this was to match the matrix of the calibration standards of dissolved and NP silver, thus minimizing any matrix differences between the two.

All solutions used in the experiments were diluted gravimetrically fresh on a daily basis before the experiments. 15 and 50 ml polypropylene (PP) centrifuge tubes and high-density polyethylene (HDPE) bottles (Abdos Life Science, VWR International, and Fisher Scientific) were used for the preparation of the samples. The matrix of all sample solutions of silver was adjusted to 0.5 mM STS before measurements to ensure the chemical stability of dissolved silver and to minimize any matrix interferences. To minimize the effect of time on the sample properties, all samples were measured within 2 h from their initial preparation.

Table 1
General instrumental parameters used in spICP-MS measurements.

Parameter	Value
ICP RF-power (W)	1600
Nebulizer gas flow (L min^{-1})	0.93–0.95
Plasma gas flow rate (L min^{-1})	18
Auxiliary gas flow rate (L min^{-1})	1.2
Spray chamber	Baffled Cyclonic, Glass (cooled to 2 °C)
Nebulizer	PFA-ST MicroFlow Concentric
Injector	1.8 mm i.d. Sapphire
Sampling depth (mm)	11
Dwell time	100 μs
Sampling time (s)	30
Readings/sample	≥2
Transport efficiency (%)	6.1–8.7
Sample uptake rate (g min^{-1})	0.265–0.314
Isotope monitored	$^{107}Ag^+$

2.3. Verification of the Ag NP standards

The certified values of the commercial Ag NPs used in the experiments were verified in our laboratory (Table S1), as at times these values have been shown to deviate from the information provided by the manufacturer [64–67]. The mass fraction of silver (mg L^{-1}) of each Ag NP dispersion was quantified in duplicate by ICP-MS (NexION350 D ICP-MS, standard mode) using ruthenium (^{102}Ru) as an internal standard. 0.25 g of each sample was accurately weighed into new 15 ml PP tubes followed by the addition of 0.4 ml of aqua regia (Analpure). For quality control purposes, an accurately weighed amount of yttrium (approximately 7.5 μg) was added, and the samples were allowed to digest at room temperature for several days. Once dissolved, samples were brought to 10 ml using 0.1% (m/v) thiourea solution (Sigma-Aldrich) and further diluted 50-fold using a solution composed of 0.1% thiourea (*w/v*), 2.4% HCl (*v/v*) and 0.5% HNO_3 (v/v). The recovery of yttrium was monitored during analysis and used to compensate for any deviations originating from the sample preparation procedure (recoveries of 92–98% were attained in all experiments).

The diameters of the commercial Ag NPs were determined with transmission electron microscopy (TEM, JEM-1400HC, JEOL, MA, USA). For the calculation of average particle diameters and to ensure the statistical significance of the results, a minimum of 250 particles were considered. The in-lab verified values of the commercial Ag NPs were found to differ <10% from the values provided by the manufacturer (Table S1) and were used throughout the study.

2.4. Environmental water samples

Several environmental water samples (lake, river, brook, and two spring waters) were collected from various locations situated in Southern Ostrobothnia and Central Finland and stored in HDPE-containers in the refrigerator at 6–8 °C until use. Samples containing any solid material were filtrated before use (Whatman grade 41) to minimize the risk of blockage of the sample introduction system. The elemental composition of all the water samples used in the experiments (environmental water samples, UP water, SWS, and HA solution) were characterized in the laboratory and is presented in Table S2 (Appendix). Silver was measured with spICP-MS as described in Chapter 2.2, while ICP-OES (PerkinElmer) was used for the characterization of other minor and major elements. Other physicochemical parameters including e.g. chemical oxygen demand (COD_{Mn}) and dissolved organic carbon (DOC) used to characterize the humic substances' content of the water samples are presented in Table S3 (Appendix).

2.5. SPE materials

Various SPE materials having the potential to extract dissolved silver from water samples were obtained from commercial vendors (Tables 2 and S4). All SPE materials used in the experiments were pre-treated in the laboratory before use to remove any possible residual impurities and the finest particles, which could cause blockage of the sample introduction system. 3–4 g of each material was weighted into new 50 ml PP centrifuge tubes (VWR International) followed by the addition of 30 ml of 1 mM nitric acid. The tubes were shaken for 10 min (800 osc./min) using a flask shaker (Stuart SF1 Flask Shaker, Cole-Parmer, IL, USA), left to stand for 5–10 min and the supernatant liquid was removed by decanting. The residue was thoroughly rinsed with UP water until a neutral pH was achieved. To avoid any pH changes of the sample solutions caused by ion-exchange processes, some of the materials were further transformed to their sodium (Na^+) form (Table 2) using 30 ml of 1 mM NaOH following the same procedure as above. The excess water was then removed by vacuum filtration. All SPE materials except for

Table 2
SPE materials used in the experiments.

SPE material (Abbreviation)	Manufacturer	Particle size (μm)	Functional group	Conversion to Na^+ form
Chelex 100	Bio-Rad	300–1180 (wet)	Iminodiacetate ion	Yes
Lewatit MonoPlus TP 214 (TP 214)	Lanxess	500–600	Thiourea	–
Purolite C115HMR (C115HMR)	Purolite	<150	Carboxylic Acid	Yes
SiliaBond Tosic Acid (SB TA)	SiliCycle	40–63	Tosic Acid	Yes
SiliaMetS DEAM (SM DEAM)	SiliCycle	40–63	N-alkyldiethanolamine	Yes
SiliaMetS DMT (SM DMT)	SiliCycle	40–63	Dimercaptotriazine (DMT)	Yes
SiliaMetS Thiol (SM Thiol)	SiliCycle	40–63	Thiol	Yes
SiliaMetS Triamine (SM Tri)	SiliCycle	40–63	Triamine	–

Chelex 100 were further oven-dried at 50 °C overnight. All materials were stored in tightly-sealed containers until use.

2.6. Separation of the solid SPE materials

To investigate the effect of centrifugation speed and duration on sample Ag NP properties, dispersions containing 50 nm Ag NPs (10^5 particles g^{-1}) were prepared both in UP and lake water and treated with SPE materials 'C115HMR' and 'SM DEAM' as described in Chapter 2.7. The two SPE materials were chosen for their different properties (Tables 2 and S4), which might affect the separation process. Samples were then centrifuged at 1500, 2500, or 3500 rpm for 3, 5, or 10 min using Heraeus Labofuge 400 centrifuge (Thermo Scientific, MA, USA).

2.7. Extraction experiments using SPE materials

The ability of the different SPE materials (Tables 2 and S4) to remove dissolved silver and their possible effect on NP properties (particle size or -concentration) was estimated. Dispersions containing either 1 μg kg^{-1} of dissolved silver or 10^5 particles g^{-1} of 50 nm Ag NPs were prepared in brook, lake, spring (1), or UP water. The dispersions were then divided on 15 ml centrifuge tubes (10 ± 1 ml each, $n = 2$) containing 45 ± 5 mg of SPE materials, which were weighted in the tubes beforehand. 2 sample tubes were used as reference samples and thus did not contain any SPE material. Sample tubes were protected from light with aluminum foils and manually shaken for 5 min to ensure efficient mixing. Samples were then centrifuged at 2500 rpm for 3 min using Heraeus Labofuge 400 centrifuge (Thermo Scientific). 6 ml of liquid samples were carefully separated from the surface of the tubes and an appropriate amount of 100 mM STS solution was added to adjust the matrix background to 0.5 mM STS. The silver content (dissolved and NP silver) of the samples was measured with spICP-MS.

The effect of different SPE materials on dissolved or NP silver was evaluated by comparing the obtained results of the samples to those of the reference samples according to Eqs. (1) and (2), where EE-% is the material's dissolved silver extraction efficiency (%), C_{Ag} is the dissolved silver concentration (μg kg^{-1}) and C_p is the particle concentration (particles g^{-1}):

$$EE - \% = \frac{C_{Ag\ (Ref.)} - C_{Ag\ (Sample)}}{C_{Ag\ (Ref.)}} \bullet 100\% \quad (1)$$

$$C_p\ recovery\ (\%) = \frac{C_{p\ (Sample)}}{C_{p\ (Ref.)}} \bullet 100\% \quad (2)$$

In addition, the possible effect of SPE materials on Ag NP size or particle size distribution was evaluated by comparing the obtained mean particle size and the size distribution histograms of the samples to those obtained for reference samples.

2.8. Interference and selectivity experiments

The SPE materials' ability to extract silver in the presence of humic substances and various competing elements (Al, Ca, Cl^-, Fe, K, Mg, Na, NO_3^- and S) was evaluated. Solutions containing 1 μg kg^{-1} dissolved silver were prepared in spring (2) and river water, SWS, and in HA solution with different physicochemical properties (Tables S2 and S3). All samples were then treated as described in Chapter 2.7 and the concentration of dissolved silver was analyzed with spICP-MS. After extracting the sample for spICP-MS measurements, 3 ml of the residual sample was further extracted for ICP-OES to determine the concentration of the extracted competing elements (Al, Ca, Fe, K, Mg, Na, and S). Following this, 0.25 ml of high-purity HNO_3 was added, and the volume was finally brought up to 5 ml with UP water for ICP-OES analysis.

3. Results

3.1. Dissolved silver interference

As discussed before, elevated concentrations of dissolved analyte can severely affect the accuracy of NP characterization by masking NP signals. The situation is particularly challenging for environmental samples, where dissolved silver usually coexists with Ag NPs due to Ag NP dissolution [20]. As the intensity of observed NP pulses is directly proportional to the NP size, the high background signal interferes foremost with the detection of small NPs as a result of increased size detection limit [31,36].

To study the effect of dissolved silver interference on NP detection, dispersions containing 30, 40, 50, and 80 nm Ag NPs in UP water were spiked with increasing concentrations of dissolved silver (0–1 μg kg^{-1}, Fig. 1). Whereas dissolved silver concentration up to 1 μg kg^{-1} was not found to affect the detection of 50 and 80 nm Ag NPs, characterization of the 30 and 40 nm Ag NPs was clearly interfered by dissolved silver concentrations of ≥0.1 μg kg^{-1}. For these NPs, increasing dissolved concentration leads to an overestimation of the particle size and a significant underestimation in particle concentration. As expected, elevated concentrations of dissolved silver affected foremost the detection of the smaller 30 nm Ag NPs, and at dissolved silver concentrations >0.5 μg kg^{-1} the majority (>80%) of the 30 nm Ag NP signals were in fact masked by the dissolved signal and thus were undetected. This is because the increased dissolved background signal masked the pulses of the smaller NPs, leading to significant bias in particle sizing (up to +80%) and concentration determination (up to −93%).

As the Ag NPs in environmental samples are usually 20 nm in size or less [68], the dissolved signal should be reduced as much as possible for accurate NP characterization. As seen in Fig. 1, for accurate characterization of ≤30 nm Ag NPs, the dissolved silver concentration should be decreased to a concentration below 0.1 μg kg^{-1}.

3.2. Separation of the solid materials

SPE materials can be highly effective in improving the accuracy of NP detection by removing dissolved analyte in NP dispersions. Even though these materials are often utilized in in-lab built columns connected on-line with spICP-MS [31,61,62], laborious washing and regeneration steps (16–60 min depending on the author [31,62]) needed to ensure the proper functioning of the SPE materials and to minimize the risk of carryover between samples often increase total sample analysis time. As such, in this paper, SPE materials were utilized as an

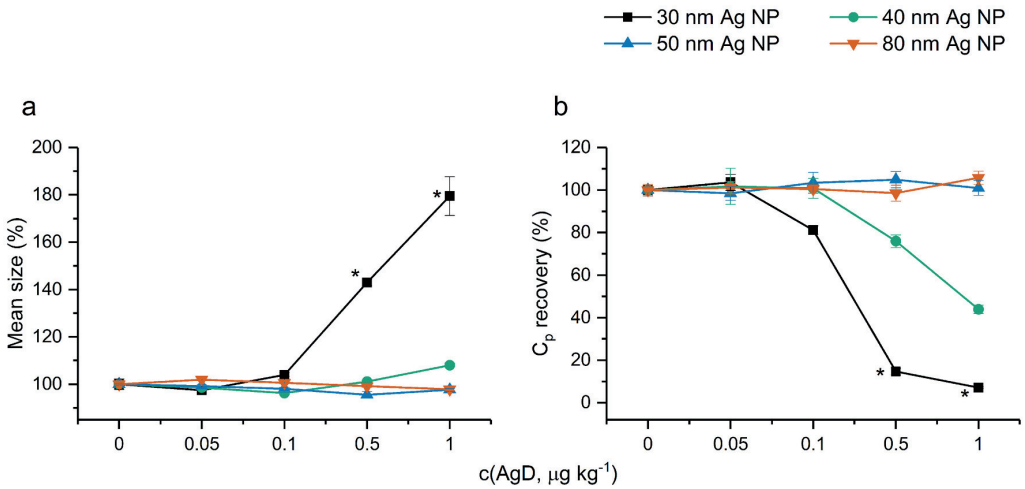

Fig. 1. The effect of dissolved silver concentration (0–1 µg kg^{-1}) on the accuracy of Ag NP characterization. Obtained Ag NP mean size (a) and particle concentration (b) as function of dissolved silver (AgD) concentration, given as percentual (%) values as compared to the values obtained at a dissolved silver concentration of 0 µg kg^{-1}. Results are given as mean ± 1 standard deviation (1 s) of three replicate samples ($n = 3$). The obtained NP size detection limits were 10, 16, 17, 26 and 30 nm at dissolved silver concentrations of 0, 0.05, 0.1, 0.5 and 1.0 µg kg^{-1}, respectively. The data points for 30 nm Ag NP at AgD concentrations of 0.5 and 1.0 µg kg^{-1} are highlighted with an asterisk, as an insufficient number of NPs (⟨100) were captured for statistically significant characterization.

off-line sample pre-treatment procedure to maximize sample throughput in spICP-MS.

For the small particle size of the solid SPE materials (Table 2), sufficient separation of the sample solution and solid materials should be achieved to prevent the risk of blockage of the sample introduction system. However, the original sample NP properties (size and concentration) should be maintained in the process. Even though centrifugation is an efficient method for the separation of the solid materials, using high centrifugation speeds and durations has in some cases shown to lead Ag NP losses [59,69–72]. As such, the effect of centrifugation conditions on sample properties was investigated.

Firstly, the effect of centrifugation duration on Ag NP recoveries was evaluated. 50 nm Ag NP dispersions prepared in UP and lake water were centrifugated for 3, 5, and 10 min at 3500 rpm (Fig. S1a and b in Appendix). Even though the Ag NP recoveries are generally observed to decrease slightly as the centrifugation duration is increased, no significant differences are observed in the Ag NP concentration in either matrix. In addition, sufficient separation of the solid SPE materials was achieved even at the shortest centrifugation duration of 3 min. As such, 3 min was chosen as the optimal centrifugation duration to minimize sample preparation time. Once the centrifugation duration of 3 min was set, the effect of centrifugation speed (1500, 2500, and 3500 rpm) on 50 nm Ag NP concentration was further studied (Fig. S1c and d in Appendix). Increasing centrifugation speed was not found to significantly affect the Ag NP concentration or separation of the SPE materials in either matrix. As such, a centrifugation speed of 2500 rpm was chosen.

A closer investigation of Fig. S1 reveals some interesting differences in the recoveries of Ag NPs between samples and matrices treated with SPE materials. Significantly (up to 40%) lower Ag NPs recoveries are obtained for samples treated with SPE material 'SM DEAM' in lake water matrix (Fig. S1b and d). Similar behavior was not observed in UP water, indicating that the SPE material itself is not responsible for the loss of the Ag NPs. It seems SPE material 'SM DEAM' interacts with sample Ag NPs to some extent leading to NP losses, however, the process is matrix dependent. The effect of different SPE materials on Ag NPs in different matrices is discussed in more detail in Chapter 3.3.1.

Neither the centrifugation speed nor duration was found to significantly affect the recovery of Ag NPs in either of the matrices studied. This is somewhat in contrast with the findings of other authors, who reported a significant reduction of the NP concentration with increasing centrifugation speed [59,69,71,72]. However, in these studies either significantly longer centrifugation times (up to 20 min) or different sample matrices were used, which could explain the differences in the findings. In addition, differences in the equipment used for centrifugation (e.g. the centrifuge itself and the size of centrifugation tubes used) can affect the results, making the direct comparison of the results challenging. As such, it seems advisable to study the effect of these variables on the sample properties in the early stages of the method development to minimize the risk of NP losses.

Compared with on-line systems, the optimized off-line procedure presented here reduces the required analysis time considerably, as laborious washing and regeneration steps needed between samples [31,39,61,62] are omitted. Up to 12 samples can be pre-treated with the proposed off-line procedure in less than 10 min (<1 min/sample), whereas 16–60 min (depending on the author [31,62]) was required for the regeneration of the resin between samples in on-line systems. In addition, the risk of carryover is minimized by washing the sample introduction system between every sample.

3.3. Extraction experiments of the SPE materials

The effect of the commercially available SPE materials used in the experiments (Table 2) on sample properties was evaluated. Considering spICP-MS analyses, the aim is to identify suitable SPE materials capable of efficient removal of dissolved silver, while maintaining the original Ag NP properties of the sample. As such, the SPE materials were evaluated based on two factors. Firstly, the effect of these materials on Ag NP properties (particle size or -concentration) and secondly, the extraction efficiency of dissolved silver.

3.3.1. Effect of SPE materials on Ag NPs properties

As the purpose of this study is to improve the accuracy of NP detection, maintaining the samples' original NP properties is of utmost importance. As such, the effect of the different SPE materials on Ag NP concentration and size was carefully investigated. To evaluate the possible effect of SPE materials on NP properties, the results obtained for samples treated with SPE materials were compared to those obtained for reference samples, which did not contain any SPE materials. The obtained results for the Ag NP concentration and size in various natural waters are presented in Fig. 2a and b, respectively, and in Table S5

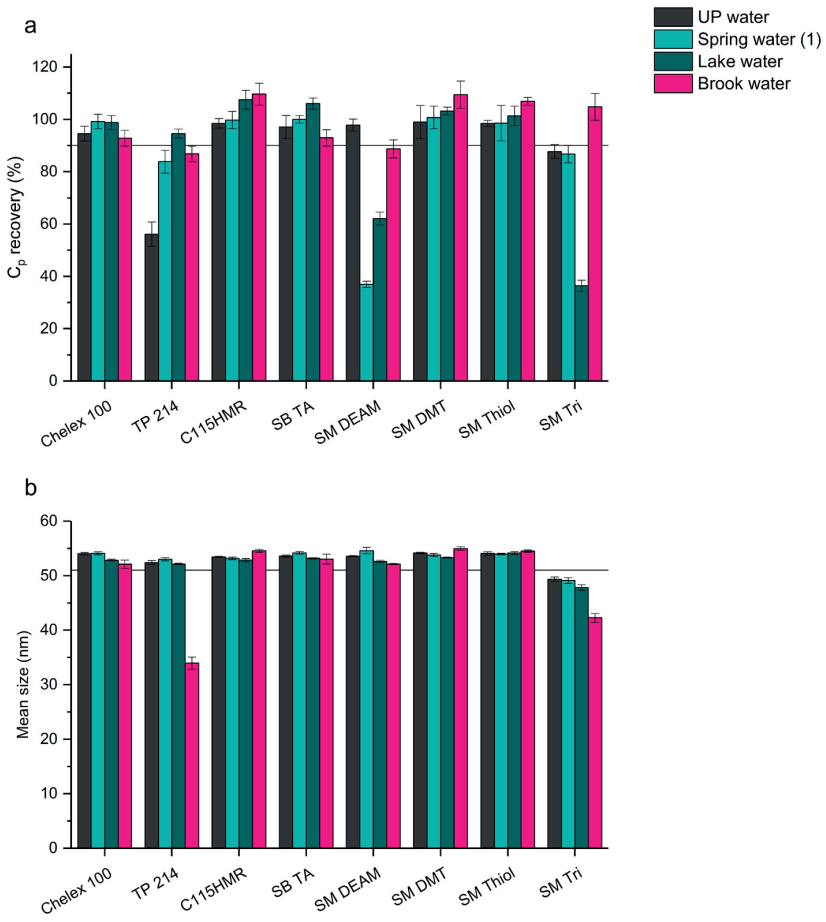

Fig. 2. The effect of SPE materials on 50 nm Ag NPs a) particle recovery (C_p recovery (%)) and b) mean size in different matrices. Results are given as mean ± 1 standard deviation of two replicate samples with 4 readings. The black reference lines given in Figs. 2 a and b represent 90% C_p recovery and the mean size of the 50 nm Ag NPs (51 nm as obtained with TEM), respectively.

(Appendix). The obtained size distribution histograms are presented in Figs. S2–S5 (Appendix).

Most of the SPE materials were not found to cause significant changes in Ag NP concentration or size (Fig. 2a and b). In addition, similar size distribution histograms were in general obtained for samples analyzed as such and after treatment with SPE materials (Figs. S2–S5 in Appendix). As such, most of the materials were not found to significantly interact with sample Ag NPs in any of the matrices studied, making them potential candidates for dissolved silver removal in NP dispersions. However, significant (up to 64%) loss of Ag NPs is observed in samples treated with SPE materials 'TP 214', 'SM DEAM' and 'SM Tri' (Fig. 2a). The effect of these materials, however, is found matrix-dependent; in general, losses are more severe in spring (1) and lake water (Tables S2 and S3 in Appendix). A significant reduction in particle size was also observed for samples containing SPE materials 'TP 214' and 'SM Tri' (Fig. 2b), indicating particle dissolution. As the observation was made for the latter in all the matrices studied, it can be expected, that the material itself is causing changes in particle size. The observed changes in particle size and concentration for the SPE materials 'TP 214', 'SM DEAM' and 'SM Tri' can also be clearly seen in the size distribution histograms (Figs. S2–S5 in Appendix).

As the observed changes in particle size or concentration are clear indicators of the material's interaction with the sample Ag NPs, materials 'TP 214', 'SM Tri', and 'SM DEAM' cannot be considered for dissolved silver removal in NP dispersions. However, SPE materials 'Chelex 100', 'SB TA', 'C115HMR', 'SM Thiol' and 'SM DMT' were able to maintain the original sample Ag NP properties in all the matrices studied. As such, these materials can be considered as viable alternatives for dissolved silver removal and the extraction efficiency of these materials is evaluated in the following chapter.

3.3.2. *Effect of SPE materials on dissolved silver*

As presented in Fig. 1 and shown before [31], even low concentrations of dissolved silver can severely interfere with the detection of Ag NPs, leading to inaccurate characterization of these materials. Efficient removal of the dissolved silver is thus required for accurate sizing and counting of the NPs. In addition, the possible effect of the sample matrix should be considered, as it is expected to affect the extraction efficiency of SPE materials [55,59,61,73].

After identification of the SPE materials capable of maintaining the original sample NP properties (Chapter 3.3.1), their ability to extract dissolved silver was evaluated in various matrices (UP, spring (1 and 2), lake, river, and brook water, SWS and HA solution). The obtained results for colorless (with dissolved organic carbon (DOC) <5 mg L^{-1}) and dark-colored (DOC >5 mg L^{-1}) waters are presented in Fig. 3a and b, respectively and in Table S6 (Appendix).

As the obtained results in colorless and dark-colored waters are compared (Fig. 3a and b), a significant difference in the dissolved silver

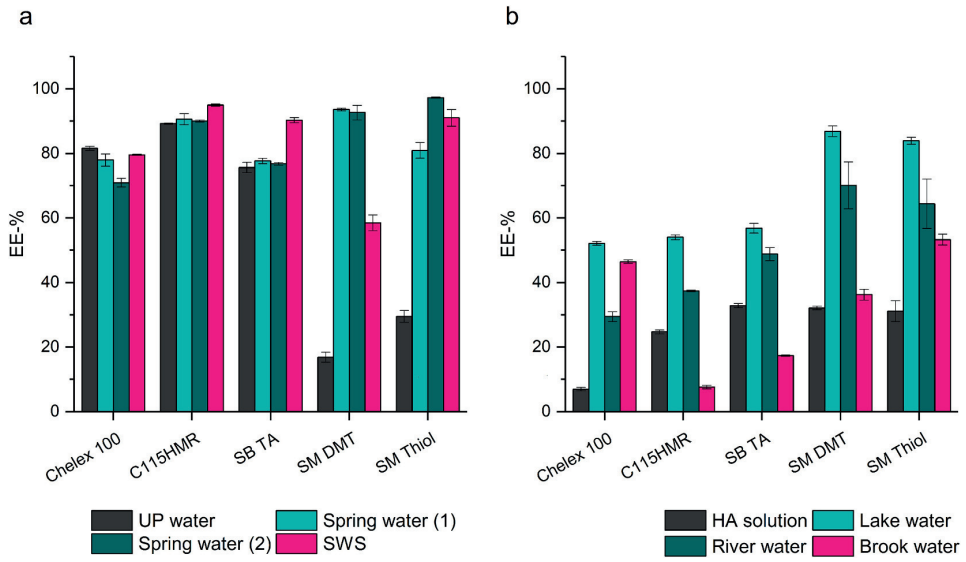

Fig. 3. The different SPE materials' dissolved silver extraction efficiency (EE-%) a) in colorless waters (DOC <5 mg L^{-1}) and b) in dark-colored waters (DOC >5 mg L^{-1}). Results are given as mean ± 1 standard deviation (1 s) of two replicate samples with 4 readings.

extraction efficiency is observed. In colorless waters, clearly higher extraction efficiencies (up to 97%) are obtained virtually unaffected by the SPE materials used. Cation exchange materials 'C115HMR', 'SB TA', and 'Chelex 100' with carboxylic or sulfonate groups proved most efficient in dissolved silver removal. The highest extraction efficiencies (89–95%) were obtained with a weak cation exchange resin 'C115HMR', followed by 'SB TA' and 'Chelex 100' with highly similar efficiencies (71–90%).

In dark-colored waters with higher amounts of humic substances (DOC >5 mg L^{-1}), however, the ability of the different SPE materials to remove dissolved silver is clearly decreased (Fig. 3b). The latter is true especially for the ion-exchange resins 'C115HMR', 'SB TA' and 'Chelex 100', which extraction efficiencies fell below 60% in dark-colored waters. A possible explanation for this observation is the presence of humic substances in these waters (Table S3, Appendix), which are known to affect the efficiency of SPE extraction [55,61]. As seen in Fig. 3b, poor dissolved extraction efficiencies (<40%) were obtained in HA solution independent of the SPE material used, which might be due to competitive binding of silver to humic substances' active sites (e.g. sulphur and carboxyl groups) [74]. The effect of humic substances can be more clearly seen in Fig. S6, where the SPE materials' dissolved silver EE-% in different waters is presented with their corresponding DOC-values indicating the humic substances' content in these waters. As can be seen, the dissolved silver extraction is found most efficient in colorless waters with DOC-values <5 mg L^{-1}, but generally lower efficiencies are obtained in waters with DOC-values >5 mg L^{-1}.

Comparing the obtained results in colorless and dark-colored waters (Fig. 3a and b and S6), two SPE materials stand out. In contrast to the other SPE materials, clearly lower extraction efficiencies are obtained for thiol-containing materials 'SM DMT' and 'SM Thiol' in UP water as compared to environmental waters. This is somewhat unexpected since UP water contains no competing elements or compounds that could interfere with the extraction process. Considering that UP water lacks buffering capacity, changes in solution pH during the extraction process might affect the extraction efficiency. As compared with the reference sample, a significantly higher pH value was indeed measured for the sample treated with SPE material 'SM DMT' (9.9 vs. 5.4), which could explain the observed results. In addition, the extraction efficiency of these materials might depend on specific compounds or elements present. When the extraction efficiency of these materials is presented with the increasing concentration of dissolved anions (Cl^- and SO_4^{2-}) present (Fig. S7 in Appendix), some correlation can be observed. The presence of these anions may be favouring the dissolved silver extraction efficiency of SPE materials 'SM DMT' and 'SM Thiol', for instance by affecting the chemical state of silver.

As the purpose of this paper is to develop a sample pre-treatment procedure for dissolved silver removal in environmental waters, it is important to evaluate the possible interfering effect of matrix components on the extraction process. Since other elements present in environmental waters might decrease the extraction efficiency of dissolved silver by competing with the SPE materials' active sites, the effect of competing elements on the dissolved silver extraction efficiency was investigated in more detail. The results for extraction of dissolved silver and other competing elements are presented in the supplementary material (Tables S7–S9 for SWS, spring (2), and river water, respectively). Due to the conversion of SPE materials into their sodium (Na^+) form, higher concentrations of sodium were measured for samples treated with SPE materials as compared to the reference samples, and thus results for the extraction of sodium were omitted. As all the SPE materials were found to extract competing elements to varying extents, none of the SPE materials were found selective towards silver. As such, the application of SPE materials on improving NP detection by dissolved signal removal can potentially be extended for other elements as well, as has already been demonstrated for Zn and La_2O_3 [55,60,61].

Because of the high molecular loading capacity of SPE materials (Table S4, Appendix) and the low elemental concentrations commonly found in natural waters, the presence of competing elements was not found to affect the materials' dissolved silver extraction efficiency. As seen in Fig. 3a and b, similar extraction efficiencies were obtained in waters containing various competing elements as in UP water, indicating that the extraction of other elements does not negatively affect the extraction of silver in the concentration range studied. Interestingly, the presence of humic substances was not found to affect the SPE materials' extraction efficiency of the competing elements (Tables S7–S9 in Appendix), especially in the case of ion-exchange resins, as was noticed for silver. This confirms that the observed decrease in dissolved silver extraction efficiency in dark waters is due to humic substances' interaction with silver ions, thereby reducing the interaction with the SPE materials.

3.4. Selection of the SPE materials for dissolved silver extraction in NP dispersions

The suitability of the SPE materials on dissolved silver removal in Ag NP dispersions was evaluated based on their effects on NP properties and dissolved silver extraction efficiency. As maintaining the original sample Ag NP properties is of utmost importance for accurate NP characterization, any SPE materials found to cause changes in the original sample NP properties were excluded ('SM Tri', 'SM DEAM' and 'TP 214', see Chapter 3.3.1). The remaining five SPE materials were assessed based on their ability to extract dissolved silver in colorless (DOC <5 mg L^{-1}) and dark-colored waters (DOC >5 mg L^{-1}), for which the numerical results are given in Table S6 (in Appendix) and summarized in Table 3.

Based on the obtained results, SPE materials 'C115HMR', 'Chelex100' and 'SB TA' were found generally most suitable for dissolved silver removal. These materials were found to extract dissolved silver efficiently especially in colorless waters and importantly, were not found to interact with the Ag NPs in any of the matrices studied. However, in dark-colored waters, these materials' extraction efficiency decreased significantly probably because of the interfering effect of humic substances. In dark-colored waters with higher amounts of humic substances (DOC >5 mg L^{-1}), SPE materials 'SM Thiol' and 'SM DMT' were found more efficient and should be preferred. As such, care should be taken in choosing SPE materials for dissolved silver removal, as the sample matrix greatly affects the efficiency of the SPE materials.

Finally, SPE materials 'C115HMR' and 'SM Thiol' were chosen as the final materials for dissolved silver removal in colorless and dark-colored environmental waters, respectively. Even though 'C115HMR' was found more efficient in colorless waters, tests were performed also with 'Chelex 100' for comparative purposes due to its frequent use in previous studies [31,62].

3.5. Analysis of environmental samples

To demonstrate the effect of the chosen SPE materials on improving the accuracy of NP characterization in environmental waters, dispersions containing 30 nm Ag NPs and 0–1 μg kg^{-1} of dissolved silver were prepared in colorless waters with COD <5 mg L^{-1} (UP and spring (2) water), and dark-colored water with COD >5 mg L^{-1} (river water). Samples were then analyzed as such and after treatment with the chosen SPE materials as described in Chapter 2.7. The results are displayed in Fig. 4a–c.

As can be seen in Fig. 4a–c, when samples are analyzed as such without treatment with the SPE materials, the coexisting dissolved concentration causes a significant interference on the detection of the 30 nm Ag NPs in all matrices. With increasing dissolved silver concentration, more and more NPs are masked by the higher background signal, causing a significant increase in particle mean size (up to +58%, from 26 to 29 nm to 42–43 nm) and a decrease in particle concentration (up to −90%). By pre-treating the samples with SPE materials before spICP-MS-measurements, however, a significant portion of the dissolved silver can be removed, allowing highly more accurate characterization of the 30 nm Ag NPs over the entire concentration range studied. It should be noted, that significantly lower (up to 40%) particle concentration is obtained in UP water for samples analyzed as such (i.e., for the reference sample) as compared to the values obtained for samples treated with SPE materials, even in the presence of low background signal (no dissolved silver added, Fig. 4a). The adsorption of Ag NPs onto solid surfaces has been previously reported [75] and shown to depend both on the surface of the Ag NPs and the sample container materials. As such, it seems possible, that the lower recoveries obtained in UP water for the reference sample might result from the interaction of Ag NPs with e.g. sample introduction system. The addition of SPE materials might reduce the adsorption of Ag NPs onto solid surfaces by e.g. affecting the physicochemical properties of the sample matrix or particle surface, thereby explaining the observed results.

Table 3
Effect of the selected SPE materials on sample properties.

SPE Material	C_p recovery (%)[1]	EE-%(AgD), colorless waters[2]	EE-%(AgD), dark-colored waters[2]
Chelex 100	Excellent	Good	Poor
C115HMR	Excellent	Excellent	Poor
SB TA	Excellent	Good	Poor
SM DMT	Excellent	Moderate	Moderate
SM Thiol	Excellent	Moderate	Moderate

[1] The effect of SPE materials on C_p recovery was estimated as follows: ≥90% in all matrices: Excellent, <90% in any matrix: Poor.

[2] Dissolved silver extraction efficiency (EE-%(AgD)) estimated as follows: >85% Excellent, 75–85% Good, 55–75% Moderate and < 55% Poor.

In clear waters (UP- and spring water (2) with DOC <5 mg L^{-1}, Fig. 4a and b), the dissolved silver interference can be minimized by treating the samples with ion-exchange materials 'Chelex 100' or 'C115HMR'. The efficient extraction of dissolved silver (up to 95%) improves the detection of the 30 nm Ag NPs, allowing more accurate sizing and particle concentration determination over the entire concentration range studied. Even though 'Chelex 100' is more often used in previous publications [31,62], 'C115HMR' proved more efficient in dissolved silver removal, as noticed already in Chapter 3.3.2. As a result, highly accurate values are obtained for the particle mean size (28 ± 2 nm) even in samples containing relatively high amounts (up to 1 μg kg^{-1}) of dissolved silver, whereas a slight increase is observed for samples treated with 'Chelex 100' (from 29/27 nm to 32/33 nm). At the same time, relatively stable particle concentration values are also obtained for samples treated with 'C115HMR' over the entire concentration range studied.

In river water with higher amounts of humic substances (DOC 11 mg L^{-1}), the detection of the 30 nm NPs can be significantly improved by pre-treating the samples with SPE material 'SM Thiol' (Fig. 4c). As a result, accurate readings are obtained for particle mean size (28 ± 2 nm) and particle concentration (<21% different) over the entire concentration range studied. For the ion-exchange materials 'Chelex 100' and 'C115HMR', the extraction efficiency is significantly decreased in the river water matrix rich with humic substances, resulting in only a slight improvement in NP detection. This demonstrates the better suitability of 'SM Thiol' for dissolved silver removal in dark-colored waters as compared to 'Chelex 100' and 'C115HMR', which were found more efficient in colorless waters.

4. Conclusions

Accurate characterization of Ag NPs in environmental samples can be severely interfered by high background (dissolved) signal, leading to inaccurate characterization of these materials. As the smallest NPs are most susceptible to the interfering effect of dissolved silver, for accurate characterization of ≤30 nm NPs, dissolved silver concentration should be decreased at least to a concentration below 0.1 μg L^{-1}. In this paper, a simple sample pre-treatment procedure for more accurate NP characterization with spICP-MS is presented using solid phase extraction (SPE) materials for dissolved silver removal in environmental waters. The developed off-line procedure maximizes sample throughput in spICP-MS with 12 samples treated in less than 10 min, as lengthy (up to 60 min) washing and regeneration steps necessary on commonly employed on-line systems are eliminated. The effect of centrifugation conditions (speed and duration) used for the separation of the solid SPE materials on the NP properties were investigated to minimize NP losses. Using the optimal conditions (2500 rpm for 3 min), the applicability of eight commercially available SPE materials was thoroughly evaluated based on their dissolved silver extraction efficiency and ability to maintain original sample Ag NP properties in various water matrices. Though many of the SPE materials were not found to interact with the sample Ag NPs, SPE materials 'SiliaMets (SM) Triamine', 'SM DEAM' and 'Lewatit

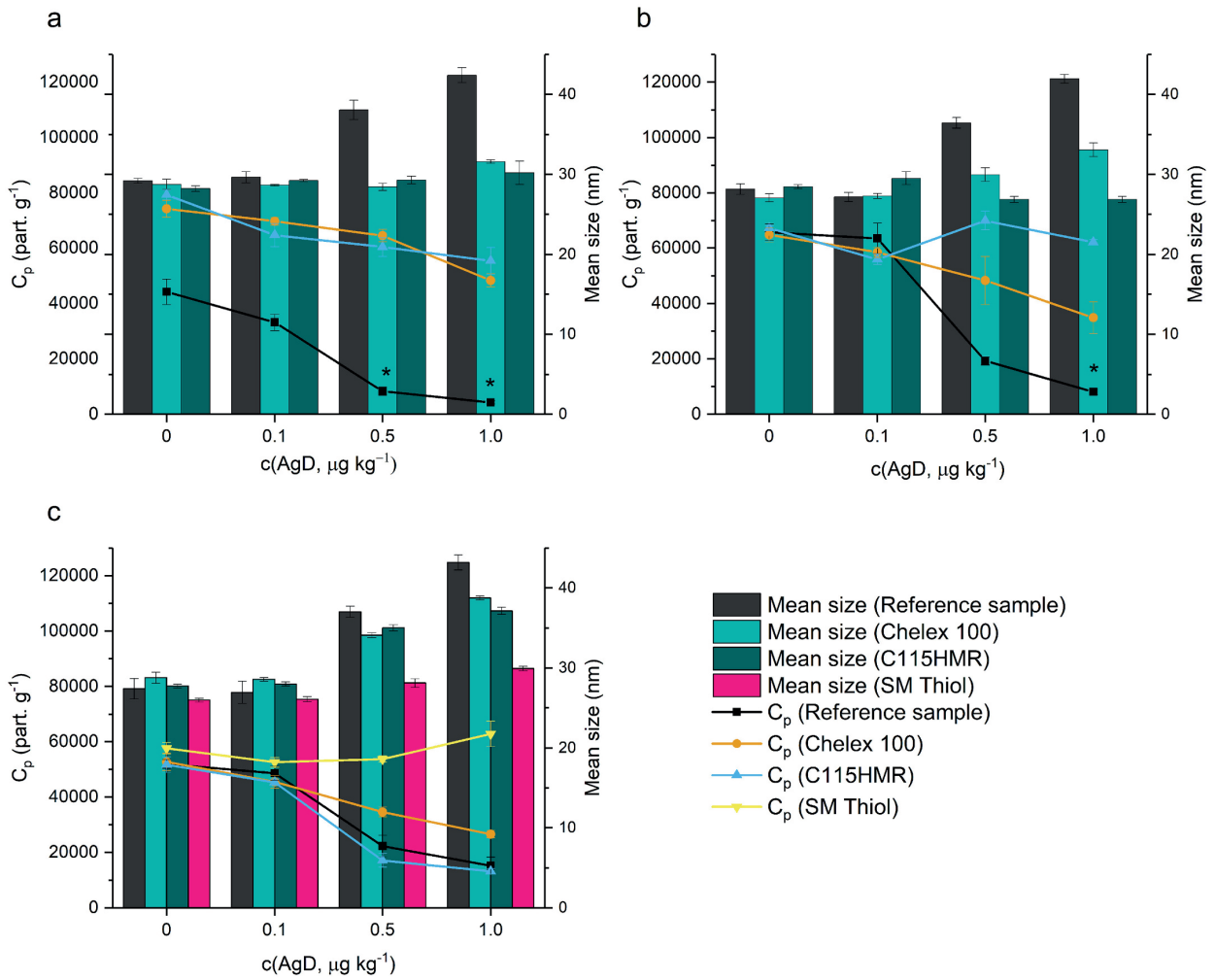

Fig. 4. The obtained results for 30 nm Ag NP dispersions spiked with increasing concentrations (0–1 µg kg^{-1}) of dissolved silver (AgD) in a) UP water, b) spring water (2) and c) river water. All samples were analyzed as such (i.e., reference sample) and after treatment with the chosen SPE materials ('Chelex 100'; 'C115HMR' and 'SM Thiol') in triplicate. The obtained results for particle concentration (C_p, given in part. g^{-1}) are represented with lines and mean size with bars. The error bars represent one standard deviation (1 s) of three replicate samples ($n = 3$). The data points for 30 nm Ag NP at AgD concentrations of 0.5 and 1.0 µg kg^{-1} are highlighted with an asterisk, as an insufficient number of NPs (<100) were captured for statistically significant characterization.

MonoPlus TP 214' were found to cause Ag NP dissolution or losses and as such were found unsuitable for dissolved silver removal in NP dispersions. The remaining SPE materials capable of maintaining original NP properties ('Chelex 100', 'Purolite C115HMR' ('C115HMR'), 'SiliaBond Tosic acid' ('SB TA'), 'SM Thiol' and 'SM DMT') were assessed based on their dissolved silver extraction efficiency in several water matrices. In addition, the effect of various competing elements commonly found in natural waters (Al, Ca, Na, Fe, K, Mg, S, NO_3^- and Cl^-) and humic substances on the extraction efficiency were evaluated. Even though competing elements were not found to affect the dissolved silver extraction efficiency due to the high molecular capacity of the SPE materials used, the presence of humic substances was shown to significantly decrease the dissolved silver extraction efficiency, especially with ion-exchange materials 'Chelex 100', 'C115HMR' and 'SB TA'. This is probably due to the competitive binding of silver through humic substances' active sites (e.g. sulphur and carboxyl groups).

Three SPE materials found most efficient in dissolved silver extraction ('C115HMR', 'Chelex 100' and 'SM Thiol') were chosen and their effect on improving the accuracy of Ag NP characterization was demonstrated in ultrapure, spring, and river water with different physicochemical properties. Whereas measurement of the samples with coexisting dissolved silver (up to 1 µg kg^{-1}) as such without treatment with SPE materials resulted in significant bias in 30 nm Ag NP sizing (up to +58% increase) and counting (up to −90% decrease), pre-treatment of the samples with SPE materials 'C115HMR' and 'SM Thiol' minimized the effect of dissolved silver interference in colorless and dark-colored waters, respectively. As a result, highly more accurate readings were obtained for NP size (28 ± 2 nm) with relatively stable particle concentration values (<21% different).

CRediT authorship contribution statement

Virva Kinnunen: Conceptualization, Validation, Formal analysis, Investigation, Visualization, Writing – original draft. **Siiri Perämäki:** Supervision, Writing – original draft. **Rose Matilainen:** Project administration, Supervision, Writing – original draft.

Declaration of Competing Interest

The authors declare that they have no known competing financial interests or personal relationships that could have appeared to influence the work reported in this paper.

Acknowledgments

This work was supported by the University of Jyväskylä, Department of Chemistry. The authors would like to thank Joona Rajahalme for the inspirational discussions regarding the subject and comments regarding the manuscript. Kaisa Lampinen and Elina Hautakangas are greatly appreciated for their help on sample preparation.

Appendix A. Supplementary data

Supplementary data to this article can be found online at https://doi.org/10.1016/j.sab.2022.106431.

References

[1] S.P. Deshmukh, S.M. Patil, S.B. Mullani, S.D. Delekar, Silver nanoparticles as an effective disinfectant: a review, Mater. Sci. Eng. C 97 (2019) 954–965, https://doi.org/10.1016/j.msec.2018.12.102.
[2] X.F. Zhang, Z.G. Liu, W. Shen, S. Gurunathan, Silver nanoparticles: synthesis, characterization, properties, applications, and therapeutic approaches, Int. J. Mol. Sci. 17 (2016), https://doi.org/10.3390/ijms17091534.
[3] L. Wei, J. Lu, H. Xu, A. Patel, Z.S. Chen, G. Chen, Silver nanoparticles: synthesis, properties, and therapeutic applications, Drug Discov. Today 20 (2015) 595–601, https://doi.org/10.1016/j.drudis.2014.11.014.
[4] E.A.J. Bleeker, S. Evertz, R.E. Geertsma, W.J.G. Peijnenburg, J. Westra, S.W. P. Wijnhoven, Assessing Health & Environmental Risks of Nanoparticles, National Institute for Public Health and the Environment, Bilthoven, The Netherlands, 2015.
[5] J.R. Lead, G.E. Batley, P.J.J. Alvarez, M.N. Croteau, R.D. Handy, M.J. McLaughlin, J.D. Judy, K. Schirmer, Nanomaterials in the environment: behavior, fate, bioavailability, and effects—an updated review, Environ. Toxicol. Chem. 37 (2018) 2029–2063, https://doi.org/10.1002/etc.4147.
[6] E. Kabir, V. Kumar, K.H. Kim, A.C.K. Yip, J.R. Sohn, Environmental impacts of nanomaterials, J. Environ. Manag. 225 (2018) 261–271, https://doi.org/10.1016/j.jenvman.2018.07.087.
[7] K. Savolainen, H. Alenius, H. Norppa, L. Pylkkänen, T. Tuomi, G. Kasper, Risk assessment of engineered nanomaterials and nanotechnologies-a review, Toxicology. 269 (2010) 92–104, https://doi.org/10.1016/j.tox.2010.01.013.
[8] K.L. Garner, S. Suh, A.A. Keller, Assessing the risk of engineered nanomaterials in the environment: development and application of the nanoFate model, Environ. Sci. Technol. 51 (2017) 5541–5551, https://doi.org/10.1021/acs.est.6b05279.
[9] Z. Ferdous, A. Nemmar, Health impact of silver nanoparticles: a review of the biodistribution and toxicity following various routes of exposure, Int. J. Mol. Sci. (2020), https://doi.org/10.3390/ijms21072375.
[10] E. McGillicuddy, I. Murray, S. Kavanagh, L. Morrison, A. Fogarty, M. Cormican, P. Dockery, M. Prendergast, N. Rowan, D. Morris, Silver nanoparticles in the environment: sources, detection and ecotoxicology, Sci. Total Environ. 575 (2017) 231–246, https://doi.org/10.1016/j.scitotenv.2016.10.041.
[11] Y. Li, J. Zhao, E. Shang, X. Xia, J. Niu, J. Crittenden, Effects of chloride ions on dissolution, ROS generation, and toxicity of silver nanoparticles under UV irradiation, Environ. Sci. Technol. 52 (2018) 4842–4849, https://doi.org/10.1021/acs.est.7b04547.
[12] S.A. Johari, M. Sarkheil, M. Behzadi Tayemeh, S. Veisi, Influence of salinity on the toxicity of silver nanoparticles (AgNPs) and silver nitrate (AgNO3) in halophilic microalgae, *Dunaliella salina*, Chemosphere 209 (2018) 156–162, https://doi.org/10.1016/j.chemosphere.2018.06.098.
[13] S. Lekamge, A.F. Miranda, A. Abraham, V. Li, R. Shukla, V. Bansal, D. Nugegoda, The toxicity of silver nanoparticles (AgNPs) to three freshwater invertebrates with different life strategies: *Hydra vulgaris*, *Daphnia carinata*, and *Paratya australiensis*, Front. Environ. Sci. 6 (2018) 1–13, https://doi.org/10.3389/fenvs.2018.00152.
[14] R. Asadi Dokht Lish, S.A. Johari, M. Sarkheil, I.J. Yu, On how environmental and experimental conditions affect the results of aquatic nanotoxicology on brine shrimp (*Artemia salina*): a case of silver nanoparticles toxicity, Environ. Pollut. 255 (2019), https://doi.org/10.1016/j.envpol.2019.113358.
[15] A. Albanese, P.S. Tang, W.C.W. Chan, The effect of nanoparticle size, shape, and surface chemistry on biological systems, Annu. Rev. Biomed. Eng. 14 (2012) 1–16, https://doi.org/10.1146/annurev-bioeng-071811-150124.
[16] J. Jiménez-Lamana, V.I. Slaveykova, Silver nanoparticle behaviour in lake water depends on their surface coating, Sci. Total Environ. 573 (2016) 946–956, https://doi.org/10.1016/j.scitotenv.2016.08.181.
[17] L.M. Furtado, B.C. Norman, M.A. Xenopoulos, P.C. Frost, C.D. Metcalfe, H. Hintelmann, Environmental fate of silver nanoparticles in boreal lake ecosystems, Environ. Sci. Technol. 49 (2015) 8441–8450, https://doi.org/10.1021/acs.est.5b01116.
[18] A. Wimmer, A. Urstoeger, N.C. Funck, F.P. Adler, L. Lenz, M. Doeblinger, M. Schuster, What happens to silver-based nanoparticles if they meet seawater? Water Res. 171 (2020), 115399 https://doi.org/10.1016/j.watres.2019.115399.
[19] L.Q. Chen, L. Fang, J. Ling, C.Z. Ding, B. Kang, C.Z. Huang, Nanotoxicity of silver nanoparticles to red blood cells: size dependent adsorption, uptake, and hemolytic activity, Chem. Res. Toxicol. 28 (2015) 501–509, https://doi.org/10.1021/tx500479m.
[20] J. Dobias, R. Bernier-Latmani, Silver release from silver nanoparticles in natural waters, Environ. Sci. Technol. 47 (2013) 4140–4146, https://doi.org/10.1021/es304023p.
[21] M.D. Montaño, J.W. Olesik, A.G. Barber, K. Challis, J.F. Ranville, Single particle ICP-MS: advances toward routine analysis of nanomaterials, Anal. Bioanal. Chem. 408 (2016) 5053–5074, https://doi.org/10.1007/s00216-016-9676-8.
[22] F. Laborda, E. Bolea, J. Jiménez-Lamana, Single particle inductively coupled plasma mass spectrometry for the analysis of inorganic engineered nanoparticles in environmental samples, Trends Environ. Anal. Chem. 9 (2016) 15–23, https://doi.org/10.1016/j.teac.2016.02.001.
[23] F. Laborda, E. Bolea, J. Jiménez-Lamana, Single particle inductively coupled plasma mass spectrometry: a powerful tool for nanoanalysis, Anal. Chem. 86 (2014) 2270–2278, https://doi.org/10.1021/ac402980q.
[24] B. Meermann, V. Nischwitz, ICP-MS for the analysis at the nanoscale – a tutorial review, J. Anal. At. Spectrom. 33 (2018) 1432–1468, https://doi.org/10.1039/C8JA00037A.
[25] D. Mozhayeva, C. Engelhard, A critical review of single particle inductively coupled plasma mass spectrometry – a step towards an ideal method for nanomaterial characterization, J. Anal. At. Spectrom. 35 (2020) 1740–1783, https://doi.org/10.1039/c9ja00206e.
[26] C. Degueldre, P.Y. Favarger, Colloid analysis by single particle inductively coupled plasma-mass spectroscopy: a feasibility study, Colloids Surfaces A Physicochem. Eng. Asp. 217 (2003) 137–142, https://doi.org/10.1016/S0927-7757(02)00568-X.
[27] F. Laborda, J. Jiménez-Lamana, E. Bolea, J.R. Castillo, Selective identification, characterization and determination of dissolved silver(i) and silver nanoparticles based on single particle detection by inductively coupled plasma mass spectrometry, J. Anal. At. Spectrom. 26 (2011) 1362–1371, https://doi.org/10.1039/c0ja00098a.
[28] H.E. Pace, N.J. Rogers, C. Jarolimek, V.A. Coleman, C.P. Higgins, J.F. Ranville, Determining transport efficiency for the purpose of counting and sizing nanoparticles via single particle inductively coupled plasma mass spectrometry, Anal. Chem. 83 (2011) 9361–9369, https://doi.org/10.1021/ac201952t.
[29] F. Laborda, J. Jiménez-Lamana, E. Bolea, J.R. Castillo, Critical considerations for the determination of nanoparticle number concentrations, size and number size distributions by single particle ICP-MS, J. Anal. At. Spectrom. 28 (2013) 1220–1232, https://doi.org/10.1039/c3ja50100k.
[30] D.M. Schwertfeger, J.R. Velicogna, A.H. Jesmer, R.P. Scroggins, J.I. Princz, Single particle-inductively coupled plasma mass spectroscopy analysis of metallic nanoparticles in environmental samples with large dissolved analyte fractions, Anal. Chem. 88 (2016) 9908–9914, https://doi.org/10.1021/acs.analchem.6b02716.
[31] M. Hadioui, C. Peyrot, K.J. Wilkinson, Improvements to single particle ICPMS by the online coupling of ion exchange resins, Anal. Chem. 86 (2014) 4668–4674, https://doi.org/10.1021/ac5004932.
[32] K. Newman, C. Metcalfe, J. Martin, H. Hintelmann, P. Shaw, A. Donard, Improved single particle ICP-MS characterization of silver nanoparticles at environmentally relevant concentrations, J. Anal. At. Spectrom. 31 (2016) 2069–2077, https://doi.org/10.1039/c6ja00221h.
[33] F. Laborda, A.C. Gimenez-Ingalaturre, E. Bolea, J.R. Castillo, About detectability and limits of detection in single particle inductively coupled plasma mass spectrometry, Spectrochim, Acta - Part B At. Spectrosc. 169 (2020), 105883, https://doi.org/10.1016/j.sab.2020.105883.
[34] D. Mozhayeva, C. Engelhard, A quantitative nanoparticle extraction method for microsecond time resolved single-particle ICP-MS data in the presence of a high background, J. Anal. At. Spectrom. 34 (2019) 1571–1580, https://doi.org/10.1039/c9ja00042a.
[35] A. Gundlach-Graham, L. Hendriks, K. Mehrabi, D. Günther, Monte carlo simulation of low-count signals in time-of-flight mass spectrometry and its application to single-particle detection, Anal. Chem. 90 (2018) 11847–11855, https://doi.org/10.1021/acs.analchem.8b01551.
[36] H.E. Pace, N.J. Rogers, C. Jarolimek, V.A. Coleman, E.P. Gray, C.P. Higgins, J. F. Ranville, Single particle inductively coupled plasma-mass spectrometry: a performance evaluation and method comparison in the determination of nanoparticle size, Environ. Sci. Technol. 46 (2012) 12272–12280, https://doi.org/10.1021/es301787d.
[37] B. Giese, F. Klaessig, B. Park, R. Kaegi, M. Steinfeldt, H. Wigger, A. Von Gleich, F. Gottschalk, Risks, release and concentrations of engineered nanomaterial in the environment, Sci. Rep. 8 (2018) 1–18, https://doi.org/10.1038/s41598-018-19275-4.
[38] T.Y. Sun, N.A. Bornhöft, K. Hungerbühler, B. Nowack, Dynamic probabilistic modeling of environmental emissions of engineered nanomaterials, Environ. Sci. Technol. 50 (2016) 4701–4711, https://doi.org/10.1021/acs.est.5b05828.
[39] M. Hadioui, S. Leclerc, K.J. Wilkinson, Multimethod quantification of Ag+ release from nanosilver, Talanta 105 (2013) 15–19, https://doi.org/10.1016/j.talanta.2012.11.048.
[40] A.L. Fabricius, L. Duester, B. Meermann, T.A. Ternes, ICP-MS-based characterization of inorganic nanoparticles-sample preparation and off-line fractionation strategies, Anal. Bioanal. Chem. 406 (2014) 467–479, https://doi.org/10.1007/s00216-013-7480-2.

[41] L. Torrent, F. Laborda, E. Marguí, M. Hidalgo, M. Iglesias, Combination of cloud point extraction with single particle inductively coupled plasma mass spectrometry to characterize silver nanoparticles in soil leachates, Anal. Bioanal. Chem. 411 (2019) 5317–5329, https://doi.org/10.1007/s00216-019-01914-y.
[42] A. Wimmer, A. Urstoeger, T. Hinke, M. Aust, P.J. Altmann, M. Schuster, Separating dissolved silver from nanoparticulate silver is the key: improved cloud-point-extraction hyphenated to single particle ICP-MS for comprehensive analysis of silver-based nanoparticles in real environmental samples down to single-digit nm particl, Anal. Chim. Acta 1150 (2021), 238198, https://doi.org/10.1016/j.aca.2021.01.001.
[43] I. López-García, Y. Vicente-Martínez, M. Hernández-Córdoba, Speciation of silver nanoparticles and Ag(I) species using cloud point extraction followed by electrothermal atomic absorption spectrometry, Spectrochim. Acta - Part B At. Spectrosc. 101 (2014) 93–97, https://doi.org/10.1016/j.sab.2014.07.017.
[44] J. Soto-Alvaredo, M. Montes-Bayón, J. Bettmer, Speciation of silver nanoparticles and silver(I) by reversed-phase liquid chromatography coupled to ICPMS, Anal. Chem. 85 (2013) 1316–1321, https://doi.org/10.1021/ac302851d.
[45] M.S. Jiménez, M. Bakir, D. Isábal, M.T. Gómez, J. Pérez-Arantegui, J.R. Castillo, F. Laborda, Evaluation of hydrodynamic chromatography coupled to inductively coupled plasma mass spectrometry for speciation of dissolved and nanoparticulate gold and silver, Anal. Bioanal. Chem. (2021) 1689–1699, https://doi.org/10.1007/s00216-020-03132-3.
[46] Y. Yang, L. Luo, H.P. Li, Q. Wang, Z.G. Yang, Z.P. Qu, R. Ding, Analysis of metallic nanoparticles and their ionic counterparts in complex matrix by reversed-phase liquid chromatography coupled to ICP-MS, Talanta 182 (2018) 156–163, https://doi.org/10.1016/j.talanta.2018.01.077.
[47] B. Hetzer, A. Burcza, V. Gräf, E. Walz, R. Greiner, Online-coupling of AF4 and single particle-ICP-MS as an analytical approach for the selective detection of nanosilver release from model food packaging films into food simulants, Food Control 80 (2017) 113–124, https://doi.org/10.1016/j.foodcont.2017.04.040.
[48] K.A. Huynh, E. Siska, E. Heithmar, S. Tadjiki, S.A. Pergantis, Detection and quantification of silver nanoparticles at environmentally relevant concentrations using asymmetric flow field-flow fractionation online with single particle inductively coupled plasma mass spectrometry, Anal. Chem. 88 (2016) 4909–4916, https://doi.org/10.1021/acs.analchem.6b00764.
[49] S.K. Mwilu, E. Siska, R.B.N. Baig, R.S. Varma, E. Heithmar, K.R. Rogers, Separation and measurement of silver nanoparticles and silver ions using magnetic particles, Sci. Total Environ. 472 (2014) 316–323, https://doi.org/10.1016/j.scitotenv.2013.10.077.
[50] L. Luo, Y. Yang, H. Li, R. Ding, Q. Wang, Z. Yang, Size characterization of silver nanoparticles after separation from silver ions in environmental water using magnetic reduced graphene oxide, Sci. Total Environ. 612 (2018) 1215–1222, https://doi.org/10.1016/j.scitotenv.2017.09.024.
[51] I. López-García, J.J. Marín-Hernández, M. Hernández-Córdoba, Freshly prepared magnetic ferrite for the speciation of silver using dispersive micro-solid phase extraction and electrothermal atomic absorption spectrometry, J. Anal. At. Spectrom. 34 (2019) 2112–2118, https://doi.org/10.1039/c9ja00241c.
[52] A. García-Figueroa, F. Pena-Pereira, I. Lavilla, C. Bendicho, Speciation of gold nanoparticles and total gold in natural waters: a novel approach based on naked magnetite nanoparticles in combination with ascorbic acid, Talanta 193 (2019) 176–183, https://doi.org/10.1016/j.talanta.2018.09.092.
[53] T. Tolessa, X.X. Zhou, M. Amde, J.F. Liu, Development of reusable magnetic chitosan microspheres adsorbent for selective extraction of trace level silver nanoparticles in environmental waters prior to ICP-MS analysis, Talanta 169 (2017) 91–97, https://doi.org/10.1016/j.talanta.2017.03.064.
[54] P. Anekthirakun, A. Imyim, Separation of silver ions and silver nanoparticles by silica based-solid phase extraction prior to ICP-OES determination, Microchem. J. 145 (2019) 470–475, https://doi.org/10.1016/j.microc.2018.11.008.
[55] L. Fréchette-Viens, M. Hadioui, K.J. Wilkinson, Quantification of ZnO nanoparticles and other Zn containing colloids in natural waters using a high sensitivity single particle ICP-MS, Talanta 200 (2019) 156–162, https://doi.org/10.1016/j.talanta.2019.03.041.
[56] L. Li, G. Hartmann, M. Döblinger, M. Schuster, Quantification of nanoscale silver particles removal and release from municipal wastewater treatment plants in Germany, Environ. Sci. Technol. 47 (2013) 7317–7323, https://doi.org/10.1021/es3041658.
[57] Di Schwertfeger, J. Velicogna, A. Jesmer, H. McShane, R. Scroggins, J. Princz, Ion exchange technique (IET) to characterise Ag+ exposure in soil extracts contaminated with engineered silver nanoparticles, Environ. Chem. 14 (2017) 123–133, https://doi.org/10.1071/EN16136.
[59] L. Li, K. Leopold, Ligand-assisted extraction for separation and preconcentration of gold nanoparticles from waters, Anal. Chem. 84 (2012) 4340–4349, https://doi.org/10.1021/ac2034437.
[60] L. Fréchette-Viens, M. Hadioui, K.J. Wilkinson, Practical limitations of single particle ICP-MS in the determination of nanoparticle size distributions and dissolution: case of rare earth oxides, Talanta 163 (2017) 121–126, https://doi.org/10.1016/j.talanta.2016.10.093.
[61] M. Hadioui, V. Merdzan, K.J. Wilkinson, Detection and characterization of ZnO nanoparticles in surface and waste waters using single particle ICPMS, Environ. Sci. Technol. 49 (2015) 6141–6148, https://doi.org/10.1021/acs.est.5b00681.
[62] P. Cervantes-Avilés, Y. Huang, A.A. Keller, Multi-technique approach to study the stability of silver nanoparticles at predicted environmental concentrations in wastewater, Water Res. 166 (2019), https://doi.org/10.1016/j.watres.2019.115072.
[63] S. Bazargan, R. Hill, H. Badiei, Systems and Methods for Automated Analysis of Output in Single Particle Inductively Coupled Plasma Mass Spectrometry and Similar Data Sets, US 9, 754,774 B2, 2017.
[64] A.R. Montoro Bustos, K.P. Purushotham, A. Possolo, N. Farkas, A.E. Vladár, K. E. Murphy, M.R. Winchester, Validation of single particle ICP-MS for routine measurements of nanoparticle size and number size distribution, Anal. Chem. 90 (2018) 14376–14386, https://doi.org/10.1021/acs.analchem.8b03871.
[65] V. Geertsen, E. Barruet, F. Gobeaux, J.L. Lacour, O. Taché, Contribution to accurate spherical gold nanoparticle size determination by single-particle inductively coupled mass spectrometry: a comparison with small-angle X-ray scattering, Anal. Chem. 90 (2018) 9742–9750, https://doi.org/10.1021/acs.analchem.8b01167.
[66] J. Liu, K.E. Murphy, R.I. Maccuspie, M.R. Winchester, Capabilities of single particle inductively coupled plasma mass spectrometry for the size measurement of nanoparticles: a case study on gold nanoparticles, Anal. Chem. 86 (2014) 3405–3414, https://doi.org/10.1021/ac403775a.
[67] R.C. Merrifield, C. Stephan, J.R. Lead, Single-particle inductively coupled plasma mass spectroscopy analysis of size and number concentration in mixtures of monometallic and bimetallic (core-shell) nanoparticles, Talanta. 162 (2017) 130–134, https://doi.org/10.1016/j.talanta.2016.09.070.
[68] B. Kim, C.S. Park, M. Murayama, M.F. Hochella, Discovery and characterization of silver sulfide nanoparticles in final sewage sludge products, Environ. Sci. Technol. 44 (2010) 7509–7514, https://doi.org/10.1021/es101565j.
[69] Y.-J. Chang, Y.-H. Shih, C.-H. Su, H.-C. Ho, Comparison of three analytical methods to measure the size of silver nanoparticles in real environmental water and wastewater samples, J. Hazard. Mater. 322 (2017) 95–104, https://doi.org/10.1016/j.jhazmat.2016.03.030.
[70] L.J. Gimbert, P.M. Haygarth, R. Beckett, P.J. Worsfold, The influence of sample preparation on observed particle size distributions for contrasting soil suspensions using flow field-flow fractionation, Environ. Chem. 3 (2006) 184–191, https://doi.org/10.1071/EN06029.
[71] D.M. Schwertfeger, J.R. Velicogna, A.H. Jesmer, S. Saatcioglu, H. McShane, R. P. Scroggins, J.I. Princz, Extracting metallic nanoparticles from soils for quantitative analysis: method development using engineered silver nanoparticles and SP-ICP-MS, Anal. Chem. 89 (2017) 2505–2513, https://doi.org/10.1021/acs.analchem.6b04668.
[72] L. Li, Q. Wang, Y. Yang, L. Luo, R. Ding, Z.G. Yang, H.P. Li, Extraction method development for quantitative detection of silver nanoparticles in environmental soils and sediments by single particle inductively coupled plasma mass spectrometry, Anal. Chem. 91 (2019) 9442–9450, https://doi.org/10.1021/acs.analchem.8b05575.
[73] Bio-Rad Laboratories, Chelex 100 Chelating Ion Exchange Resin Instruction Manual, Bio-Rad Lab, 2017, pp. 1–24.
[74] Edward Tipping, Cation Binding by Humic Substances, 1st ed., Cambridge University Press, New York, 2002.
[75] R. Sekine, K. Khurana, K. Vasilev, E. Lombi, E. Donner, Quantifying the adsorption of ionic silver and functionalized nanoparticles during ecotoxicity testing: test container effects and recommendations, Nanotoxicology 9 (2015) 1005–1012, https://doi.org/10.3109/17435390.2014.994570.

III

APPLICATION OF 3D PRINTED SCAVENGERS FOR IMPROVING THE ACCURACY OF SINGLE-PARTICLE INDUCTIVELY COUPLED PLASMA MASS SPECTROMETRY ANALYSES OF SILVER NANOPARTICLES BY DISSOLVED SILVER REMOVAL

by

Virva Kinnunen, Janne Frimodig, Siiri Perämäki & Rose Matilainen 2023

Spectrochimica Acta Part B: Atomic Spectroscopy vol 203, 106662

DOI: 10.1016/j.sab.2023.106662

Spectrochimica Acta Part B: Atomic Spectroscopy 203 (2023) 106662

Contents lists available at ScienceDirect

Spectrochimica Acta Part B: Atomic Spectroscopy

journal homepage: www.elsevier.com/locate/sab

Application of 3D printed scavengers for improving the accuracy of single-particle inductively coupled plasma mass spectrometry analyses of silver nanoparticles by dissolved silver removal

Virva Kinnunen *, Janne Frimodig, Siiri Perämäki, Rose Matilainen

Department of Chemistry, Chemistry in Circular Economy, University of Jyväskylä, P.O. Box 35, FI-40014 Jyväskylä, Finland

ARTICLE INFO

Keywords:
SP-ICP-MS
Silver nanoparticles
Functional 3D scavengers
Dissolved silver interference
3D printing

ABSTRACT

The determination of silver nanoparticles (Ag NPs) with single-particle inductively coupled plasma mass spectrometry can be severely interfered with coexisting dissolved silver causing high background signals, which can lead to inaccurate quantification of NP size and particle concentration. In this paper, chemically active and reusable 3D printed scavengers are applied for highly efficient dissolved silver removal in Ag NP dispersions, allowing more accurate determination of particle concentration and size. Selective laser sintering was used for constructing the porous 3D scavengers constituting of polystyrene used as a supporting material and ion-exchange material SiliaBond Tosic acid (TA), which were chosen based on their high dissolved silver extraction efficiency and ability to maintain original NP properties. The macroporous structure of the final 3D TA scavengers allowed Ag NPs to pass freely through the object without affecting their original properties. The efficient contact between the sample solution and the functional material resulted in rapid (ca. <1 min/sample), and highly efficient dissolved silver removal (≥98%). The 3D TA scavengers showed potential to be used for preconcentration of dissolved silver, and the retained dissolved silver can be eluted with a 0.5 mM solution of sodium thiosulphate with excellent recoveries (≥99%). Competitive adsorption of elements commonly found in natural waters (Ca, K, Mg, Na, S, Si, and Sr) were not found to affect the dissolved silver extraction efficiency. The developed pre-treatment method was applied for the determination of 30 nm Ag NPs in ultrapure and clear environmental waters with coexisting dissolved silver (0.2 μg kg^{-1}). Whereas measurement of the samples as such led to a significant bias in NP sizing (up to +12% increase) and counting (up to −51% decrease), pre-treatment of samples with the functional 3D TA scavengers eliminated the interfering effect of dissolved silver. This resulted in significant improvement in NP detection and determination. Highly similar values were obtained for both NP mean size (30 ± 1 nm, <4% different) and concentration (<13% different) in all matrices studied as compared to samples in the absence of dissolved silver.

1. Introduction

The antimicrobial properties of silver nanoparticles (Ag NPs) are increasingly used in various applications and consumer products, which has raised concerns about their potential adverse effects on the environment and human health [1–5]. The realistic risk assessment of these materials requires sensitive analytical techniques, for which single-particle inductively coupled plasma mass spectrometry (SP-ICP-MS) has evolved as a viable alternative [6–9]. In SP-ICP-MS, the analyte intensity is recorded as a function of time using very short dwell times (e.g. ≤10 ms [6]). Whereas the ionization of the dissolved element results in a constant flow of ions to the detector and thus a relative steady-state signal, ionization of individual NPs generates a discrete pulse of ions separating from the baseline. The intensities originating from NPs can be obtained by the separation of pulse intensities over a certain threshold limit, which is typically determined using an iterative 'mean + 3σ' computation [7,10–13]. In the presence of high concentration of dissolved element, however, separation of the NP events from the background signal can prove challenging. In these cases, the dissolved signal might overlap NP pulses and lead to the computation of a threshold value being larger than some or possibly all NP signals, and thus, biased determination (overestimation of the NP size and underestimation of the

* Corresponding author.
E-mail address: virva.v-t.kinnunen@jyu.fi (V. Kinnunen).

https://doi.org/10.1016/j.sab.2023.106662
Received 13 July 2022; Received in revised form 15 March 2023; Accepted 16 March 2023
Available online 17 March 2023

particle concentration) [14,15]. The situation is particularly challenging for samples containing elevated concentrations of dissolved analyte and/or small NPs, e.g. for environmental samples [15–17].

In the presence of high concentrations of dissolved elements, the use of high data acquisition frequencies (with dwell times ≤100 μs) [7,18,19] or sophisticated mathematical models [20,21] can be used to improve the separation of NP events from the background signal. However, these methods are often found inadequate to eliminate the interfering effect of coexisting dissolved element or may require laborious manual data processing. The background signal can be decreased efficiently by physical removal of the dissolved element as well, for which several options have been suggested over the years. The simplest solution for reducing the dissolved concentration of the sample is sample dilution, as proposed by Schwertfeger et al. [16]. However, considering environmental samples with low NP concentration [2,16,17,22,23], sampling times often need to be extended to ensure the capture of a sufficient amount of NP events for reliable determination [24]. Sample dilution can also promote NP instability in highly diluted solutions [25–28], which should be avoided.

Over the years, several authors have demonstrated the beneficiation of solid phase extraction (SPE) materials for efficient separation of NPs from their ionic counterparts followed by SP-ICP-MS detection [14,15,29–31]. These materials have been used either for sample pre-treatment in off-line systems [14,30] or in-lab built columns connected directly on-line with ICP-MS [15,29,31,32]. The use of powdery SPE materials, however, can be challenging requiring either separation of the solid materials from the sample solution or time-consuming washing and regeneration steps in on-line systems (up to 60 min). These problems can be avoided by the utilization of 3D printing, which has gained great interest in a wide array of applications [33–36]. In addition to producing complex objects with precise dimensions, 3D printing technique can be used for manufacturing of objects possessing actual chemical functionalities, such as catalysts [24,37] and 3D printed scavengers used for the recovery of pharmaceuticals [38] and precious metals [39,40] from waste streams. In selective laser sintering (SLS), polymer particles used as printing material are partially sintered together to obtain an object with desired size and shape. The partial melting of the particles allows the formation of a highly porous structure with accessible voids between the sintered polymer grains, allowing the sample solution to pass through the object. The porosity, as well as other physical and mechanical properties of the 3D printed objects, can be controlled by adjusting the printing parameters (e.g. laser speed and power) [41]. An additional benefit of SLS is the wide range of materials used for printing [35], and the possibility to incorporate chemically active materials with specific desired functionalities [37,38,42,43]. Instead of using materials in their powdery form, the incorporation of SPE materials into 3D objects with fully customizable size, shape, porosity, and functionality increases their usability in a wide range of applications.

This paper presents a novel sample pre-treatment procedure using a functional 3D printed scavenger for the efficient removal of dissolved silver in NP dispersions, allowing more accurate determination of Ag NP size and concentration. The effect of 3D scavengers on Ag NP properties and their ability to extract dissolved silver is thoroughly investigated. In addition, the selectivity towards silver in the presence of various competing elements commonly found in natural waters (Ca, K, Mg, Na, S, Si, and Sr) and the adsorption behaviour of the 3D scavengers is studied. Finally, the proposed method is applied for the determination of 30 nm Ag NPs in ultrapure (UP) and clear natural waters. To the best of our knowledge, this study is the first to demonstrate the beneficiation of functional 3D scavengers for improving the accuracy of Ag NP size and concentration determination by dissolved silver removal.

2. Experimental

2.1. Materials

UP water (18.2 MΩ•cm) obtained from PURELAB Ultra water purification system (ELGA LabWater, Buckinghamshire, UK) was used for the preparation of all aqueous solutions and sample dilutions. Single-element stock solutions of silver and ruthenium (1000 mg L^{-1}) and multi-element standard solutions (29-Element and 12-Element Solution, 10 mg L^{-1}) were obtained from PerkinElmer (MA, USA). Sodium thiosulfate (STS, ≥98.0%) and thiourea (TU, ≥99.0%) were obtained from Sigma-Aldrich (Saint Louis, MO, USA). High-purity nitric (HNO_3) and hydrochloric (HCl) acids were obtained from Analytika spol. s r.o. (Prague, Chech Republic). A 1 mol L^{-1} solution of nitric acid was prepared from nitric acid (≥65%) obtained from Sigma-Aldrich. Polystyrene (PS) was obtained from Axalta Polymer Powders (Bulle, Switzerland) and SPE material SiliaBond Tosic acid (TA) from SiliCycle (Québec, Canada).

Citrate-stabilized Ag NPs with nominal sizes of 30, 40, 50, and 80 nm were obtained from NanoComposix (San Diego, CA, USA). Ultra-uniform 50 nm PEG-Carboxyl-stabilized Au NPs specially designed for SP-ICP-MS calibration were obtained from PerkinElmer. The certified values of all commercial NP dispersions were verified in the laboratory before performing any experiments. More details of the verification measurements can be found in the supplementary material (Table S1 in Appendix) and our previous publications [14,44].

Environmental water samples used in this study were collected from different locations situated in Central Finland and stored in the refrigerator at 6–8 °C until use. Before conducting any experiments, the elemental composition and other physicochemical parameters of the water samples were determined in the laboratory. More detailed information on the experimental procedure and the obtained results are presented in Tables S2 and S3 (Appendix).

2.2. Instrumentation

2.2.1. SP-ICP-MS and ICP-MS (standard mode) measurements

All ICP-MS measurements were performed using a NexION350D ICP-MS (PerkinElmer, Table S4 in Appendix) equipped with an ESI 4DX autosampler (Elemental Scientific, NE, USA). The SP-ICP-MS measurements were performed operating the instrument in single-particle mode. A commercially available Syngistix Nano Application Module software (v. 2.5) by PerkinElmer was used for SP-ICP-MS data acquisition and processing of the raw data. The software automatically discriminates the NP events from the continuous background (dissolved) signal using an intensity threshold value determined using an iterative "mean + 3σ" computation [44].

Dissolved silver calibration standards ranging from 0.1 to 2 μg kg^{-1} were prepared from a stock solution of silver (1000 mg L^{-1}). Citrate-stabilized Ag NPs with nominal sizes of 40, 50, and 80 nm were used for the preparation of the particle calibration standards. 50 nm PEG-Carboxyl-stabilized Au NPs were used for transport efficiency determination after dilution to a particle concentration of approximately 10^5 particles g^{-1} using the particle frequency method described by Pace et al. [13]. The sample flow rate was determined daily at least in duplicate by quantifying the water uptake after 3 min of aspiration. To minimize the adsorptive losses of dissolved silver onto solid surfaces [28,45,46] and eliminate any matrix interferences, the matrix of all solutions of silver (both NP and dissolved silver) were adjusted to 0.5 mM of STS before measurement.

ICP-MS operating in standard mode was used in some experiments for the concentration measurements of silver from acidified samples. Calibration standards ranging from 1 to 100 μg kg^{-1} were prepared by diluting the stock solution of silver (1000 mg L^{-1}) with a solution composed of 0.1% TU (*w/v*), 2.25% HCl (*v/v*) and 0.75% HNO_3 (*v/v*). ^{102}Ru was used as the internal standard. All solutions used in the

experiments were diluted gravimetrically daily prior to the experiments.

2.2.2. Scanning electron microscopy

Scanning electron microscope analysis of the 3D scavengers was conducted using Zeiss EVO-50XVP (Carl Zeiss AG, Oberkochen, Germany). Samples were plated with a thin layer of gold using a gold sputter machine to enhance conductivity and improve imaging. Images were produced using backscatter electron detection with an acceleration voltage of 20 kV and a working distance of 9.5 mm.

2.2.3. Preparation of the 3D printed scavengers

The designing of the 3D scavengers was performed using FreeCad (v. 0.16) and Slic3r (v. 1.2.9) softwares to obtain objects with desired size and shape (5 mm in height and 16.5 mm in diameter with an average mass of 0.53 g). The material used for 3D printing was prepared by manually mixing PS and TA in a mass ratio of 1:10 (10 m-% of TA), with an estimated cost of 0.25 €/3D TA scavenger (ca. 0.27 USD). The materials used for constructing the 3D TA scavengers were chosen based on their negligible effects on original NP properties (Table S5 and Fig. S1 in Appendix) and highly efficient dissolved silver extraction efficiency in clear waters [14]. The printing of the 3D scavengers was performed with a Sharebot SnowWhite SLS 3D printer (Nibionno LC, Italy) using the operational parameters shown in Table S6 (Appendix). The 3D TA scavengers were then tightly fit into 10 ml syringes (one 3D scavenger/syringe) and washed with UP water and 1 M HNO_3 to remove any unsintered material or residual impurities. Finally, all 3D scavengers were thoroughly rinsed with UP water until a neutral pH was achieved.

2.2.4. Effect of 3D TA scavengers on analyte properties and regeneration of the scavengers

The ability of the 3D TA scavengers to extract dissolved silver and their possible effect on Ag NPs properties was investigated. Dispersions containing either 1 μg kg^{-1} of dissolved silver or 10^5 part. g^{-1} of 50 nm Ag NPs were passed through a 10 ml syringe containing one 3D TA scavenger within approximately 1 min (flow rate ca. 10 ml min^{-1}). The solution containing Ag NPs was collected from the tip of the syringe into a 15 ml PP tube, whereas dissolved silver is retained in the 3D scavenger during the process. All experiments were performed in triplicate ($n = 3$). The concentration of silver (both dissolved and NP silver) was then analysed with SP-ICP-MS as described in paragraph 2.2. The effect of the 3D scavengers on Ag NP properties was evaluated by comparing the mean particle size and size distribution histograms obtained for samples before (i) and after (f) passing through the 3D scavengers and using eq. 1, where C_p is the obtained particle concentration (part. g^{-1}):

$$C_p recovery\ (\%) = \frac{C_{p(f)}}{C_{p(i)}} \bullet 100\% \quad (1)$$

The dissolved silver extraction efficiency (EE-%) of the 3D TA scavengers was calculated according to Eqs. (2) or (3), where C_{Ag} is the concentration of dissolved silver (μg kg^{-1}) before (i) and after (f) passing through the 3D TA scavenger. Limit of quantification (LOQ) of 0.02 μg kg^{-1} for silver was determined as the mean + 10*standard deviation of blank samples ($n = 50$) and considered in the calculations as follows:

$C_{Ag\ (f)} > LOQ$:

$$EE - \% = \frac{C_{Ag\ (i)} - C_{Ag\ (f)}}{C_{Ag\ (i)}} \bullet 100\% \quad (2)$$

$C_{Ag\ (f)} < LOQ$:

$$EE - \% \geq \frac{C_{Ag\ (i)} - LOQ}{C_{Ag\ (i)}} \bullet 100\% \quad (3)$$

After use, all 3D scavengers were post-treated allowing the reusability of the scavengers and to investigate the possibility to retain the adsorbed silver. First, 3D scavengers were rinsed with UP water (10 ml) to remove any sample residues, after which blank samples constituting of 10 ml of UP water were passed through the 3D scavengers within one minute to evaluate possible carry-over. Following this, the adsorbed dissolved silver was eluted using 10 ml of 0.5 mM STS solution with a flow rate of ca. 10 ml min^{-1}. The silver content of the solutions was then measured with SP-ICP-MS as described in paragraph 2.2. The desorption efficiency (DE-%) was calculated according to Eqs. 4 or 5, where $C_{Ag\ (e)}$ is the concentration of dissolved silver (μg kg^{-1}) in the elution solution and V_e and V_i are the amounts of the elution and sample solutions (in kg), respectively:

$C_{Ag\ (f)} > LOQ$:

$$DE - \% = \frac{C_{Ag\ (e)} \bullet V_e}{\left(C_{Ag\ (i)} - C_{Ag\ (f)}\right) \bullet V_i} \bullet 100\% \quad (4)$$

$C_{Ag\ (f)} < LOQ$:

$$DE - \% \geq \frac{C_{Ag\ (e)} \bullet V_e}{\left(C_{Ag\ (i)} - 0\right) \bullet V_i} \bullet 100\% \quad (5)$$

After desorption, any STS residues were rinsed off with ca. 40 ml of UP water, and the 3D TA scavengers regenerated by passing 10 ml of 1 M HNO_3 through the 3D scavengers within approximately one minute. Finally, 3D scavengers were thoroughly rinsed with UP water until a neutral pH was achieved (ca. 40 ml).

2.2.5. Selectivity experiments

The selectivity of the 3D TA scavenger towards silver in the presence of competing elements commonly found in natural waters (Ca, K, Mg, Na, S, Si, and Sr) was investigated by comparing the elemental composition of spring water (1) spiked with 1 μg kg^{-1} of dissolved silver before and after passing through the 3D TA scavenger. Experiments were performed in duplicate ($n = 2$) as described in paragraph 2.4. After extracting the sample for SP-ICP-MS, a second aliquot of the residual sample was further extracted for ICP-OES to determine the concentration of the other elements. Finally, 3D TA scavengers were treated as described in paragraph 2.4 to elute the adsorbed dissolved silver and regenerate the scavengers.

2.2.6. Breakthrough experiments

The adsorption performance of the 3D TA scavengers was studied by performing flow-through experiments. A solution containing 1 mg L^{-1} of dissolved silver was prepared in UP water and 10 ml of the solution was set aside for direct analysis to determine the initial concentration (C_0) of silver. Following this, the solution was passed through a 10 ml syringe containing one 3D TA scavenger in 6 or 10 ml portions using a peristaltic pump (Shenchen LabV1, Baoding Shenchen Precision Pump Co., Ltd., China) with a flow rate of 2 ml min^{-1}. The concentration of silver was then determined with ICP-MS (standard mode) after an appropriate dilution. Experiments were performed on duplicate samples ($n = 2$). The adsorption performance of the 3D TA scavenger was estimated by comparing the concentration of the samples passed through the 3D TA scavenger (C_e) to the initial concentration (C_0).

2.2.7. Reusability of the 3D TA scavenger

The reusability of the 3D TA scavengers was estimated by monitoring the dissolved silver extraction efficiency and the particle concentration recoveries of the 3D TA scavengers over extended time periods. As the 3D TA scavengers can be used either for dissolved silver removal in NP dispersions or potentially also for preconcentration of dissolved silver, the reusability of the scavengers was evaluated on two different occasions. Firstly, the reusability of the scavengers was estimated for the purpose of dissolved silver removal only ("short-term reusability"). Secondly, the adsorbed silver was desorbed between samples, and the 3D scavengers were exposed to the full adsorption-elution cycle ("long-term reusability").

For the evaluation of the short-term reusability, a total of 100 ml of a dispersion containing 1 μg kg^{-1} of dissolved silver and ca. 10^5 particles

g^{-1} of 50 nm Ag NPs was passed through a 10 ml syringe containing one 3D TA scavenger in 10 ml increments. Between samples, the 3D TA scavenger was rinsed with 10 ml of UP water to remove any sample residues. Following this, blank samples were taken by passing 10 ml of UP water through the syringe to monitor possible carry-over. The silver content of the samples (both NP and dissolved silver) was then measured with SP-ICP-MS. The evaluation of the long-term reusability was performed similarly as above, however, between samples the adsorbed silver was eluted using 10 ml of 0.5 mM STS solution, and the scavenger was regenerated as described in paragraph 2.4.

2.2.8. Analysis of environmental water samples

The applicability of the proposed pre-treatment method for dissolved silver removal in NP dispersions was demonstrated by analysing water samples (UP and two spring waters) spiked with 30 nm Ag NPs (10^5 part. g^{-1}) and 0 or 0.2 μg kg^{-1} of dissolved silver. To evaluate the performance of the 3D TA scavengers, samples were analysed as such and after passing through the 3D TA scavengers as described in paragraph 2.4 in triplicate ($n = 3$). For comparative purposes, samples spiked with 0.2 μg kg^{-1} of dissolved silver were analysed also from 4-fold diluted samples. In these cases, sampling times were increased to 120 s to ensure the capture of a sufficient number of NP pulses for reliable NP determination (>100 events). The silver content of all samples was then measured with SP-ICP-MS as described in paragraph 2.2.

3. Results and discussion

3.1. Effect of 3D TA scavengers on sample properties

Fig. 1 presents the effect of the 3D TA scavengers on the mean size, particle concentration, and size distribution histograms of the 50 nm Ag NPs. The highly porous structure of the 3D TA scavengers (Fig. S2 in Appendix) allows Ag NPs to pass through the object without significantly interacting with the 3D scavenger, as confirmed by the highly similar values obtained for the samples before and after passing through the 3D TA scavengers (Fig. 1). No significant changes were either observed in the size distribution histograms, confirming the suitability of the 3D TA scavengers on NP dispersions.

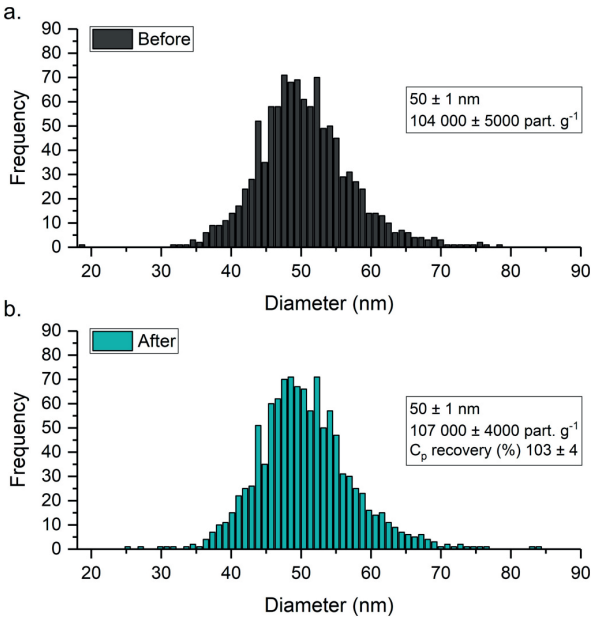

Fig. 1. The obtained values for the 50 nm Ag NP mean size and particle concentration and the size distribution histograms before (a) and after (b) passing through the 3D TA scavengers. Results are presented as a mean ± standard deviation (1 s) of three replicates ($n = 3$).

Once the 3D TA scavengers' ability to maintain the original Ag NP properties of the samples was confirmed, their dissolved silver extraction efficiency was further investigated. The macroporous structure of the 3D scavengers allowed an effective contact between the sample and the functional material, resulting in rapid (ca. 1 min/sample) and highly efficient extraction of dissolved silver (≥98%, n = 3). The dissolved silver concentrations in the solutions after passage through the 3D scavengers were near or below the LOQ of 0.02 μg kg^{-1}, indicating nearly complete adsorption. In addition, no silver was detected in the blank samples passed through the 3D TA scavengers after samples, proving that the dissolved silver was efficiently retained in the scavengers.

After confirming the suitability of the 3D TA scavengers on dissolved silver removal in NP dispersions, the possibility to desorb the adsorbed dissolved silver by elution was further investigated. STS was chosen as the most promising eluent, as it is a well-known efficient complexing agent for Ag^+ [47–49] and directly compatible with the calibration standards' matrix used in this study. Based on the preliminary studies conducted, 0.5 mM STS with 10 ml of volume was chosen as the eluent for its high efficiency and direct combability with the calibration standards (Table S7 in Appendix). Using the 0.5 mM STS solution with 10 ml of volume, excellent desorption efficiencies (≥99%, $n = 3$) were achieved. These observations indicate, that preconcentration of dissolved silver in 3D TA scavengers is possible, and efficient elution can be achieved with a 0.5 mM solution of STS.

3.2. Selectivity experiments

The selectivity of the 3D TA scavenger towards Ag was studied by investigating the competitive adsorption of various elements from a spiked spring water sample. The elemental composition of the sample before and after passing through the 3D TA scavenger is presented in Table S8 (Appendix). 3D TA scavenger was shown to extract various elements except for S and Si. Similar findings were obtained also for TA in our previous study [14], indicating that the printing process does not alter the functionality of the SPE material. The competitive adsorption of other elements was, however, not found to affect the extraction or elution efficiencies of dissolved silver, as highly efficient dissolved silver extraction (95%) and desorption efficiencies (101%) were still achieved ($n = 2$, Table S8 in Appendix). This proves the usability of the proposed method for dissolved silver removal in NP dispersion from environmental waters.

3.3. Breakthrough experiments

The experimental breakthrough curve obtained for the 3D TA scavengers using a flow rate of 2 ml min^{-1} is presented in Fig. S3 (Appendix). A gradual upward trending curve is obtained, indicating the slow saturation of the SPE materials' active sites with the increasing amount of retained silver. The 3D TA scavenger extracts dissolved silver efficiently (EE-% > 90%, i.e. $C_e/C_0 < 0.1$) until reaching the breakthrough point, which is observed after adsorption of ca. 0.10 mg of silver. After this point, the dissolved silver extraction efficiency is observed to fall below 90% (i.e., $C_e/C_0 > 0.1$), indicating the need for regeneration of the 3D TA scavenger. Eventually, full saturation is reached after the adsorption of approximately 0.60 mg of silver, after which the extraction efficiency of dissolved silver remains relatively constant (EE-% < 10%, i.e., $C_e/C_0 > 0.9$). For a 1 μg L^{-1} solution of dissolved silver, the breakthrough point would be achieved after the passage of 100 l of solution.

In samples containing other elements commonly found in natural waters (e.g. Ca and Na), the competitive binding of other elements needs to be taken into account, as these affect the capacity of the 3D TA scavenger. However, a major benefit of using 3D scavengers is that the

adsorption capacity can be easily increased by adjusting the portion of the chemically active component in the scavengers. Additionally, multiple scavengers can be used in the syringe, or the dimensions of the scavengers can be increased.

3.4. Reusability of the 3D TA scavenger

The reusability of the 3D scavengers was estimated by assessing the performance of the 3D TA scavengers over extended time periods. As seen in Fig. S4 (Appendix), 3D TA scavengers can be reused at least 10 times without a loss of dissolved silver extraction efficiency (≥98%) or significant changes in the properties of the Ag NPs. No dissolved silver nor significant amounts of particles (<5 peaks) were detected in the blank samples taken between samples, confirming the lack of significant interactions of the Ag NPs with the 3D TA scavengers, as already noticed in paragraph 3.1. Considering the long-term reusability, the 3D TA scavengers can be reused at least 5 times without affecting the functioning of the scavengers. Excellent dissolved silver extraction (≥98%) and elution (≥87%) efficiencies were achieved during the experiment, with no significant changes in NP size or concentration (Fig. S5 in Appendix).

3.5. Analysis of environmental water samples

As shown before [14,15,50], even low concentrations of dissolved silver can severely interfere with the detection of Ag NPs, leading to the inaccurate determination of these materials. As the intensity of observed NP events is related to particle mass, coexisting dissolved silver interferes foremost with the detection of the smallest NPs by increasing the size critical values [14,15,19,50,51]. Results obtained in this study confirm these observations. The presence of even 0.2 μg kg^{-1} of dissolved silver increased the size critical values from 15 nm to 19–21 nm (Table S9 in Appendix) and clearly interfered with the determination of the 30 nm Ag NPs (Fig. S6 in Appendix). As a result, a significant decrease in particle concentration (up to −51%) and an increase in particle diameter (up to +12%) was observed. The interfering effect of coexisting dissolved silver on the determination of the 30 nm Ag NPs can also be clearly seen in the size distribution histograms (Figs. S7 – S9 in Appendix). By pre-treating the samples with 3D TA scavengers, however, the interfering effect of dissolved silver can be eliminated by efficient removal of dissolved silver (≥89%, dissolved silver concentrations < LOQ, Table S10 in Appendix). This significantly improves the detection of NP events, thus allowing more accurate NP determination. When compared to samples with no added dissolved silver, highly similar values were obtained for both NP mean size (30 ± 1 nm, <4%

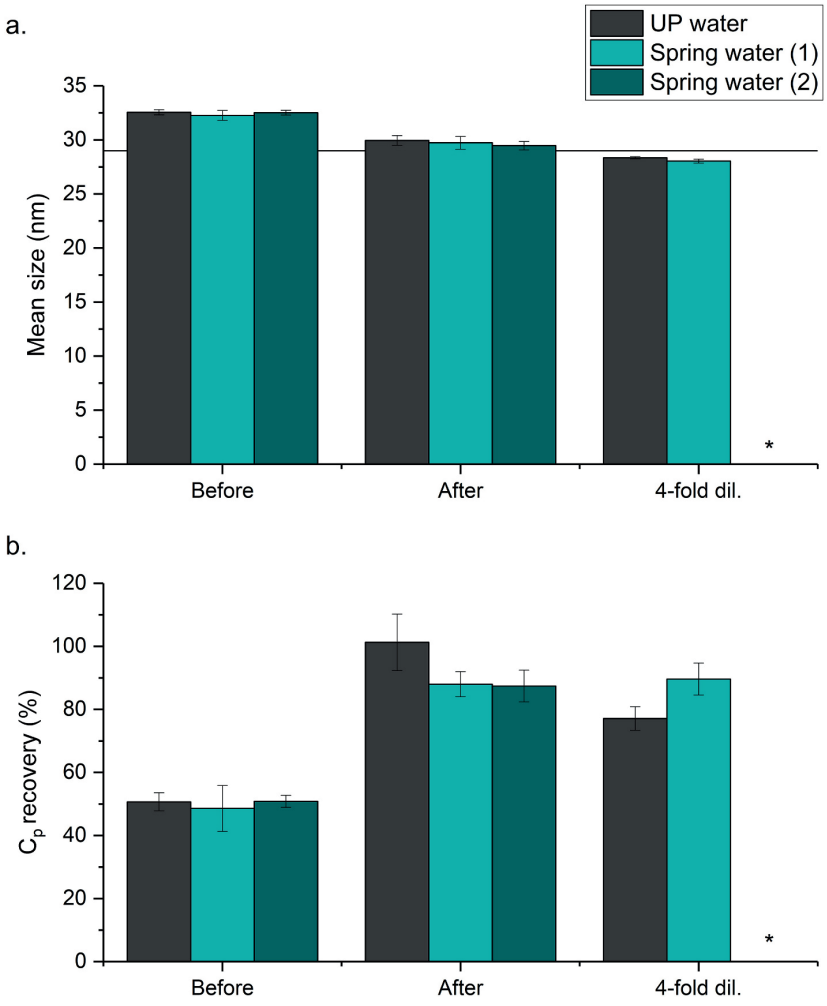

Fig. 2. The obtained results for particle mean size (a) and concentration (b) for the 30 nm Ag NP dispersions spiked with 0.2 μg kg^{-1} of dissolved silver before and after passing through the 3D TA scavenger. For comparative purposes, results are presented also for the 4-fold diluted samples. Results are given as mean ± standard deviation (1 s) of three replicates (n = 3). The reference line in Fig. 2a indicates the certified value of the 30 nm Ag NPs used in the experiments (29 ± 3 nm). Please note that the results obtained for 4-fold diluted spring water (2) sample are not shown for the occurrence of false positives (please see paragraph 10.2 in Appendix for a more detailed discussion).

different) and concentration (<13% different, Fig. 2) in all matrices studied. In addition, the adsorbed dissolved silver was recovered with satisfactory results (≥75%, Table S10 in Appendix), indicating the possibility of beneficiation of the 3D TA scavengers for preconcentration of dissolved silver in NP dispersions.

Generally, similar results were obtained for the 4-fold diluted UP and spring water (1) samples (Fig. 2), further confirming the suitability of the proposed method for dissolved silver removal in NP dispersions. However, changes in the size distribution histogram were observed for the 4-fold diluted spring water (2) sample, leading to significantly biased Ag NP determination (Fig. S9 and Table S9 in Appendix). As the observed low intensity events result presumably from the occurrence of false positives (please see paragraph 10.2 in Appendix for a more detailed discussion), these results were discarded. On the other hand, the pre-treatment of samples with the 3D TA scavengers eliminated the interfering effect of coexisting dissolved silver in all matrices while preserving the original NP properties (Figs. S7 – S9), highlighting the benefits of the proposed sample pre-treatment method. In addition, whereas the characterization of NPs in diluted samples often requires the extension of sampling times to ensure the capture of a sufficient amount of NP events [16,24,25], sample pre-treatment with the 3D TA scavengers can be performed extremely fast (ca. 1 min/sample).

4. Conclusions

This paper presents a novel sample pre-treatment method using functional 3D printed scavengers for more accurate NP determination by efficient removal of dissolved silver in Ag NP dispersions. The sample pre-treatment method proposed here offers a simple, extremely fast, and cost-effective alternative for the previously reported methods for dissolved analyte removal. The 3D printed scavengers are easy to handle, reusable, and fully customizable, allowing their widespread beneficiation in numerous applications. The 3D scavengers composed of polystyrene used as a supporting matrix and ion-exchange material SiliaBond Tosic acid (TA) were able to extract dissolved silver highly efficiently (≥98%) while maintaining the original Ag NP properties (size and concentration). The presence of various elements commonly found in natural waters (Ca, K, Mg, Na, S, Si, and Sr) was not shown to affect the 3D TA scavengers' dissolved silver extraction efficiency. In addition, the 3D TA scavengers can potentially be used for the preconcentration of dissolved silver, and efficient desorption (≥99%) can be achieved with 0.5 mM sodium thiosulfate solution. The applicability of the proposed sample pre-treatment method was further demonstrated in clear waters (ultrapure and two spring waters) containing 30 nm Ag NPs and 0.2 μg kg^{-1} of dissolved silver. Whereas measurement of samples as such resulted in significant bias in NP determination (up to +12% increase in NP sizing and up to −51% decrease in particle concentration), pre-treatment of samples with 3D TA scavengers eliminated the interfering effect of dissolved silver. This allowed more accurate determination of Ag NP concentration (<13% different) and NP mean size (30 ± 1 nm, <4% different) in all matrices studied as compared to samples in the absence of dissolved silver.

CRediT authorship contribution statement

Virva Kinnunen: Conceptualization, Validation, Formal analysis, Investigation, Visualization, Writing – original draft, Writing – review & editing. **Janne Frimodig:** Writing – original draft, Investigation, Resources. **Siiri Perämäki:** Supervision, Writing – original draft. **Rose Matilainen:** Project administration, Supervision, Writing – original draft, Writing – review & editing.

Declaration of Competing Interest

The authors declare that they have no known competing financial interests or personal relationships that could have appeared to influence the work reported in this paper.

Data availability

Data will be made available on request.

Acknowledgements

This work was supported by the University of Jyväskylä, Department of Chemistry. The authors would like to thank Joona Rajahalme and Joni Niskanen for the inspirational discussions regarding the subject and comments on the manuscript. Kaisa Lampinen and Elina Hautakangas are greatly appreciated for their help with sample preparation and Hannu Salo for SEM imaging.

Appendix A. Supplementary data

Supplementary data to this article can be found online at https://doi.org/10.1016/j.sab.2023.106662.

References

[1] E.A.J. Bleeker, S. Evertz, R.E. Geertsma, W.J.G.M. Peijnenburg, J. Westra, S.W. P. Wijnhoven, Assessing Health & Environmental Risks of Nanoparticles, National Institute for Public Health and the Environment, Bilthoven, The Netherlands, 2015.
[2] J.R. Lead, G.E. Batley, P.J.J. Alvarez, M.N. Croteau, R.D. Handy, M.J. McLaughlin, J.D. Judy, K. Schirmer, Nanomaterials in the environment: behavior, fate, bioavailability, and effects—an updated review, Environ. Toxicol. Chem. 37 (2018) 2029–2063, https://doi.org/10.1002/etc.4147.
[3] Z. Ferdous, A. Nemmar, Health impact of silver nanoparticles: a review of the biodistribution and toxicity following various routes of exposure, Int. J. Mol. Sci. 21 (2020), https://doi.org/10.3390/ijms21072375.
[4] S.P. Deshmukh, S.M. Patil, S.B. Mullani, S.D. Delekar, Silver nanoparticles as an effective disinfectant: a review, Mater. Sci. Eng. C 97 (2019) 954–965, https://doi.org/10.1016/j.msec.2018.12.102.
[5] X.F. Zhang, Z.G. Liu, W. Shen, S. Gurunathan, Silver nanoparticles: synthesis, characterization, properties, applications, and therapeutic approaches, Int. J. Mol. Sci. 17 (2016), https://doi.org/10.3390/ijms17091534.
[6] D. Mozhayeva, C. Engelhard, A critical review of single particle inductively coupled plasma mass spectrometry – a step towards an ideal method for nanomaterial characterization, J. Anal. At. Spectrom. 35 (2020) 1740–1783, https://doi.org/10.1039/c9ja00206e.
[7] B. Meermann, V. Nischwitz, ICP-MS for the analysis at the nanoscale - a tutorial review, J. Anal. At. Spectrom. 33 (2018) 1432–1468, https://doi.org/10.1039/C8JA00037A.
[8] E. Bolea, M.S. Jimenez, J. Perez-Arantegui, J.C. Vidal, M. Bakir, K. Ben-Jeddou, A. C. Gimenez-Ingalaturre, D. Ojeda, C. Trujillo, F. Laborda, Analytical applications of single particle inductively coupled plasma mass spectrometry: a comprehensive and critical review, Anal. Methods 13 (2021) 2742–2795, https://doi.org/10.1039/d1ay00761k.
[9] F. Laborda, E. Bolea, G. Cepriá, M.T. Gómez, M.S. Jiménez, J. Pérez-Arantegui, J. R. Castillo, Detection, characterization and quantification of inorganic engineered nanomaterials: a review of techniques and methodological approaches for the analysis of complex samples, Anal. Chim. Acta 904 (2016) 10–32, https://doi.org/10.1016/j.aca.2015.11.008.
[10] M.D. Montaño, J.W. Olesik, A.G. Barber, K. Challis, J.F. Ranville, Single particle ICP-MS: advances toward routine analysis of nanomaterials, Anal. Bioanal. Chem. 408 (2016) 5053–5074, https://doi.org/10.1007/s00216-016-9676-8.
[11] C. Degueldre, P.Y. Favarger, Colloid analysis by single particle inductively coupled plasma-mass spectroscopy: a feasibility study, Colloids Surf. A Physicochem. Eng. Asp. 217 (2003) 137–142, https://doi.org/10.1016/S0927-7757(02)00568-X.
[12] F. Laborda, J. Jiménez-Lamana, E. Bolea, J.R. Castillo, Selective identification, characterization and determination of dissolved silver(i) and silver nanoparticles based on single particle detection by inductively coupled plasma mass spectrometry, J. Anal. At. Spectrom. 26 (2011) 1362–1371, https://doi.org/10.1039/c0ja00098a.
[13] H.E. Pace, N.J. Rogers, C. Jarolimek, V.A. Coleman, C.P. Higgins, J.F. Ranville, Determining transport efficiency for the purpose of counting and sizing nanoparticles via single particle inductively coupled plasma mass spectrometry, Anal. Chem. 83 (2011) 9361–9369, https://doi.org/10.1021/ac201952t.
[14] V. Kinnunen, S. Perämäki, R. Matilainen, Solid phase extraction materials as a key for improving the accuracy of silver nanoparticle characterization with single-particle inductively coupled plasma mass spectrometry in natural waters through dissolved silver removal, Spectrochim Acta Part B At Spectrosc. 193 (2022), 106431, https://doi.org/10.1016/j.sab.2022.106431.
[15] M. Hadioui, C. Peyrot, K.J. Wilkinson, Improvements to single particle ICPMS by the online coupling of ion exchange resins, Anal. Chem. 86 (2014) 4668–4674, https://doi.org/10.1021/ac5004932.

[16] D.M. Schwertfeger, J.R. Velicogna, A.H. Jesmer, R.P. Scroggins, J.I. Princz, Single particle-inductively coupled plasma mass spectroscopy analysis of metallic nanoparticles in environmental samples with large dissolved Analyte fractions, Anal. Chem. 88 (2016) 9908–9914, https://doi.org/10.1021/acs.analchem.6b02716.
[17] K. Newman, C. Metcalfe, J. Martin, H. Hintelmann, P. Shaw, A. Donard, Improved single particle ICP-MS characterization of silver nanoparticles at environmentally relevant concentrations, J. Anal. At. Spectrom. 31 (2016) 2069–2077, https://doi.org/10.1039/c6ja00221h.
[18] F. Laborda, J. Jiménez-Lamana, E. Bolea, J.R. Castillo, Critical considerations for the determination of nanoparticle number concentrations, size and number size distributions by single particle ICP-MS, J. Anal. At. Spectrom. 28 (2013) 1220–1232, https://doi.org/10.1039/c3ja50100k.
[19] F. Laborda, A.C. Gimenez-Ingalaturre, E. Bolea, J.R. Castillo, About detectability and limits of detection in single particle inductively coupled plasma mass spectrometry, Spectrochim Acta Part B At Spectrosc. 169 (2020), 105883, https://doi.org/10.1016/j.sab.2020.105883.
[20] D. Mozhayeva, C. Engelhard, A quantitative nanoparticle extraction method for microsecond time resolved single-particle ICP-MS data in the presence of a high background, J. Anal. At. Spectrom. 34 (2019) 1571–1580, https://doi.org/10.1039/c9ja00042a.
[21] A. Gundlach-Graham, L. Hendriks, K. Mehrabi, D. Günther, Monte Carlo simulation of low-count signals in time-of-flight mass spectrometry and its application to single-particle detection, Anal. Chem. 90 (2018) 11847–11855, https://doi.org/10.1021/acs.analchem.8b01551.
[22] B. Giese, F. Klaessig, B. Park, R. Kaegi, M. Steinfeldt, H. Wigger, A. von Gleich, F. Gottschalk, Risks, release and concentrations of engineered nanomaterial in the environment, Sci Rep. 8 (2018) 1–18, https://doi.org/10.1038/s41598-018-19275-4.
[23] T.Y. Sun, N.A. Bornhöft, K. Hungerbühler, B. Nowack, Dynamic probabilistic modeling of environmental emissions of engineered nanomaterials, Environ. Sci. Technol. 50 (2016) 4701–4711, https://doi.org/10.1021/acs.est.5b05828.
[24] E. Lahtinen, E. Kukkonen, V. Kinnunen, M. Lahtinen, K. Kinnunen, S. Suvanto, A. Vaïsänen, M. Haukka, Gold nanoparticles on 3D-printed filters: from waste to catalysts, ACS Omega. 4 (2019) 16891–16898, https://doi.org/10.1021/acsomega.9b02113.
[25] K.E. Murphy, J. Liu, A.R. Montoro, B.M.E. Johnson, M.R. Winchester, Characterization of nanoparticle suspensions using single particle inductively coupled plasma mass spectrometry, in: NIST Special Publication 1200-21, 2011, pp. 1200–1221, https://doi.org/10.6028/NIST.SP.1200-21.
[26] I. Römer, T.A. White, M. Baalousha, K. Chipman, M.R. Viant, J.R. Lead, Aggregation and dispersion of silver nanoparticles in exposure media for aquatic toxicity tests, J. Chromatogr. A 1218 (2011) 4226–4233, https://doi.org/10.1016/j.chroma.2011.03.034.
[27] J. Wan, Y. Kim, M.J. Mulvihill, T.K. Tokunaga, Dilution destabilizes engineered ligand-coated nanoparticles in aqueous suspensions, Environ. Toxicol. Chem. 37 (2018) 1301–1308, https://doi.org/10.1002/etc.4103.
[28] J. Liu, K.E. Murphy, M.R. Winchester, V.A. Hackley, Overcoming challenges in single particle inductively coupled plasma mass spectrometry measurement of silver nanoparticles, Anal. Bioanal. Chem. 409 (2017) 6027–6039, https://doi.org/10.1007/s00216-017-0530-4.
[29] P. Cervantes-Avilés, Y. Huang, A.A. Keller, Multi-technique approach to study the stability of silver nanoparticles at predicted environmental concentrations in wastewater, Water Res. 166 (2019), https://doi.org/10.1016/j.watres.2019.115072.
[30] L. Fréchette-Viens, M. Hadioui, K.J. Wilkinson, Quantification of ZnO nanoparticles and other Zn containing colloids in natural waters using a high sensitivity single particle ICP-MS, Talanta. 200 (2019) 156–162, https://doi.org/10.1016/j.talanta.2019.03.041.
[31] M. Hadioui, V. Merdzan, K.J. Wilkinson, Detection and characterization of ZnO nanoparticles in surface and waste waters using single particle ICPMS, Environ. Sci. Technol. 49 (2015) 6141–6148, https://doi.org/10.1021/acs.est.5b00681.
[32] L. Fréchette-Viens, M. Hadioui, K.J. Wilkinson, Practical limitations of single particle ICP-MS in the determination of nanoparticle size distributions and dissolution: case of rare earth oxides, Talanta. 163 (2017) 121–126, https://doi.org/10.1016/j.talanta.2016.10.093.
[33] H. Agrawaal, J.E. Thompson, Additive manufacturing (3D printing) for analytical chemistry, Talanta Open. 3 (2021), 100036, https://doi.org/10.1016/j.talo.2021.100036.
[34] B. Gross, S.Y. Lockwood, D.M. Spence, Recent advances in analytical chemistry by 3D printing, Anal. Chem. 89 (2017) 57–70, https://doi.org/10.1021/acs.analchem.6b04344.
[35] B.C. Gross, J.L. Erkal, S.Y. Lockwood, C. Chen, D.M. Spence, Evaluation of 3D printing and its potential impact on biotechnology and the chemical sciences, Anal. Chem. 86 (2014) 3240–3253, https://doi.org/10.1021/ac403397r.
[36] U. Kalsoom, P.N. Nesterenko, B. Paull, Current and future impact of 3D printing on the separation sciences, TrAC Trends Anal. Chem. 105 (2018) 492–502, https://doi.org/10.1016/j.trac.2018.06.006.
[37] E. Lahtinen, L. Turunen, M.M. Hänninen, K. Kolari, H.M. Tuononen, M. Haukka, Fabrication of porous hydrogenation catalysts by a selective laser sintering 3D printing technique, ACS Omega. 4 (2019) 12012–12017, https://doi.org/10.1021/acsomega.9b00711.
[38] J. Frimodig, A. Autio, E. Lahtinen, M. Haukka, Recovery of 17β-Estradiol using 3D printed polyamide-12 scavengers, 3D Print Addit Manuf. (2022), https://doi.org/10.1089/3dp.2021.0063.
[39] E. Lahtinen, M.M. Hänninen, K. Kinnunen, H.M. Tuononen, A. Väisänen, K. Rissanen, M. Haukka, Porous 3D printed scavenger filters for selective recovery of precious metals from electronic waste, Adv Sustain Syst. 2 (2018) 1–5, https://doi.org/10.1002/adsu.201800048.
[40] E. Lahtinen, L. Kivijärvi, R. Tatikonda, A. Väisänen, K. Rissanen, M. Haukka, Selective recovery of gold from electronic waste using 3D-printed scavenger, ACS Omega. 2 (2017) 7299–7304, https://doi.org/10.1021/acsomega.7b01215.
[41] S.F.S. Shirazi, S. Gharehkhani, M. Mehrali, H. Yarmand, H.S.C. Metselaar, N. Adib Kadri, N.A.A. Osman, A review on powder-based additive manufacturing for tissue engineering: selective laser sintering and inkjet 3D printing, Sci Technol, Adv. Mater. 16 (2015) 1–20, https://doi.org/10.1088/1468-6996/16/3/033502.
[42] S. Kulomäki, E. Lahtinen, S. Perämäki, A. Väisänen, Preconcentration and speciation analysis of mercury: 3D printed metal scavenger-based solid-phase extraction followed by analysis with inductively coupled plasma mass spectrometry, Talanta. 240 (2022), https://doi.org/10.1016/j.talanta.2021.123163.
[43] S. Kulomäki, E. Lahtinen, S. Perämäki, A. Väisänen, Determination of mercury at picogram level in natural waters with inductively coupled plasma mass spectrometry by using 3D printed metal scavengers, Anal. Chim. Acta 1092 (2019) 24–31, https://doi.org/10.1016/j.aca.2019.09.075.
[44] V. Kinnunen, S. Perämäki, R. Matilainen, Optimization of instrumental parameters for improving sensitivity of single particle inductively-coupled plasma mass spectrometry analysis of gold, Spectrochim Acta Part B At Spectrosc. 177 (2021), https://doi.org/10.1016/j.sab.2021.106104.
[45] R. Sekine, K. Khurana, K. Vasilev, E. Lombi, E. Donner, Quantifying the adsorption of ionic silver and functionalized nanoparticles during ecotoxicity testing: test container effects and recommendations, Nanotoxicology. 9 (2015) 1005–1012, https://doi.org/10.3109/17435390.2014.994570.
[46] W. Chen, P. Wee, I.D. Brindle, Elimination of the memory effects of gold, mercury and silver in inductively coupled plasma atomic emission spectroscopy, J. Anal. At. Spectrom. 15 (2000) 409–413, https://doi.org/10.1039/A908658G.
[47] I. López-García, Y. Vicente-Martínez, M. Hernández-Córdoba, Speciation of silver nanoparticles and Ag(I) species using cloud point extraction followed by electrothermal atomic absorption spectrometry, Spectrochim Acta Part B At Spectrosc. 101 (2014) 93–97, https://doi.org/10.1016/j.sab.2014.07.017.
[48] J.F. Liu, J.B. Chao, R. Liu, Z.Q. Tan, Y.G. Yin, Y. Wu, G. Bin Jiang, Cloud point extraction as an advantageous preconcentration approach for analysis of trace silver nanoparticles in environmental waters, Anal. Chem. 81 (2009) 6496–6502, https://doi.org/10.1021/ac900918e.
[49] J. Soto-Alvaredo, M. Montes-Bayón, J. Bettmer, Speciation of silver nanoparticles and silver(I) by reversed-phase liquid chromatography coupled to ICPMS, Anal. Chem. 85 (2013) 1316–1321, https://doi.org/10.1021/ac302851d.
[50] A.C. Gimenez-Ingalaturre, K. Ben-Jeddou, J. Perez-Arantegui, M.S. Jimenez, E. Bolea, F. Laborda, How to trust size distributions obtained by single particle inductively coupled plasma mass spectrometry analysis, Anal. Bioanal. Chem. (2022), https://doi.org/10.1007/s00216-022-04215-z.
[51] H.E. Pace, N.J. Rogers, C. Jarolimek, V.A. Coleman, E.P. Gray, C.P. Higgins, J. F. Ranville, Single particle inductively coupled plasma-mass spectrometry: a performance evaluation and method comparison in the determination of nanoparticle size, Environ. Sci. Technol. 46 (2012) 12272–12280, https://doi.org/10.1021/es301787d.

DEPARTMENT OF CHEMISTRY, UNIVERSITY OF JYVÄSKYLÄ
RESEARCH REPORT SERIES

1. Vuolle, Mikko: Electron paramagnetic resonance and molecular orbital study of radical ions generated from (2.2)metacyclophane, pyrene and its hydrogenated compounds by alkali metal reduction and by thallium(III)trifluoroacetate oxidation. (99 pp.) 1976
2. Pasanen, Kaija: Electron paramagnetic resonance study of cation radical generated from various chlorinated biphenyls. (66 pp.) 1977
3. Carbon-13 Workshop, September 6-8, 1977. (91 pp.) 1977
4. Laihia, Katri: On the structure determination of norbornane polyols by NMR spectroscopy. (111 pp.) 1979
5. Nyrönen, Timo: On the EPR, ENDOR and visible absorption spectra of some nitrogen containing heterocyclic compounds in liquid ammonia. (76 pp.) 1978
6. Talvitie, Antti: Structure determination of some sesquiterpenoids by shift reagent NMR. (54 pp.) 1979
7. Häkli, Harri: Structure analysis and molecular dynamics of cyclic compounds by shift reagent NMR. (48 pp.) 1979
8. Pitkänen, Ilkka: Thermodynamics of complexation of 1,2,4-triazole with divalent manganese, cobalt, nickel, copper, zinc, cadmium and lead ions in aqueous sodium perchlorate solutions. (89 pp.) 1980
9. Asunta, Tuula: Preparation and characterization of new organometallic compounds synthesized by using metal vapours. (91 pp.) 1980
10. Sattar, Mohammad Abdus: Analyses of MCPA and its metabolites in soil. (57 pp.) 1980
11. Bibliography 1980. (31 pp.) 1981
12. Knuuttila, Pekka: X-Ray structural studies on some divalent 3d metal compounds of picolinic and isonicotinic acid N-oxides. (77 pp.) 1981
13. Bibliography 1981. (33 pp.) 1982
14. 6^{th} National NMR Symposium, September 9-10, 1982, Abstracts. (49 pp.) 1982
15. Bibliography 1982. (38 pp.) 1983
16. Knuuttila, Hilkka: X-Ray structural studies on some Cu(II), Co(II) and Ni(II) complexes with nicotinic and isonicotinic acid N-oxides. (54 pp.) 1983
17. Symposium on inorganic and analytical chemistry May 18, 1984, Program and Abstracts. (100 pp.) 1984
18. Knuutinen, Juha: On the synthesis, structure verification and gas chromatographic determination of chlorinated catechols and guaiacols occuring in spent bleach liquors of kraft pulp mill. (30 pp.) 1984
19. Bibliography 1983. (47 pp.) 1984
20. Pitkänen, Maija: Addition of BrCl, B_2 and Cl_2 to methyl esters of propenoic and 2-butenoic acid derivatives and ^{13}C NMR studies on methyl esters of saturated aliphatic mono- and dichlorocarboxylic acids. (56 pp.) 1985
21. Bibliography 1984. (39 pp.) 1985
22. Salo, Esa: EPR, ENDOR and TRIPLE spectroscopy of some nitrogen heteroaromatics in liquid ammonia. (111 pp.) 1985

23. Humppi, Tarmo: Synthesis, identification and analysis of dimeric impurities of chlorophenols. (39 pp.) 1985
24. Aho, Martti: The ion exchange and adsorption properties of sphagnum peat under acid conditions. (90 pp.) 1985
25. Bibliography 1985 (61 pp.) 1986
26. Bibliography 1986. (23 pp.) 1987
27. Bibliography 1987. (26 pp.) 1988
28. Paasivirta, Jaakko (Ed.): Structures of organic environmental chemicals. (67 pp.) 1988
29. Paasivirta, Jaakko (Ed.): Chemistry and ecology of organo-element compounds. (93 pp.) 1989
30. Sinkkonen, Seija: Determination of crude oil alkylated dibenzothiophenes in environment. (35 pp.) 1989
31. Kolehmainen, Erkki (Ed.): XII National NMR Symposium Program and Abstracts. (75 pp.) 1989
32. Kuokkanen, Tauno: Chlorocymenes and Chlorocymenenes: Persistent chlorocompounds in spent bleach liquors of kraft pulp mills. (40 pp.) 1989
33. Mäkelä, Reijo: ESR, ENDOR and TRIPLE resonance study on substituted 9,10-anthraquinone radicals in solution. (35 pp.) 1990
34. Veijanen, Anja: An integrated sensory and analytical method for identification of off-flavour compounds. (70 pp.) 1990
35. Kasa, Seppo: EPR, ENDOR and TRIPLE resonance and molecular orbital studies on a substitution reaction of anthracene induced by thallium(III) in two fluorinated carboxylic acids. (114 pp.) 1990
36. Herve, Sirpa: Mussel incubation method for monitoring organochlorine compounds in freshwater recipients of pulp and paper industry. (145 pp.) 1991
37. Pohjola, Pekka: The electron paramagnetic resonance method for characterization of Finnish peat types and iron (III) complexes in the process of peat decomposition. (77 pp.) 1991
38. Paasivirta, Jaakko (Ed.): Organochlorines from pulp mills and other sources. Research methodology studies 1988-91. (120 pp.) 1992
39. Veijanen, Anja (Ed.): VI National Symposium on Mass Spectrometry, May 13-15, 1992, Abstracts. (55 pp.) 1992
40. Rissanen, Kari (Ed.): The 7. National Symposium on Inorganic and Analytical Chemistry, May 22, 1992, Abstracts and Program. (153 pp.) 1992
41. Paasivirta, Jaakko (Ed.): CEOEC'92, Second Finnish-Russian Seminar: Chemistry and Ecology of Organo-Element Compounds. (93 pp.) 1992
42. Koistinen, Jaana: Persistent polychloroaromatic compounds in the environment: structure-specific analyses. (50 pp.) 1993
43. Virkki, Liisa: Structural characterization of chlorolignins by spectroscopic and liquid chromatographic methods and a comparison with humic substances. (62 pp.) 1993
44. Helenius, Vesa: Electronic and vibrational excitations in some

biologically relevant molecules. (30 pp.) 1993

45. Leppä-aho, Jaakko: Thermal behaviour, infrared spectra and x-ray structures of some new rare earth chromates(VI). (64 pp.) 1994
46. Kotila, Sirpa: Synthesis, structure and thermal behavior of solid copper(II) complexes of 2-amino-2- hydroxymethyl-1,3-propanediol. (111 pp.) 1994
47. Mikkonen, Anneli: Retention of molybdenum(VI), vanadium(V) and tungsten(VI) by kaolin and three Finnish mineral soils. (90 pp.) 1995
48. Suontamo, Reijo: Molecular orbital studies of small molecules containing sulfur and selenium. (42 pp.) 1995
49. Hämäläinen, Jouni: Effect of fuel composition on the conversion of fuel-N to nitrogen oxides in the combustion of small single particles. (50 pp.) 1995
50. Nevalainen, Tapio: Polychlorinated diphenyl ethers: synthesis, NMR spectroscopy, structural properties, and estimated toxicity. (76 pp.) 1995
51. Aittola, Jussi-Pekka: Organochloro compounds in the stack emission. (35 pp.) 1995
52. Harju, Timo: Ultrafast polar molecular photophysics of (dibenzylmethine)borondifluoride and 4-aminophthalimide in solution. (61 pp.) 1995
53. Maatela, Paula: Determination of organically bound chlorine in industrial and environmental samples. (83 pp.) 1995
54. Paasivirta, Jaakko (Ed.): CEOEC'95, Third Finnish-Russian Seminar: Chemistry and Ecology of Organo-Element Compounds. (109 pp.) 1995
55. Huuskonen, Juhani: Synthesis and structural studies of some supramolecular compounds. (54 pp.) 1995
56. Palm, Helena: Fate of chlorophenols and their derivatives in sawmill soil and pulp mill recipient environments. (52 pp.) 1995
57. Rantio, Tiina: Chlorohydrocarbons in pulp mill effluents and their fate in the environment. (89 pp.) 1997
58. Ratilainen, Jari: Covalent and non-covalent interactions in molecular recognition. (37 pp.) 1997
59. Kolehmainen, Erkki (Ed.): XIX National NMR Symposium, June 4-6, 1997, Abstracts. (89 pp.) 1997
60. Matilainen, Rose: Development of methods for fertilizer analysis by inductively coupled plasma atomic emission spectrometry. (41 pp.) 1997
61. Koistinen, Jari (Ed.): Spring Meeting on the Division of Synthetic Chemistry, May 15-16, 1997, Program and Abstracts. (36 pp.) 1997
62. Lappalainen, Kari: Monomeric and cyclic bile acid derivatives: syntheses, NMR spectroscopy and molecular recognition properties. (50 pp.) 1997
63. Laitinen, Eira: Molecular dynamics of cyanine dyes and phthalimides in solution: picosecond laser studies. (62 pp.) 1997
64. Eloranta, Jussi: Experimental and theoretical studies on some

quinone and quinol radicals. (40 pp.) 1997

65. Oksanen, Jari: Spectroscopic characterization of some monomeric and aggregated chlorophylls. (43 pp.) 1998
66. Häkkänen, Heikki: Development of a method based on laser-induced plasma spectrometry for rapid spatial analysis of material distributions in paper coatings. (60 pp.) 1998
67. Virtapohja, Janne: Fate of chelating agents used in the pulp and paper industries. (58 pp.) 1998
68. Airola, Karri: X-ray structural studies of supramolecular and organic compounds. (39 pp.) 1998
69. Hyötyläinen, Juha: Transport of lignin–type compounds in the receiving waters of pulp mills. (40 pp.) 1999
70. Ristolainen, Matti: Analysis of the organic material dissolved during totally chlorine-free bleaching. (40 pp.) 1999
71. Eklin, Tero: Development of analytical procedures with industrial samples for atomic emission and atomic absorption spectrometry. (43 pp.) 1999
72. Välisaari, Jouni: Hygiene properties of resol-type phenolic resin laminates. (129 pp.) 1999
73. Hu, Jiwei: Persistent polyhalogenated diphenyl ethers: model compounds syntheses, characterization and molecular orbital studies. (59 pp.) 1999
74. Malkavaara, Petteri: Chemometric adaptations in wood processing chemistry. (56 pp.) 2000
75. Kujala Elena, Laihia Katri, Nieminen Kari (Eds.): NBC 2000, Symposium on Nuclear, Biological and Chemical Threats in the 21st Century. (299 pp.) 2000
76. Rantalainen, Anna-Lea: Semipermeable membrane devices in monitoring persistent organic pollutants in the environment. (58 pp.) 2000
77. Lahtinen, Manu: *In situ* X-ray powder diffraction studies of Pt/C, CuCl/C and Cu_2O/C catalysts at elevated temperatures in various reaction conditions. (92 pp.) 2000
78. Tamminen, Jari: Syntheses, empirical and theoretical characterization, and metal cation complexation of bile acid-based monomers and open/closed dimers. (54 pp.) 2000
79. Vatanen, Virpi: Experimental studies by EPR and theoretical studies by DFT calculations of α-amino-9,10-anthraquinone radical anions and cations in solution. (37 pp.) 2000
80. Kotilainen, Risto: Chemical changes in wood during heating at 150-260 °C. (57 pp.) 2000
81. Nissinen, Maija: X-ray structural studies on weak, non-covalent interactions in supramolecular compounds. (69 pp.) 2001
82. Wegelius, Elina: X-ray structural studies on self-assembled hydrogen-bonded networks and metallosupramolecular complexes. (84 pp.) 2001
83. Paasivirta, Jaakko (Ed.): CEOEC'2001, Fifth Finnish-Russian Seminar: Chemistry and Ecology of Organo-Element Compounds. (163 pp.) 2001
84. Kiljunen, Toni: Theoretical studies on spectroscopy and

atomic dynamics in rare gas solids. (56 pp.) 2001

85. Du, Jin: Derivatives of dextran: synthesis and applications in oncology. (48 pp.) 2001
86. Koivisto, Jari: Structural analysis of selected polychlorinated persistent organic pollutants (POPs) and related compounds. (88 pp.) 2001
87. Feng, Zhinan: Alkaline pulping of non-wood feedstocks and characterization of black liquors. (54 pp.) 2001
88. Halonen, Markku: Lahon havupuun käyttö sulfaattiprosessin raaka-aineena sekä havupuun lahontorjunta. (90 pp.) 2002
89. Falábu, Dezsö: Synthesis, conformational analysis and complexation studies of resorcarene derivatives. (212 pp.) 2001
90. Lehtovuori, Pekka: EMR spectroscopic studies on radicals of ubiquinones Q-*n*, vitamin K_3 and vitamine E in liquid solution. (40 pp.) 2002
91. Perkkalainen, Paula: Polymorphism of sugar alcohols and effect of grinding on thermal behavior on binary sugar alcohol mixtures. (53 pp.) 2002
92. Ihalainen, Janne: Spectroscopic studies on light-harvesting complexes of green plants and purple bacteria. (42 pp.) 2002
93. Kunttu, Henrik, Kiljunen, Toni (Eds.): 4th International Conference on Low Temperature Chemistry. (159 pp.) 2002
94. Väisänen, Ari: Development of methods for toxic element analysis in samples with environmental concern by ICP-AES and ETAAS. (54 pp.) 2002
95. Luostarinen, Minna: Synthesis and characterisation of novel resorcarene derivatives. (200 pp.) 2002
96. Louhelainen, Jarmo: Changes in the chemical composition and physical properties of wood and nonwood black liquors during heating. (68 pp.) 2003
97. Lahtinen, Tanja: Concave hydrocarbon cyclophane π-prismands. (65 pp.) 2003
98. Laihia, Katri (Ed.): NBC 2003, Symposium on Nuclear, Biological and Chemical Threats – A Crisis Management Challenge. (245 pp.) 2003
99. Oasmaa, Anja: Fuel oil quality properties of wood-based pyrolysis liquids. (32 pp.) 2003
100. Virtanen, Elina: Syntheses, structural characterisation, and cation/anion recognition properties of nano-sized bile acid-based host molecules and their precursors. (123 pp.) 2003
101. Nättinen, Kalle: Synthesis and X-ray structural studies of organic and metallo-organic supramolecular systems. (79 pp.) 2003
102. Lampiselkä, Jarkko: Demonstraatio lukion kemian opetuksessa. (285 pp.) 2003
103. Kallioinen, Jani: Photoinduced dynamics of $Ru(dcbpy)_2(NCS)_2$ – in solution and on nanocrystalline titanium dioxide thin films. (47 pp.) 2004
104. Valkonen, Arto (Ed.): VII Synthetic Chemistry Meeting and XXVI Finnish NMR Symposium. (103 pp.) 2004

105. Vaskonen, Kari: Spectroscopic studies on atoms and small molecules isolated in low temperature rare gas matrices. (65 pp.) 2004
106. Lehtovuori, Viivi: Ultrafast light induced dissociation of $Ru(dcbpy)(CO)_2I_2$ in solution. (49 pp.) 2004
107. Saarenketo, Pauli: Structural studies of metal complexing Schiff bases, Schiff base derived *N*-glycosides and cyclophane π-prismands. (95 pp.) 2004
108. Paasivirta, Jaakko (Ed.): CEOEC'2004, Sixth Finnish-Russian Seminar: Chemistry and Ecology of Organo-Element Compounds. (147 pp.) 2004
109. Suontamo, Tuula: Development of a test method for evaluating the cleaning efficiency of hard-surface cleaning agents. (96 pp.) 2004
110. Güneş, Minna: Studies of thiocyanates of silver for nonlinear optics. (48 pp.) 2004
111. Ropponen, Jarmo: Aliphatic polyester dendrimers and dendrons. (81 pp.) 2004
112. Vu, Mân Thi Hong: Alkaline pulping and the subsequent elemental chlorine-free bleaching of bamboo (*Bambusa procera*). (69 pp.) 2004
113. Mansikkamäki, Heidi: Self-assembly of resorcinarenes. (77 pp.) 2006
114. Tuononen, Heikki M.: EPR spectroscopic and quantum chemical studies of some inorganic main group radicals. (79 pp.) 2005
115. Kaski, Saara: Development of methods and applications of laser-induced plasma spectroscopy in vacuum ultraviolet. (44 pp.) 2005
116. Mäkinen, Riika-Mari: Synthesis, crystal structure and thermal decomposition of certain metal thiocyanates and organic thiocyanates. (119 pp.) 2006
117. Ahokas, Jussi: Spectroscopic studies of atoms and small molecules isolated in rare gas solids: photodissociation and thermal reactions. (53 pp.) 2006
118. Busi, Sara: Synthesis, characterization and thermal properties of new quaternary ammonium compounds: new materials for electrolytes, ionic liquids and complexation studies. (102 pp.) 2006
119. Mäntykoski, Keijo: PCBs in processes, products and environment of paper mills using wastepaper as their raw material. (73 pp.) 2006
120. Laamanen, Pirkko-Leena: Simultaneous determination of industrially and environmentally relevant aminopolycarboxylic and hydroxycarboxylic acids by capillary zone electrophoresis. (54 pp.) 2007
121. Salmela, Maria: Description of oxygen-alkali delignification of kraft pulp using analysis of dissolved material. (71 pp.) 2007
122. Lehtovaara, Lauri: Theoretical studies of atomic scale impurities in superfluid ^{4}He. (87 pp.) 2007
123. Rautiainen, J. Mikko: Quantum chemical calculations of structures, bonding, and spectroscopic properties of some sulphur and selenium iodine cations. (71 pp.) 2007
124. Nummelin, Sami: Synthesis, characterization, structural and

retrostructural analysis of self-assembling pore forming dendrimers. (286 pp.) 2008

125. Sopo, Harri: Uranyl(VI) ion complexes of some organic aminobisphenolate ligands: syntheses, structures and extraction studies. (57 pp.) 2008
126. Valkonen, Arto: Structural characteristics and properties of substituted cholanoates and *N*-substituted cholanamides. (80 pp.) 2008
127. Lähde, Anna: Production and surface modification of pharmaceutical nano- and microparticles with the aerosol flow reactor. (43 pp.) 2008
128. Beyeh, Ngong Kodiah: Resorcinarenes and their derivatives: synthesis, characterization and complexation in gas phase and in solution. (75 pp.) 2008
129. Välisaari, Jouni, Lundell, Jan (Eds.): Kemian opetuksen päivät 2008: uusia oppimisympäristöjä ja ongelmalähtöistä opetusta. (118 pp.) 2008
130. Myllyperkiö, Pasi: Ultrafast electron transfer from potential organic and metal containing solar cell sensitizers. (69 pp.) 2009
131. Käkölä, Jaana: Fast chromatographic methods for determining aliphatic carboxylic acids in black liquors. (82 pp.) 2009
132. Koivukorpi, Juha: Bile acid-arene conjugates: from photoswitchability to cancer cell detection. (67 pp.) 2009
133. Tuuttila, Tero: Functional dendritic polyester compounds: synthesis and characterization of small bifunctional dendrimers and dyes. (74 pp.) 2009
134. Salorinne, Kirsi: Tetramethoxy resorcinarene based cation and anion receptors: synthesis, characterization and binding properties. (79 pp.) 2009
135. Rautiainen, Riikka: The use of first-thinning Scots pine (*Pinus sylvestris*) as fiber raw material for the kraft pulp and paper industry. (73 pp.) 2010
136. Ilander, Laura: Uranyl salophens: synthesis and use as ditopic receptors. (199 pp.) 2010
137. Kiviniemi, Tiina: Vibrational dynamics of iodine molecule and its complexes in solid krypton - Towards coherent control of bimolecular reactions? (73 pp.) 2010
138. Ikonen, Satu: Synthesis, characterization and structural properties of various covalent and non-covalent bile acid derivatives of N/O-heterocycles and their precursors. (105 pp.) 2010
139. Siitonen, Anni: Spectroscopic studies of semiconducting single-walled carbon nanotubes. (56 pp.) 2010
140. Raatikainen, Kari: Synthesis and structural studies of piperazine cyclophanes – Supramolecular systems through Halogen and Hydrogen bonding and metal ion coordination. (69 pp.) 2010
141. Leivo, Kimmo: Gelation and gel properties of two- and three-component Pyrene based low molecular weight organogelators. (116 pp.) 2011
142. Martiskainen, Jari: Electronic energy transfer in light-harvesting complexes isolated from *Spinacia oleracea* and from three

photosynthetic green bacteria *Chloroflexus aurantiacus*, *Chlorobium tepidum*, and *Prosthecochloris aestuarii*. (55 pp.) 2011

143. Wichmann, Oula: Syntheses, characterization and structural properties of [O,N,O,X´] aminobisphenolate metal complexes. (101 pp.) 2011
144. Ilander, Aki: Development of ultrasound-assisted digestion methods for the determination of toxic element concentrations in ash samples by ICP-OES. (58 pp.) 2011
145. The Combined XII Spring Meeting of the Division of Synthetic Chemistry and XXXIII Finnish NMR Symposium. Book of Abstracts. (90 pp.) 2011
146. Valto, Piia: Development of fast analysis methods for extractives in papermaking process waters. (73 pp.) 2011
147. Andersin, Jenni: Catalytic activity of palladium-based nanostructures in the conversion of simple olefinic hydro- and chlorohydrocarbons from first principles. (78 pp.) 2011
148. Aumanen, Jukka: Photophysical properties of dansylated poly(propylene amine) dendrimers. (55 pp.) 2011
149. Kärnä, Minna: Ether-functionalized quaternary ammonium ionic liquids – synthesis, characterization and physicochemical properties. (76 pp.) 2011
150. Jurček, Ondřej: Steroid conjugates for applications in pharmacology and biology. (57 pp.) 2011
151. Nauha, Elisa: Crystalline forms of selected Agrochemical actives: design and synthesis of cocrystals. (77 pp.) 2012
152. Ahkola, Heidi: Passive sampling in monitoring of nonylphenol ethoxylates and nonylphenol in aquatic environments. (92 pp.) 2012
153. Helttunen, Kaisa: Exploring the self-assembly of resorcinarenes: from molecular level interactions to mesoscopic structures. (78 pp.) 2012
154. Linnanto, Juha: Light excitation transfer in photosynthesis revealed by quantum chemical calculations and exiton theory. (179 pp.) 2012
155. Roiko-Jokela, Veikko: Digital imaging and infrared measurements of soil adhesion and cleanability of semihard and hard surfaces. (122 pp.) 2012
156. Noponen, Virpi: Amides of bile acids and biologically important small molecules: properties and applications. (85 pp.) 2012
157. Hulkko, Eero: Spectroscopic signatures as a probe of structure and dynamics in condensed-phase systems – studies of iodine and gold ranging from isolated molecules to nanoclusters. (69 pp.) 2012
158. Lappi, Hanna: Production of Hydrocarbon-rich biofuels from extractives-derived materials. (95 pp.) 2012
159. Nykänen, Lauri: Computational studies of Carbon chemistry on transition metal surfaces. (76 pp.) 2012
160. Ahonen, Kari: Solid state studies of pharmaceutically important molecules and their derivatives. (65 pp.) 2012

161. Pakkanen, Hannu: Characterization of organic material dissolved during alkaline pulping of wood and non-wood feedstocks. (76 pp.) 2012
162. Moilanen, Jani: Theoretical and experimental studies of some main group compounds: from closed shell interactions to singlet diradicals and stable radicals. (80 pp.) 2012
163. Himanen, Jatta: Stereoselective synthesis of Oligosaccharides by *De Novo* Saccharide welding. (133 pp.) 2012
164. Bunzen, Hana: Steroidal derivatives of nitrogen containing compounds as potential gelators. (76 pp.) 2013
165. Seppälä, Petri: Structural diversity of copper(II) amino alcohol complexes. Syntheses, structural and magnetic properties of bidentate amino alcohol copper(II) complexes. (67 pp.) 2013
166. Lindgren, Johan: Computational investigations on rotational and vibrational spectroscopies of some diatomics in solid environment. (77 pp.) 2013
167. Giri, Chandan: Sub-component self-assembly of linear and non-linear diamines and diacylhydrazines, formulpyridine and transition metal cations. (145 pp.) 2013
168. Riisiö, Antti: Synthesis, Characterization and Properties of Cu(II)-, Mo(VI)- and U(VI) Complexes With Diaminotetraphenolate Ligands. (51 pp.) 2013
169. Kiljunen, Toni (Ed.): Chemistry and Physics at Low Temperatures. Book of Abstracts. (103 pp.) 2013
170. Hänninen, Mikko: Experimental and Computational Studies of Transition Metal Complexes with Polydentate Amino- and Aminophenolate Ligands: Synthesis, Structure, Reactivity and Magnetic Properties. (66 pp.) 2013
171. Antila, Liisa: Spectroscopic studies of electron transfer reactions at the photoactive electrode of dye-sensitized solar cells. (53 pp.) 2013
172. Kemppainen, Eeva: Mukaiyama-Michael reactions with α-substituted acroleins – a useful tool for the synthesis of the pectenotoxins and other natural product targets. (190 pp.) 2013
173. Virtanen, Suvi: Structural Studies of Dielectric Polymer Nanocomposites. (49 pp.) 2013
174. Yliniemelä-Sipari, Sanna: Understanding The Structural Requirements for Optimal Hydrogen Bond Catalyzed Enolization – A Biomimetic Approach.(160 pp.) 2013
175. Leskinen, Mikko V: Remote β-functionalization of β'-keto esters. (105 pp.) 2014
176. 12th European Conference on Research in Chemistry Education (ECRICE2014). Book of Abstracts. (166 pp.) 2014
177. Peuronen, Anssi: N-Monoalkylated DABCO-Based N-Donors as Versatile Building Blocks in Crystal Engineering and Supramolecular Chemistry. (54 pp.) 2014
178. Perämäki, Siiri: Method development for determination and recovery of rare earth elements from industrial fly ash. (88 pp.) 2014

179. Chernyshev, Alexander, N.: Nitrogen-containing ligands and their platinum(IV) and gold(III) complexes: investigation and basicity and nucleophilicity, luminescence, and aurophilic interactions. (64 pp.) 2014
180. Lehto, Joni: Advanced Biorefinery Concepts Integrated to Chemical Pulping. (142 pp.) 2015
181. Tero, Tiia-Riikka: Tetramethoxy resorcinarenes as platforms for fluorescent and halogen bonding systems. (61 pp.) 2015
182. Löfman, Miika: Bile acid amides as components of microcrystalline organogels. (62 pp.) 2015
183. Selin, Jukka: Adsorption of softwood-derived organic material onto various fillers during papermaking. (169 pp.) 2015
184. Piisola, Antti: Challenges in the stereoselective synthesis of allylic alcohols. (210 pp.) 2015
185. Bonakdarzadeh, Pia: Supramolecular coordination polyhedra based on achiral and chiral pyridyl ligands: design, preparation, and characterization. (65 pp.) 2015
186. Vasko, Petra: Synthesis, characterization, and reactivity of heavier group 13 and 14 metallylenes and metalloid clusters: small molecule activation and more. (66 pp.) 2015
187. Topić, Filip: Structural Studies of Nano-sized Supramolecular Assemblies. (79 pp.) 2015
188. Mustalahti, Satu: Photodynamics Studies of Ligand-Protected Gold Nanoclusters by using Ultrafast Transient Infrared Spectroscopy. (58 pp.) 2015
189. Koivisto, Jaakko: Electronic and vibrational spectroscopic studies of gold-nanoclusters. (63 pp.) 2015
190. Suhonen, Aku: Solid state conformational behavior and interactions of series of aromatis oligoamide foldamers. (68 pp.) 2016
191. Soikkeli, Ville: Hydrometallurgical recovery and leaching studies for selected valuable metals from fly ash samples by ultrasound-assisted extraction followed by ICP-OES determination. (107 pp.) 2016
192. XXXVIII Finnish NMR Symposium. Book of Abstracts. (51 pp.) 2016
193. Mäkelä, Toni: Ion Pair Recognition by Ditopic Crown Ether Based bis-Urea and Uranyl Salophen Receptors. (75 pp.) 2016
194. Lindholm-Lehto, Petra: Occurrence of pharmaceuticals in municipal wastewater treatment plants and receiving surface waters in Central and Southern Finland. (98 pp.) 2016
195. Härkönen, Ville: Computational and Theoretical studies on Lattice Thermal conductivity and Thermal properties of Silicon Clathrates. (89 pp.) 2016
196. Tuokko, Sakari: Understanding selective reduction reactions with heterogeneous Pd and Pt: climbing out of the black box. (85 pp.) 2016
197. Nuora, Piia: Monitapaustutkimus LUMA-Toimintaan liittyvissä oppimisympäristöissä tapahtuvista kemian oppimiskokemuksista. (171 pp.) 2016

198. Kumar, Hemanathan: Novel Concepts on The Recovery of By-Products from Alkaline Pulping. (61 pp.) 2016
199. Arnedo-Sánchez, Leticia: Lanthanide and Transition Metal Complexes as Building Blocks for Supramolecular Functional Materials. (227 pp.) 2016
200. Gell, Lars: Theoretical Investigations of Ligand Protected Silver Nanoclusters. (134 pp.) 2016
201. Vaskuri, Juhani: Oppiennätyksistä opetussuunnitelman perusteisiin - lukion kemian kansallisen opetussuunnitelman kehittyminen Suomessa vuosina 1918-2016. (314 pp.) 2017
202. Lundell Jan, Kiljunen Toni (Eds.): 22nd Horizons in Hydrogen Bond Research. Book of Abstracts. 2017
203. Turunen, Lotta: Design and construction of halogen-bonded capsules and cages. (61 pp.) 2017
204. Hurmalainen, Juha: Experimental and computational studies of unconventional main group compounds: stable radicals and reactive intermediates. (88 pp.) 2017
205. Koivistoinen Juha: Non-linear interactions of femtosecond laser pulses with graphene: photo-oxidation, imaging and photodynamics. (68 pp.) 2017
206. Chen, Chengcong: Combustion behavior of black liquors: droplet swelling and influence of liquor composition. (39 pp.) 2017
207. Mansikkamäki, Akseli: Theoretical and Computational Studies of Magnetic Anisotropy and Exchange Coupling in Molecular Systems. (190 p. + included articles) 2018.
208. Tatikonda, Rajendhraprasad: Multivalent N-donor ligands for the construction of coordination polymers and coordination polymer gels. (62 pp.) 2018
209. Budhathoki, Roshan: Beneficiation, desilication and selective precipitation techniques for phosphorus refining from biomass derived fly ash. (64 pp.) 2018
210. Siitonen, Juha: Synthetic Studies on 1-azabicyclo[5.3.0]decane Alkaloids. (140 pp.) 2018
211. Ullah, Saleem: Advanced Biorefinery Concepts Related to Non-wood Feedstocks. (57 pp.) 2018
212. Ghalibaf, Maryam: Analytical Pyrolysis of Wood and Non-Wood Materials from Integrated Biorefinery Concepts. (106 pp.) 2018

DEPARTMENT OF CHEMISTRY, UNIVERSITY OF JYVÄSKYLÄ
DISSERTATIONS PUBLISHED IN THE JYU DISSERTATIONS RESEARCH SERIES

1. Bulatov, Evgeny: Synthetic and structural studies of covalent and non-covalent interactions of ligands and metal center in platinum(II) complexes containing 2,2′-dipyridylamine or oxime ligands. (58 pp.) 2019. JYU Dissertations 70.
2. Annala, Riia: Conformational Properties and Anion Complexes of Aromatic Oligoamide Foldamers. (80 pp.) 2019. JYU Dissertations 84.
3. Isoaho, Jukka Pekka: Dithionite Bleaching of Thermomechanical Pulp - Chemistry and Optimal Conditions. (73 pp.) 2019. JYU Dissertations 85.
4. Nygrén, Enni: Recovery of rubidium from power plant fly ash. (98 pp.) 2019. JYU Dissertations 136.
5. Kiesilä, Anniina: Supramolecular chemistry of anion-binding receptors based on concave macromolecules. (68 pp.) 2019. JYU Dissertations 137.
6. Sokolowska, Karolina: Study of water-soluble p-MBA-protected gold nanoclusters and their superstructures. (60 pp.) 2019. JYU Dissertations 167.
7. Lahtinen, Elmeri: Chemically Functional 3D Printing: Selective Laser Sintering of Customizable Metal Scavengers. (71 pp.) 2019. JYU Dissertations 175.
8. Larijani, Amir: Oxidative reactions of cellulose under alkaline conditions. (102 pp.) 2020. JYU Dissertations 217.
9. Kolari, Kalle: Metal-metal contacts in late transition metal polymers. (60 pp.) 2020. JYU Dissertations 220.
10. Kauppinen, Minttu: Multiscale computational investigation of catalytic properties of zirconia supported noble metals. (87 pp.) 2020. JYU Dissertations 231.
11. Ding, Xin: Halogen Bond in Crystal Engineering: Structural Studies on Crystals with Ruthenium Centered Complexes and 1-(4-Pyridyl)-4-thiopyridine Zwitterion as Halogen Bond Acceptors. (59 pp.) 2020. JYU Dissertations 323.
12. Neuvonen, Antti: Toward an Understanding of Hydrogen-Bonding Bifunctional Organocatalyst Conformations and Their Activity in Asymmetric Mannich Reactions. (77 pp.) 2020. JYU Dissertations 336.
13. Kortet, Sami: 2,5-Diarylpyrrolidines and Pyroglutamic-Acid-Derived 2-Diarylmethyl-5-Aryl-Pyrrolidines: Their Synthesis and Use in Asymmetric Synthesis. (221 pp.) 2020. JYU Dissertations 337.
14. Saarnio, Ville: Fluorescent probes, noble metal nanoparticles and their nanocomposites: detection of nucleic acids and other biological targets. (80 pp.) 2021. JYU Dissertations 361.
15. Chernysheva, Maria: σ-hole interactions: the effect of the donors and acceptors nature in selenoureas, thioureas, halogenated species, substituted benzenes, and their adducts. (72 pp.) 2021. JYU Dissertations 370.
16. Bulatova, Margarita: Noncovalent interactions as a tool for supramolecular self-assembly of metallopolymers. (62 pp.) 2021. JYU Dissertations 377.

17. Romppanen, Sari: Laser-spectroscopic studies of rare earth element- and lithium-bearing minerals and rocks. (66 pp.) 2021. JYU Dissertations 393.
18. Kukkonen, Esa: Nonlinear optical materials through weak interactions and their application in 3D printing. (58 pp.) 2021. JYU Dissertations 441.
19. Kuosmanen, Riikka: The Effect of Structure on the Gel Formation Ability and the Properties of Bile Acid Based Supramolecular Organogels. (68 pp.) 2021. JYU Dissertations 465.
20. Reuna, Sini: Development of a Method for Phosphorus Recovery from Wastewaters. (67 pp.) 2022. JYU Dissertations 486.
21. Taipale, Essi: Synthetic and Structural Studies on the Effect of Non-Covalent Interactions on N(*sp2*)-Heterocyclic Molecules. (67 pp.) 2022. JYU Dissertations 496.
22. Järvinen, Teemu: Molecular Dynamics View on Matrix Isolation. (143 pp.) 2022. JYU Dissertations 544.
23. Kumar, Parveen: Synthesis and Structural Studies on Halogen(I) Complexes. (160 pp.) 2022. JYU Dissertations 549.
24. Forsblom, Samu: Design and Construction of Metal-Organic Polyhedra. (212 pp.) 2022. JYU Dissertations 569.
25. Korpelin, Ville: Computational Studies of Catalytic Active Site Properties and Reactions at the Metal–Oxide Interface. (78 pp.) 2022. JYU Dissertations 578.
26. Vuori, Hannu: Extending Benson Group Increment Theory to Compounds of Phosphorus, Silicon, and Boron with Computational Chemistry. (59 pp.) 2022. JYU Dissertations 581.
27. Pallerla, Rajanish: Studies Towards Synthesis of Favipiravir & Humilisin E. (139 pp.) 2023. JYU Dissertations 611.
28. Taponen, Anni: Radical-Ion Salts based on Thiazyls and Tetracyanoquinodimethane: Hysteretic Magnetic Bistability in a Multicomponent System. (66 pp.) 2023. JYU Dissertations 613.
29. Aho, Noora: Molecular Dynamics Simulations of Acids and Bases in Biomolecular Environments. (78 pp.) 2023. JYU Dissertations 614.
30. Sabooni Asre Hazer, Maryam: Electronic and Optical Properties of Gold Clusters with Carbene Ligands using Density Functional Theory Calculations. (68 pp.) 2023. JYU Dissertations 650.